DISSERTATION

A COMPREHENSIVE INVESTIGATION OF HALOGENATED PLASMAS: FROM MECHANISTIC STUDIES TO APPLICATIONS

Submitted by

Ina Taylor Martin

Department of Chemistry

In partial fulfillment of the requirements

For the degree of Doctor of Philosophy

Colorado State University

Fort Collins, Colorado

Fall, 2005

UMI Number: 3200685

INFORMATION TO USERS

COLORADO STATE UNIVERSITY

November 8, 2005

WE HEREBY RECOMMEND THAT THE DISSERTATION PREPARED UNDER OUR SUPERVISION BY INA T. MARTIN ENTITLED **A COMPREHENSIVE INVESTIGATION OF HALOGENATED PLASMAS: FROM MECHANISTIC STUDIES TO APPLICATIONS** BE ACCEPTED AS FULFILLING IN PART THE REQUIREMENTS FOR THE DEGREE OF DOCTOR OF PHILOSPHY.

Committee on Graduate Work

Advisor

Department Head/Director

ABSTRACT OF DISSERTATION

A COMPREHENSIVE INVESTIGATION OF HALOGENATED PLASMAS: FROM MECHANISTIC STUDIES TO APPLICATIONS

Octafluoropropane (C_3F_8) and octafluorocyclobutane (C_4F_8) plasmas were used to deposit thin fluorocarbon (FC) films on Si substrates. The effects of applied rf power (*P*), substrate position and pulsing the plasma on film composition and thickness were studied. Plasma parameters that limited ion bombardment of the substrate during film deposition, such as pulsing the plasma, and placing the substrate downstream from the source, resulted in more F rich, less crosslinked materials. After developing the FC deposition systems, a C_3F_8 plasma treatment was chosen to modify polymer microfluidic devices, with the intent of coating the device with a non-ionizable film to reduce the electroosmotic flow (EOF). Acrylic acid (AA) plasmas were also used to treat the microfluidic devices. Both treatments resulted in modified EOF flow values compared to untreated devices. Plasma treated substrates were analyzed using FTIR, X-ray photoelectron spectroscopy (XPS), scanning Auger microcopy (SAM), scanning electron microscopy (SEM), and ellipsometry.

Gas-phase studies were performed using laser-induced fluorescence (LIF) and mass spectrometry with energy analysis capabilities. Gas-surface interaction studies of

CF_2 molecules in these FC systems were performed using our imaging of radicals interacting with surfaces (IRIS) technique, with an emphasis on ion effects. High scattering coefficients ($S > 1$) indicate CF_2 molecules are generated at the surface. Ions were found to contribute to the surface production of CF_2 during FC plasma treatment of Si. Specifically, a linear correlation exists between CF_2 surface production and the mean energy of ions produced in the plasma. There is also a linear correlation present between S (CF_2) values measured and the degree of crosslinking in the deposited FC materials. Additionally, relative density measurements and rotational temperature studies of CF are discussed.

This dissertation also summarizes preliminary work involving tetrachlorosilane ($SiCl_4$) plasmas, including gas-phase and $SiCl_2$ gas-surface interaction data collected for $SiCl_4$ and $SiCl_4/H_2$ plasma systems. Initial IRIS investigations of $SiCl_2$ molecules during $SiCl_4$ plasma processing of Si demonstrate that there is significant $SiCl_2$ surface production in the parameter range studied. Higher values correspond to systems where etching is the dominant process.

Ina Taylor Martin
Department of Chemistry
Colorado State University
Fort Collins, Colorado 80523-1872
Fall 2005

ACKNOWLEDGMENTS

I gratefully acknowledge all of the people who have participated in my education, both formally and informally. I am especially indebted to my advisor, Prof. Ellen R. Fisher. Your wisdom and guidance have been invaluable; thank you for being my teacher, my mentor, and my friend. I thank my current and former group members for their help and support in this process. A special thanks to Keri and Michelle for training me, and for a lot of encouragement when I needed it the most. Bernie, our grad school motto is going to see us both a long way.

I acknowledge my undergraduate advisor, Prof. Jeanne E. Pemberton for sparking my interest in research, and for her encouragement and advice when I was considering graduate school. Thank you to my committee members, and all the amazing teachers I have had over the years, you have been a source of inspiration- both to learn, and to educate. And finally, I acknowledge my family, and my friends who are my family. You give me buoyancy.

DEDICATION

I dedicate this dissertation to my family, with love.

To my mother Daphne, thank you for giving me the opportunities you never had. Thank you a million times over for your constant support, emotional and financial, and for your unswerving belief that I can do anything. Thank you for taking care of our family. I love you and I am proud to be your daughter.

To Joyce, you are my favorite person to laugh with, and you know me as only a sister can. Thank you for all of your support and encouragement, our off-key harmonies, and for being the one person I know who truly gets my sense of humor. I love the amazing, witty, dramatic human being that you are.

To my father Taylor, you introduced me to science. Because of you I know Invictus, and why ice floats. I love old songs, new people, and tapioca pudding. Most of all, you were the best dad with the best stories. I miss you, I love you, and know you are proud.

TABLE OF CONTENTS

TABLE OF ABBREVIATIONS

AA	acrylic acid
a-Si:H	amorphous silicon
CW	continuous wave
d.c.	duty cycle
$<E_i>$	mean ion energy
EOF	electroosmotic flow
FC	fluorocarbon
FTIR	Fourier transform infrared
g.m.	grounded mesh
IED	ion energy distribution
IRIS	imaging of radicals interacting with surfaces
LIF	laser induced fluorescence
MS	mass spectrometer
OES	optical emission spectroscopy
P	applied rf power
PDMS	polydimethylsiloxane
PECVD	plasma enhanced chemical vapor deposition
S	scatter coefficient
SAM	scanning Auger microscopy
sccm	standard cubic centimeters per minute
SEM	scanning electron microscopy
T_e	electron temperature

T_g	gas temperature
T_S	substrate temperature
XPS	x-ray photoelectron spectroscopy

CHAPTER 1

INTRODUCTION TO PLASMAS

This dissertation chapter provides an introduction to basic phenomena occurring in plasmas with a focus on the role of ions in plasma processing. This chapter also presents general information on fluorocarbon and chlorosilane plasmas, and an overview of the research presented in Chapters 2-8.

1.1. Introduction

Plasmas are complex gas-phase mixtures of ions, electrons, excited state species, photons, and neutral species. The densities and energies of these plasma components can change dramatically depending on the power-pressure regime of the system.[1] Low-temperature, or cold plasmas, have been used to make and modify numerous materials. The combination of highly reactive species and low bulk temperatures make them ideal for processing polymers and semiconductors without causing thermal damage. Both fluorocarbon (FC) and chlorosilane plasmas are widely used industrially for Si-based etch processes and the deposition of thin films. This dissertation investigates FC and chlorosilane plasma processes used to etch Si, and deposit thin FC materials. A combination of gas-phase diagnostics, bulk and surface materials analysis techniques, and, most importantly, gas-surface interaction studies are used to elucidate a more complete picture of the plasma process.

1.2. Plasmas 101

The word plasma is used to describe a range of energetically and functionally diverse systems, which include lightning, the cores of stars, neon lights and the non-thermal plasmas we use in our laboratories for materials modification. Specific terminology has developed to describe and discuss these systems; the following sections are relevant to understanding this dissertation.

1.2.A. Igniting and sustaining plasmas.

1.2.A.1. Overview. Plasmas, the fourth state of matter, are created by applying energy to a gas. This leads to the ionization of some fraction of the particles, resulting in the formation of charge carriers.[1,2] The term plasma covers an energetically diverse series of systems, which can be classified based on the temperatures of the species. Complete thermodynamic equilibrium (CTE) plasmas are thus named because the electron temperatures (T_e) and gas temperatures (T_g) are equivalent. These conditions exist in stars, such as the interior of the sun, with temperatures of several keV (1keV=11.8 x 10^6 K).[1] Thermal plasmas can also reach gas temperatures of several keV; these systems contain areas of local thermodynamic equilibrium (LTE). In contrast, non-local thermodynamic equilibrium (non-LTE) plasmas have significantly different T_e and T_g values throughout the plasma. In these systems, $T_g \leq 1000$ K, whereas $T_e \sim 10^4$-10^6 K.[1] Also referred to as glow discharges or "cold" plasmas, the energies available (~1-20 eV) are high enough to break chemical bonds (<10 eV), but do not completely atomize molecular monomers.[3] The combination of highly reactive species and low bulk temperatures makes glow discharges ideal for inducing chemical reactions on a surface with minimal to no thermal degradation of the substrate. Glow discharges are generated and sustained electrically by applying direct current, radio frequency (rf), or microwave power to a gas.[1] This dissertation is based on inductively coupled rf plasmas; particulars for these systems are discussed further in the following section.

1.2.A.2. Radio frequency plasmas. Rf power sources supply frequencies in the range of those used in radio transmissions. An alternating electric field is applied across a gas, and the anode and cathode switch polarities based on the frequency of the rf field (ω). The plasma is sustained when $\omega > f_{ci}$, a critical ion frequency. Also known as the ion transition frequency, f_{ci} is defined as:

$$f_{ci} = \frac{\langle v \rangle_{di}}{2L} \qquad (1.1)$$

where $\langle v \rangle_{di}$ is the average ion drift velocity, and L is the distance between the electrodes.[1] When $\omega > f_{ci}$, the time necessary for positive ions to move between the two electrodes is greater than half the period of the electric field. Similar to f_{ci}, the critical electron frequency, f_{ce}, is defined as:

$$f_{ce} = \frac{\langle v \rangle_{de}}{2L} \qquad (1.2)$$

where $\langle v \rangle_{de}$ is the average electron drift velocity.[1] Electrons have a much smaller mass than ions; thus, electron mobility in the AC field is considerably greater and electrons gain more energy from the external electric field than ions do. This results in $T_e >> T_g$.

1.2.A.3. Sheath effects. The bulk of a cold plasma is quasi-neutral, i.e. the densities of positive and negative species are roughly equivalent. The degree of ionization, α, is defined as the ratio of ion density (n_i) to neutral density (n), and typically ranges from $10^{-6} - 10^{-3}$.[1] Although n_i is proportionally a small part of the plasma, ions are critical to numerous plasma processes because of their high energies. The higher mobility of electrons vs. ions in cold plasmas results in a greater initial electron loss to any surface in the plasma including reactor walls and substrates. This causes the formation of a plasma sheath, an electron depletion region around all surfaces within the plasma.[4] Consequently, surfaces are always at a negative potential relative to the bulk plasma, which results in the acceleration of positive ions towards surfaces. This ion bombardment is a critical component to many plasma processes. In FC plasma deposition systems, ions physically sputter the surface, participate in film deposition, and significantly affect the morphology and hardness of the resulting films.[2,5] Ions are also crucial to etch systems; controlling ion densities and energies results in more efficient and selective etch processes.[6] Because ions have such a considerable effect on materials during plasma treatment, investigating ion compositions, energies and fluxes is a necessary component of any complete analytical study of a plasma system.

1.2.B. Uses of low pressure plasmas. Low pressure plasmas have a multitude of applications, ranging from the deposition of hydrogenated amorphous silicon for solar cells, to improving adhesion between polymers, to making lighting devices.[7-9] Plasma processes involving materials can generally be categorized as etching of a material, surface modification, or thin film deposition.

Plasmas can etch a material either physically or chemically. The former is simply sputtering of the surface caused by energetic particle bombardment, whereas the latter occurs when species from the plasma react with the substrate to form volatile etch products, which subsequently desorb and are removed through the vacuum system.[10] Plasma surface modifications include crosslinking polymers and functionalizing surfaces.[11-13] Thin film deposition occurs when gas-phase species physisorb or chemisorb to a surface. Film growth can occur via several different pathways. The activation growth model (AGM) proposed by D'Agostino involves surface activation via energetic particle bombardment, followed by the reaction of radicals with active sites.[2] Alternatively, oligomerization can occur primarily in the gas-phase, followed by deposition of high molecular weight species onto the substrate.[14] Specific etch and deposition systems are discussed in the following sections.

1.3. Fluorocarbon Plasmas

FC plasmas are among the most widely studied plasma systems; over 1000 journal publications related to CF_4 plasmas alone have been published in the last decade. The dual nature of FC plasmas allows them to be used in both etch and deposition systems. Overlap between these two regimes exists such that during film formation, sputtering of the film via energetic particle bombardment often occurs.[2] Additionally, in systems used for FC etching of Si-based materials, etch rates, selectivity and anisotropy rely on the formation of thin steady state FC films.[6,10,15,16]

Over the last 2 decades, industrial etch and deposition processes have moved from using smaller FC monomers such as CF_4 to larger monomers such as C_4F_8. With increasing monomer size, both the types of gas-phase species produced and possible gas-surface interactions increase. The versatility of FC plasmas results from the formation of an array of different neutral and ionic species. F atoms promote etching of Si via the production of SiF_x etch products, whereas neutral CF_x and C_xF_y species are thought to contribute to film growth.[2,17] FC ion bombardment affects the composition and deposition rate of FC films, and control of ion bombardment is used to enhance etch processes.[16,18] Excellent correlations exist in the literature between gas-phase species and plasma treated materials that help explain etch and deposition chemistry.[19] Harder to find are studies that directly relate to gas-surface interactions under conditions that are relevant to those present in plasmas. Thus, gas-surface investigations of FC species may offer an insight not garnered by the correlations that indirectly study these processes.

1.4. Tetrachlorosilane Plasmas

Similar to FC systems, tetrachlorosilane ($SiCl_4$) plasmas can be used in both etch and deposition systems. $SiCl_4$ plasmas have been used to etch Si, metals such as Al and Ta, and III-V semiconductor materials such as GaAs.[20-22] When combined with other feed gases, $SiCl_4$-containing plasmas have been used to deposit materials such as amorphous silicon and microcrystalline silicon for thin film solar cell applications, and silicon nitride films, which function as diffusion barriers in microelectronic devices.[23-26] These studies typically focus on optimizing desirable film qualities via careful parameter control (feed gas ratios, pressure, power etc), without exploring gas-surface interactions. Although gas-phase studies have implicated $SiCl_2$ as a growth precursor in chlorinated *a*-Si:H materials, no definitive mechanisms for growth have been determined.[23] Thus, gas-surface studies of molecules such as $SiCl_2$ may offer insight into film formation in these systems.

1.5. Overview of Research

1.5.A. Approach. The complete characterization of a plasma system requires gas-phase diagnostics, materials analyses, and gas-surface interaction studies. Gas-phase diagnostics such as optical emission spectroscopy (OES), mass spectrometry (MS), and laser-induced fluorescence (LIF) are used in this work to investigate the gas-phase composition of plasmas and to identify possible reactive species. The physical and chemical properties of plasma-deposited and plasma-modified materials are also investigated using several standard analytical methods including Fourier-transform infrared (FTIR) spectroscopy, x-ray photoelectron spectroscopy (XPS), contact angle measurements, variable-angle spectroscopic ellipsometry, profilometry, scanning Auger microscopy (SAM) and scanning electron microscopy (SEM). Gas-phase data provide information about reactive species in the plasmas, and bulk and surface materials analyses yield information on the overall effects of plasma processes. However, to probe the chemistry that occurs during substrate processing, it is critical to study the plasma-surface interface. We use our Imaging of Radicals Interacting with Surfaces (IRIS) technique to study the steady-state reactivity of molecules during bombardment of the substrate by the full range of plasma species.

1.5.B. Fluorocarbon plasmas. FC plasmas have enormous utility in both deposition and etch processes; this dissertation focuses on studying deposition processes in C_3F_8 and C_4F_8 plasmas. Chapter 3 describes a film deposition study based on continuous wave (CW) and pulsed C_3F_8 and C_4F_8 plasmas. Control of film characteristics was achieved by minimizing the exposure of the growing film to energetic species.

The use of low temperature plasmas to change surface properties of polymers is expounded upon earlier in this chapter. Chapter 4 describes the use of depositing FC and acrylic acid (AA) plasmas to modify polydimethylsiloxane (PDMS) capillary electrophoresis (CE) microfluidic devices. These devices are used for separations; the basis of the separations is the electroosmotic flow (EOF) of solution through the system. The EOF depends on the overall surface charge of the capillary channel in solution. FC plasmas coated the devices with a hydrophobic, inert material, resulting in lower EOF values. The AA plasmas deposited a hydrophilic thin film in the device, resulting in highly pH dependent EOF values. This chapter demonstrates proof-of-concept that low temperature plasmas can be used to tailor the surface of PDMS microfluidic devices.

Chapters 5, 6 and 7 detail gas-phase and gas-surface interaction studies of the depositing C_3F_8 and C_4F_8 plasmas. Specifically, Chapter 5 investigates the surface interactions of CF_2 during FC plasma processing of Si, with a focus on ion effects; ion bombardment was found to enhance CF_2 surface production. Chapter 6 characterizes the ions present in the plasma molecular beams used in these studies, including the ion energy distributions (IEDs) and relative fluxes. These are the first IED data for plasma molecular beams collected for an IRIS system. For the first time, CF_2 surface production measurements are directly correlated with average ion energies in these systems. Chapter 7 describes some preliminary CF LIF measurements for these systems, as well as unsuccessful attempts to detect C_2.

Collectively, these studies have yielded correlations between the plasma-surface interface, the surface, and the gas-phase that are important for the advancement of molecular level understanding of plasma systems.

1.5.C. Tetrachlorosilane plasmas. Chapter 8 describes initial IRIS studies of $SiCl_2$ in $SiCl_4$ and $SiCl_4/H_2$ plasmas. $SiCl_2$ was present in all plasma systems presented. LIF signal intensity measurements showed that relative $SiCl_2$ densities were dependent on applied rf power (P), pressure and feedgas composition. Significant $SiCl_2$ surface production was observed during $SiCl_4$ plasma etching of Si. These data are compared to previous Fisher group work involving SiF_4 and SiF_4/H_2 plasma processing of Si. These studies show the feasibility of investigating Cl-based systems using IRIS.

References

1. Grill, A. *Cold Plasma in Materials Fabrication: From Fundamentals to Applications*; IEEE Press: New York, NY, 1994.

2. d'Agostino, R.; Cramarossa, F.; Fracassi, F. Plasma Polymerization of Fluorocarbons. In *Plasma Deposition, Treatment, and Etching of Fluorocarbons*; d'Agostino, R., Ed.; Academic Press, Inc.: San Diego, 1990; pp 95.

3. Boenig, H. V. *Fundamentals of Plasma Chemistry and Technology*; Technomic Publishing Co: Lancaster (UK), 1988.

4. Lieberman, M. A.; Lichtenberg, A. J. *Principles of Plasma Discharges and Material Processing*; Wiley and Sons: New York, 1994.

5. Fuoco, E. R.; Hanley, L. *J. Appl. Phys.* **2002**, *92*, 37.

6. Li, X.; Ling, L.; Hua, X.; Oehrlein, G. S.; Wang, Y.; Vasenkov, A. V.; Kushner, M. J. *J. Vac. Sci. Technol. A* **2004**, *22*, 500.

7. Shah, A. V.; Schade, H.; Vanecek, M.; Meier, J.; Vallat-Sauvain, E.; Wyrsch, N.; Kroll, U.; Droz, C.; Bailat, J. *Progress in Photovoltaics* **2004**, *12*, 113.

8. Shon, C. H.; Lee, J. K. *Appl. Surf. Sci.* **2002**, *192*, 258.

9. Klemberg-Sapieha, J. E.; Martinu, L.; Yamasaki, N. L. S.; Lantman, C. W. *Thin Solid Films* **2005**, *476*, 101.

10. Standaert, T. E. F. M.; Hedlund, C.; Joseph, E. A.; Oehrlein, G. S.; Dalton, T. J. *J. Vac. Sci. Technol. A* **2004**, *22*, 53.

11. Steen, M. L.; Jordan, A. C.; Fisher, E. R. *J. Membr. Sci.* **2002**, *204*, 341.

12. Steen, M. L.; Hymas, L.; Havey, E. D.; Capps, N. E.; Castner, D. G.; Fisher, E. R. *J. Membr. Sci.* **2001**, *188*, 97.

13. Egitto, F. D.; Matienzo, L. J. *IBM J. Res. Develop.* **1994**, *38*, 423.

14. Takahashi, K.; Tachibana, K. *J. Appl. Phys.* **2001**, *89*, 893.

15. Cunge, G.; Booth, J. P. *J. Appl. Phys.* **1999**, *85*, 3952.

16. Li, X.; Ling, L.; Hua, X.; Oehrlein, G. S.; Wang, Y.; Anderson, H. M. *J. Vac. Sci. Technol. A* **2003**, *21*, 1955.

17. Yasuda, H. K. *Plasma Polymerization*; Academic Press: New York, 1985.

18. Li, X.; Ling, L.; Hua, X.; Oehrlein, G. S.; Wang, Y.; Vasenkov, A.; Kushner, M. J. *J. Vac. Sci. Technol. A* **2004**, *22*, 500.

19. Nakamura, M.; Hori, M.; Goto, T.; Ito, M.; Ishii, N. *J. Vac. Sci. Technol. A* **2001**, *19*, 2134.

20. Kuo, Y. *J. Electrochem. Soc.* **1995**, *142*, 2486.

21. Rahman, M.; Deng, L. G.; van den Berg, J.; Wilkinson, C. D. W. *J. Phys. Chem. D* **2001**, *34*, 2792.

22. Hope, D. A. O.; Monnington, G. J.; Gill, S. S.; Borsing, N.; Smith, J. A.; Rees, J. A. *Vacuum* **1993**, *44*, 245.

23. Bruno, G.; Capezzuto, P.; Cicala, G.; Cramarossa, F. *J. Appl. Phys.* **1987**, *62*, 2050.

24. Lejuene, M.; Beyer, W.; Carius, R.; Muller, J.; Rech, B. *Thin Solid Films* **2004**, *450-451*, 280.

25. Bruno, G.; Capezzuto, G.; Cicala, G.; Cramarossa, F. *J. Appl. Phys.* **1987**, *62*, 2050.

26. Klaus, J. W.; Ott, A. W.; Dillon, A. C.; George, S. M. *Surf. Sci.* **1998**, *418*, L14.

CHAPTER 2

EXPERIMENTAL METHODS

This dissertation chapter is divided into five sections which describe the experimental methods used to collect the data discussed in this work. Section 2.1 describes the plasma reactor used to deposit thin films and modify materials. The materials characterization techniques used to analyze these plasma deposited and modified materials are described in section 2.2. Section 2.3 describes methods used to fabricate and analyze plasma modified polydimethylsiloxane (PDMS) microchip capillary electrophoresis (CE) devices. Section 2.4 involves gas-phase analytical techniques used to both identify excited state species and ions, and to measure ion energy distributions in the plasmas. Lastly, Section 2.5 describes the IRIS technique, the heart of this work.

2.1. Plasma Reactor

All of the plasma generated materials in Chapters 3 and 4 were produced in our home-built, inductively coupled rf plasma reactor, Figure. 2.1. The reactor consists of two cylindrical Pyrex tubes held together by a 50 mm o-ring joint and a Thomas pinch clamp. Glass sleeves were used to minimize material deposition and plasma damage to the reactor walls. An 8.5 turn, 10 gauge nickel-plated copper coil was used to couple rf power to the chamber, and was tuned with a Jennings 100 pF variable capacitor. Power was supplied to the inductor coil by an 13.56 MHz Advanced Energy RFPP 5S power supply, which has a power range of 0-500 W and pulsing capabilities. Gases were introduced to the chamber through a 0.75 inch port located directly in front of the inductor coil. Gas products were removed from the system through a liquid N_2 cold trap by an Alcatel 2012A mechanical pump with a pumping speed of 4.2 L/sec. The pressure in the chamber was monitored with an MKS Baratron capacitance manometer which is insensitive to differing gas compositions. All samples treated in the plasmas were oriented parallel to the gas flow, and removed from the chamber for analysis.

2.1.A. Fluorocarbon material deposition. Films deposited from C_3F_8 and C_4F_8 plasmas in the plasma reactor described above are discussed in Chapters 3 and 4. For materials discussed in Chapter 3, the applied rf power (*P*) for continuous wave (CW) depositions varied from 5 to 150 W, and the applied peak power was kept constant at 300 W for pulsed experiments.

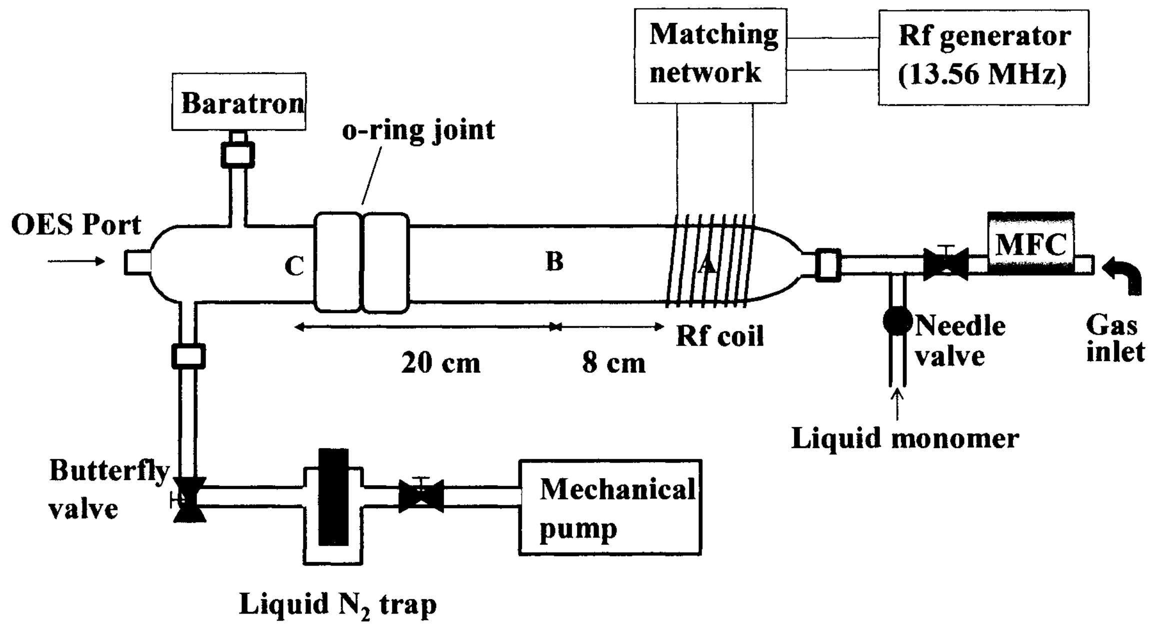

Figure 2.1 Schematic diagram of the inductively coupled plasma reactor used for thin film deposition. Optical emission spectra were collected through the quartz window located at the downstream end of the reactor.

Pulsed plasmas are defined by their duty cycle (d.c.):

$$\text{d.c. (\%)} = [\text{pulse on time/total cycle time}] * 100 \qquad (2.1)$$

A 10 ms on-time was used in all pulsed plasma experiments. The equivalent CW power of pulsed systems, P_{eq}, was calculated using:

$$P_{eq} = \text{d.c.} * \text{peak power} \qquad (2.2)$$

thus, a plasma with a 5% d.c. and an applied peak power of 300 W corresponds to a 15 W CW plasma.

Reactant gases C_3F_8 (Air Products, 99%) and C_4F_8 (Matheson, 99.99%) were used without further purification. For all experiments, the gas flow was kept constant at 10 sccm (standard cubic centimeters per minute), resulting in a pressure of ~220 mTorr for the C_3F_8 system and ~210 mTorr for the C_4F_8 system. For depositions discussed in Chapter 3, a freshly pressed FTIR grade KBr (Aldrich) pellet and a silicon wafer (p-type, 100) were used as substrates. These were placed on glass microscope slides oriented parallel to the gas flow within the coil region (position A) as well as at 8 and 28 cm downstream from the coil (positions B and C, respectively). These positions were chosen for direct comparison to previous work.[1] A Cu wire (diameter = 0.25 mm) was placed perpendicular to the flow of the gas during some depositions. The wires were twisted into a loop after film deposition to investigate the flexibility of the deposited material. Deposition times ranged from 30 sec to 150 min, and substrates were removed from the chamber for analysis. For FC plasma treatments discussed in Chapter 4, C_3F_8 gas flow was kept constant at 10 sccm (pressure ~220 mTorr), with $P = 50$ W, samples were located at position B, and the deposition time was 4 min.

2.1.B. Plasma polymerized acrylic acid deposition. AA (Aldrich, 99%), a liquid monomer, was placed in a 50 mL Pyrex glass sidearm vacuum flask with a Teflon stopcock. It was subjected to multiple freeze-pump-thaw cycles to remove dissolved gases prior to use. A Nupro bellows-sealed valve was used to control AA vapor entry into the reactor, resulting in a pressure of ~ 150 mTorr. These depositions employed a pulsed plasma with a 16% d.c., a 10 ms on-time, an applied peak power of 150 W, and a 5 min deposition time.

2.1.C. Ar plasma treatments of PDMS. Prior to film deposition, some of the PDMS samples discussed in Chapter 4 were subjected to a 10 min Ar (General Air, 99.985%) plasma pretreatment wherein gas flow and P were kept constant at 10 sccm (pressure ~ 300 mTorr) and 30 W respectively. After this pretreatment, the reactor was evacuated, and the film deposition step was performed immediately.

2.1.D. Tetrachlorosilane based plasma treatments. $SiCl_4$-based plasmas were used for both Si etching and the deposition of a-Si materials, Chapter 6. $SiCl_4$ (Sigma-Aldrich technical grade, >99%), a liquid monomer, was placed in a 50 mL Pyrex glass sidearm vacuum flask with a Teflon stopcock and subjected to multiple freeze-pump-thaw cycles to remove dissolved gases prior to use. Note that $SiCl_4$ is highly corrosive and reacts violently with H_2O.[2] For safety purposes, and to prevent degradation from reactions with water vapor, the

$SiCl_4$ was stored in a glove-box under a N_2 atmosphere, and all transfers from the source to the vacuum flask were performed in the glove-box.

Control of $SiCl_4$ vapor entry into the reactor was achieved via a Nupro bellows-sealed valve, resulting in pressure increments ranging from 20-100 mTorr. For $SiCl_4/H_2$ plasmas, a steady $SiCl_4$ pressure was established, and H_2 (General Air, 99.9%) was admitted into the plasma chamber through an MKS mass flow controller such that the total pressure in the reactor was 100 mTorr. The CW *P* ranged from 10-160 W, and Si substrates were placed 8 cm downstream from the coil. Plasma exposure time ranges from 10 to 60 min.

2.2. Materials Characterization Techniques

2.2.A. Fourier transform infrared spectroscopy. A Nicolet Magna 760 FTIR spectrometer (resolution of 8 cm^{-1} and averaging 128 scans) was used to obtain transmission FTIR spectra for films deposited on KBr substrates. Spectra shown are corrected for residual carbon dioxide peaks (absorbance bands at ~2340 and 2360 cm^{-1}), and for sloping baselines.

2.2.B. X-Ray photoelectron spectroscopy. XPS analyses were performed on a Physical Electronics PE5800 ESCA/AES system. Spectra were collected using either a 2 mm or a 7 mm monochromatic Al K_α X-ray source (1486.6 eV), hemispherical analyzer, and multichannel detector. A low energy (~1 eV) electron neutralizer was used for charge neutralization. Survey spectra were collected using a pass energy of 93.90 eV. High resolution spectra were acquired at an analyzer pass energy of 11.75 or 23.50 eV. Unless otherwise specified, curve fitting was performed using Gaussian functions with the FWHM (full widths at half maximum) ≤ 2 eV, which is expected for plasma polymers.[3] A photoelectron take-off angle of 45° was used for all spectra, which corresponds to a sampling depth of ~45 Å. The take-off angle is defined as the angle between the surface and the axis of the analyzer lens system.

2.2.B.1. Fluorocarbon materials. The binding energy (BE) scales for the samples were referenced by setting the CF_2 peak maxima in the C_{1s} spectra to 292.1 eV. High resolution C_{1s} and F_{1s} spectra were used to calculate the F/C ratio of the materials; high resolution C_{1s} spectra were deconvoluted to analyze the C bonding environments in the films. Specifically, CF_3 (294.0 eV) and CF_2 (292.1 eV) groups function as chain termination and chain elongation groups, respectively, whereas -$\underline{C}$F-CF (289.5 eV), -$\underline{C}$F-C (288.2 eV), $\underline{C}$-CF_x (287.3 eV) and C-C/C-H (285.0 eV) species contribute to crosslinking and branching in the film.[1,4] The -$\underline{C}$F-CF and -$\underline{C}$F-C peaks are fit as one curve in all the C_{1s} high resolution spectra shown and are referred to simply as -CF. As expected, the Gaussian line width for this peak is broader (2-3 eV) than that used for the other C_{1s} moieties. For FC materials, percent crosslinking is defined as the sum of the crosslinking species (%CF + %C-CF_x + %C-H).[4] Data reported in Chapter 3 are for samples over 65 Å thick. Elemental analysis of films thinner than 65 Å showed atomic concentrations of up to 16% Si and ~16% O, indicating that the underlying Si substrate was included in the analysis.

2.2.C. Scanning Auger microscopy. Scanning Auger microscopy (SAM) was carried out using the PE 5800 with the analyzer in the fixed retarding ratio mode. The Auger images were obtained using an accelerating potential of 10 kV. The electron beam had a current of 10 nA, operating in a vacuum better than 10^{-9} Torr. Images shown in Chapter 4 are 32 x 32 pixels.

2.2.D. Scanning electron microscopy. A JEOL, JSM-6500F field emission scanning electron microscope was used to investigate the morphology and flexibility of deposited materials in Chapter 3. A 3.0 or 4.7 kV accelerating voltage was used to obtain the images. All samples were sputtered with 5 nm of gold prior to analysis.

2.2.E. Contact angle measurements. The hydrophobicity or hydrophilicity of plasma treated materials was evaluated using static contact angles measured by the sessile drop method with a contact angle goniometer (Krüss DSA 10) by applying ~ 1 μL drops of room temperature deionized water to the surface. Reported contact angles are the mean of two to five measurements on each of two to three samples for each experimental condition. The water drop profiles were fit using the tangent method.

2.2.F. Variable angle spectroscopic ellipsometry. Film thicknesses were measured using variable angle spectroscopic ellipsometry (J.A. Woolam Company Inc., model HS 190). Spectra from 300 to 1500 nm in 20 nm increments were collected at 75° and 85° for three locations per sample. Experimental data were modeled using a Cauchy model for non-absorbing low k dielectric materials. Deposition rates were calculated by dividing the film thickness by the total deposition time for both CW and pulsed plasmas.

2.3. Microfluidic Device Characterization

2.3.A. Fabrication of PDMS devices. PDMS devices were fabricated using a replica molding method.[5] Briefly, for molding device construction, SU-8 2035 negative photoresist was spin-coated onto a 4 in silicon wafer that was cleaned and oxidized with piranha solution (2:1 H_2SO_4:H_2O_2) for 10 min. The wafer was then baked at 65 °C for 2 min and 95 °C for 5 min to evaporate the solvent. A mask containing the channel pattern was placed over the coated wafer, and exposed to a near-UV light source for 5 min. This was followed by a 5 min post bake at 95 °C to cross-link the exposed portions of the film to the wafer.

Developing and hard baking of the exposed SU-8 patterns were followed by pouring a degassed mixture of Sylgard 184 (Dow Corning) silicone elastomer and its curing agent (10:1 ratio) onto the mold. After 2 h of curing at 65 °C, the PDMS replica was removed from the mold to yield a pattern of negative relief channels and reservoirs in the PDMS. Buffer reservoirs were opened with a circular punch. The bottom layers (blanks) of the PDMS chips were formed by casting the PDMS mixture on a clean, dry silicon wafer. Irreversible sealing was accomplished by rinsing two PDMS replicas with methanol and drying them separately in an oven at 65 °C. The two pieces were then air plasma treated for 30 sec in a Harrick plasma cleaner/sterilizer (PDC-32 G), and immediately brought into conformal contact, resulting in irreversible sealing of the device. Alternatively, reversible sealing was achieved by rinsing the pieces with methanol and bringing them into conformal contact, followed by drying at 65 °C for 10 min. Unless otherwise specified, chips were irreversibly sealed. In all cases, a simple straight channel design was used. The channel was 4.5 cm long, 150 μm wide and 50 μm deep.

2.3.B. Dye absorption measurements. Dye absorption experiments were performed using an inverted fluorescence microscope (Nikon Eclipse TE2000-4) with a Photometrics Cool Snap *cf* camera to image and measure the intensity of fluorescence from a buffer (10 mM borate, pH 10) containing rhodamine 6G fluorescent dye (Lambda Physik, Ft. Lauderdale, FL). The channel was filled with the rhodamine solution and images were collected at regular time intervals. The extent of the dye absorption into the PDMS channel walls was monitored by the change in the width of fluorescence signal across the channel with time. The chips were stored in a light proof box in a dark room between measurements to avoid quenching the fluorescent dye.

2.3.C. EOF measurements. EOF was measured using the current monitoring method as reported previously.[6-8] The running buffer for electrophoresis experiments was pH 4-9 phosphate buffer. All buffers were prepared in deionized water, passed through a 0.20 μm pore size syringe filter (Whatman) and degassed for 5 min in a sonicator (Fisher Scientific, FS 20) before use. Electrical connections to the microfluidic devices were made with platinum electrodes placed into reservoirs at the ends of each channel. The current monitoring experiments were performed by measuring the voltage drop across a 1 kΩ resistor (0.5 W, RadioShack) using a voltmeter (RadioShack) and a high voltage power supply (Spellman CZE1000R). For a typical current monitoring measurement, the first reservoir and the channel were filled with 20 mM buffer and the second reservoir was filled with 18 mM buffer. When the voltage (900 V) was applied and electroosmosis occured, the lower concentration buffer from the second reservoir gradually displaced the higher concentration buffer in the channel, resulting in an increase in the electrical resistance of the channel. The change in current under a constant applied voltage difference was monitored using a 1 kΩ resistor in series between the cathode and ground. After a constant voltage was obtained, the potential was applied to the reservoir with concentrated buffer and the above procedure was repeated. The time required to reach a current plateau was used to calculate EOF based on Equation 2.3, where L is the length of the separation channel (4.5 cm), V is the total applied voltage (900 V), and t is the time in seconds required to reach the new current plateau.

$$\mu_{EOF} = L^2/Vt \qquad (2.3)$$

2.4. Gas Phase Analytical Techniques

2.4.A. Optical emission spectroscopy. Optical emission spectra (OES) from 240-906 nm were obtained using the inductively coupled plasma reactor shown in Figure 2.1. Emitted light was collected through the quartz window situated ~ 15 cm downstream of the coil region, resulting in coaxial sampling of the plasma emission. Signal was imaged onto a 10 μm entrance slit of an Ocean Optics S2000 spectrograph using an optical fiber. The spectrograph was equipped with five 1800 grooves/mm holographic gratings and five 2048-element linear CCD-arrays.

2.4.B. Mass spectrometry. Two mass spectrometers (MS) were used to analyze plasma ions. For both instruments, the MS was coupled to the IRIS apparatus, so that the detector was directly in line with the plasma molecular beam. This allowed sampling of species at the position of the interaction region. Data presented in Chapter 5 were collected using a Dycor LC200S quadrupole MS. Plasma-ion mass spectra (PI-MS) refers to data collected when the MS ionizer was disabled to identify nascent ions in C_3F_8 and C_4F_8 plasma systems, as well as to determine the extent of their removal when a grounded mesh (g.m.) was placed in the path of the molecular beam. The data presented in Chapter 6 were collected using a Hiden PSM003 mass spectrometer with energy analysis capabilities. Experimental details for the Hiden MS are presented in Section 6.2.

2.5. Plasma Surface Interaction Studies

The IRIS method has been described in detail previously;[9] a schematic of the apparatus is shown in Figure. 2.2. Briefly, IRIS uses molecular beam techniques and laser induced fluorescence (LIF) to measure the steady state surface reactivity of gas-phase species during plasma processing of a surface, as well as the relative gas phase densities of the species as a function of different plasma parameters such as P and pressure. In a typical IRIS experiment, the feed gas or vapor enters the rear of a glass reactor tube similar to that shown in Figure 2.1. 13.56 MHz rf power is applied to an inductor coil and a plasma is produced. Expansion of the plasma into a differentially pumped vacuum chamber, and ultimately into a high-vacuum region, generates an effusive molecular beam

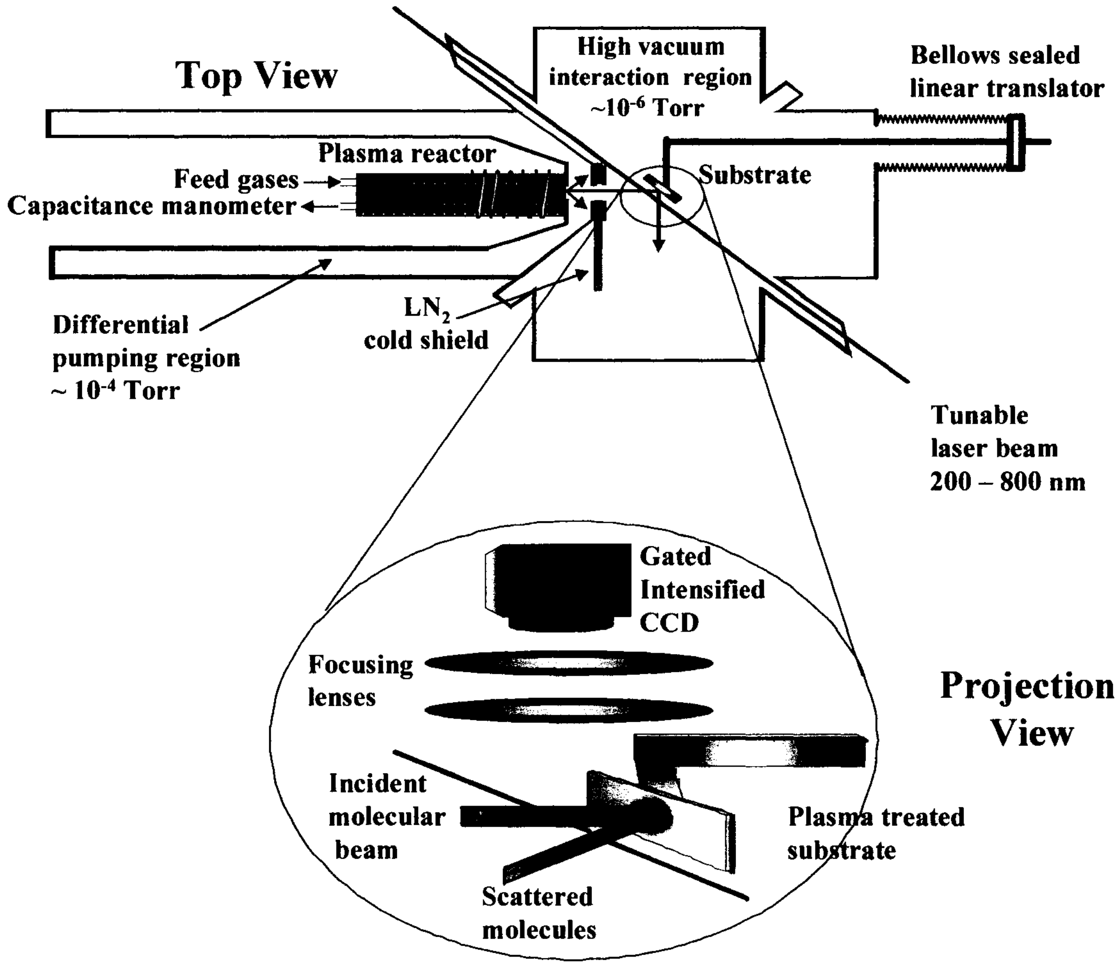

Figure 2.2 Schematic diagram of the IRIS apparatus. The ICCD is located directly above the interaction region. For measurements made under ion-limited conditions, a grounded mesh was placed on the main chamber side slit mounted to the liquid N_2 cold shield.

consisting of virtually all species present in the plasma, including the species of interest. An excimer-pumped (XeCl, 150 mJ/pulse, 308 nm) tunable dye laser beam intersects the molecular beam downstream from the plasma source and excites the species of interest. Spatially resolved LIF signals are collected by an electronically gated, intensified charge coupled device (ICCD) located perpendicular to both the molecular beam and the laser beam, directly above the interaction region. For density measurements, this is repeated as plasma parameters such as the source gas or *P* are changed. For reactivity measurements, a substrate is rotated directly into the path of the molecular beam and LIF signals are again collected. Differences between the spatial distributions with the surface in and out of the path of the molecular beam are used to measure radical-surface reactivity.

Spatially resolved LIF data are interpreted using a quantitative model of the experiment which reproduces the scattering data in one dimension. A detailed description of the simulation is given elsewhere.[10] Briefly, the simulation is based on the known geometry of the experiment and calculates the spatial distribution of the radical number density in the molecular beam at the interaction region as well as the radical number density along the laser beam for molecules scattering from the substrate surface. To adequately describe the spatial distribution of molecules from a surface, a specific scattering mechanism is assumed, either specular or adsorption-desorption scattering. In the present work, the distribution of the scattered molecules is consistent with adsorption-desorption scattering; the scatter profiles have the increased peak width and shift in peak-maximum position that is

1.3 mJ/pulse). For CF_2 density and reactivity measurements, the laser was tuned to 234.323 nm, corresponding to the (0,11,0)$\leftarrow$ (0,0,0) vibronic band of the $A^1B_1 \leftarrow X^1A_1$ transition. LIF was directly imaged onto one of two ICCD cameras, as a newer model was integrated into the system midway through data collection for this project. The first camera has a 586 x 384 pixel display and imaged a 55 x 35 mm area. The second camera has a 512 x 512 pixel display, which imaged a 51.2 x 51.2 mm area. Pixels were binned (4 x 4) to increase the signal-to-noise ratio and reduce processing time. With both ICCD cameras, a 100 ns gate width was used for the CF_2 radical (radiative lifetime of 61 ± 3 ns).[11] LIF signals were collected for 7-20 accumulations of 1000-10,000 counts/accumulation with multiple sets taken for each experiment. Background images were acquired with the laser tuned to an off-resonance wavelength (λ = 235.000 nm) and subtracted from the corresponding on-resonance image. A 1-D cross-section of each image was made by averaging a column 20 pixels wide (8.0 mm) containing the LIF signal and plotting signal intensity as a function of distance along the laser beam path. The laser was operated in the power-saturated regime (E > 0.6 mJ/pulse), so no corrections were made for laser fluctuations.

For CF measurements, a single slit (1.4-1.8 mm) was used to collimate the molecular beam. Tunable laser light in the 223.500 – 224.200 nm range was produced by frequency doubling the output of an excimer-pumped dye laser (coumarin 120, 0.2-1.5 mJ/pulse). For CF density measurements, the doubled light was produced at 223.837 nm, which corresponds to the P_{11} bandhead of the $A^2\Sigma^+$-$X^2\Pi$ (1,0) transition. CF rotational temperatures (Θ_R) calculations were expected for molecules desorbing with a cosine angular distribution. The calculated curve for adsorption-desorption scattering assumes that all incident radicals leave the surface with a cosine distribution about the surface normal. To determine surface reactivity of a specific molecule, the fraction of radicals scattering from the surface, *S*, relative to those in the molecular beam is adjusted to best fit the experimental data. For the molecules discussed in this work, surface production dominates so results are presented in terms of *S*. Ion effects were studied by placing a g.m. in the path of the molecular beam to remove charged species.

2.5.A. CF and CF_2 in fluorocarbon plasmas. For FC plasma/IRIS experiments, the source of the molecular beam was either a 100% C_3F_8 (Air Products, 99%) or a 100% C_4F_8 (Matheson, 99.99%) plasma. Unless otherwise specified, the gas flow was kept constant at 10 sccm, which yielded a total pressure in the source of ~45 mTorr as measured by a capacitance manometer.

For CF_2 experiments, the molecular beam was collimated by two slits, one 1.00-1.10 mm wide, and the other 1.25-1.45 mm wide. The first slit was mounted on a liquid nitrogen cooled shield, which was maintained at -160°C during data collection; the second slit further collimated the molecular beam. Substrates used were 25 x 40 mm *p*-type silicon (100) wafers with ~20 Å of native oxide. The substrate was mounted with the polished side facing the plasma molecular beam and positioned 3.0-6.0 mm away from the laser.

Tunable laser light in the 230.000-238.000 nm range was produced by frequency doubling the output of an excimer pumped dye laser (coumarin 47, 0.5-

based on a comparison of the relative height of the neighboring P_{12} (J=17.5) and P_{12} (J=1.5) lines at 224.149 and 224.155 nm respectively. LIF excitation spectra were collected from 224.140 to 224.160 nm in 0.001 nm increments, and Θ_R was then determined through comparison to simulations of CF rotational lines created using LIFBASE.[12] A partially saturated LIF regime was used for the Θ_R simulations, based on saturation curves collected for CF.

2.5.B. $SiCl_2$ in $SiCl_4$ and $SiCl_4/H_2$ plasmas. In this work, the source of the molecular beam consists of either 100% $SiCl_4$ (Sigma Aldrich technical grade, $\geq$ 99%), or a mixture of $SiCl_4$ and H_2 (General Air, 99.9%). The plasma beam sources were created using the plasma parameters described in Section 2.1.D. The molecular beam was collimated by two slits, 1.00-1.60 mm wide, which were mounted on a liquid N_2 cold shield maintained at -160 °C during data collection.

Substrates used were 25 x 40 mm *p*-type silicon (100) wafers with ~20 Å of native oxide. The substrate was mounted with the polished side facing the plasma molecular beam and positioned 3.0-6.0 mm away from the laser. Tunable laser light in the 315.000-323.000 nm range was produced by frequency doubling the output of an excimer pumped dye laser (sulforhodamine 640, 0.2-0.3 mJ/pulse). For the excitation spectrum, data points were collected in 0.010 nm increments over the above wavelength range. For $SiCl_2$ density and reactivity measurements, the laser was tuned to 320.340 nm, corresponding to the 2^8_0 vibronic band of the $A^1B_1 \leftarrow X^1A_1$ transition.[13] LIF was directly imaged onto the ICCD camera with the 512 x 512 pixel display. Pixels were binned (4 x 4) to increase the signal-to-noise ratio and reduce processing time. LIF signals were collected for 1-10 accumulations of 40-400 counts/accumulation, with multiple sets taken for each experiment. Background images were collected with the laser off and subtracted from the corresponding on-resonance image. The ICCD camera had a 1000 ns gate width for $SiCl_2$ radical.

References

1. Butoi, C. I.; Mackie, N. M.; Gamble, L. J.; Castner, D. G.; Barnd, J.; Miller, A. M.; Fisher, E. R. *Chem. Mater.* **2000**, *12*, 2014.

2. Kapias, T.; Griffiths, R. F.; Stefanidis, C. *J. Hazard. Mater.* **2001**, *A81*, 209.

3. Sandrin, L.; Silverstein, M. S.; Sacher, E. *Polymer* **2001**, *42*, 3761.

4. Luginbuhl, R.; Garrison, M. D.; Overney, R. M.; Weiss, L.; Schieferdecker, H.; Hild, S.; Ratner, B. D. Chemical and Contact Mechanical Characterization of Thin Plasma-Deposited Hexafluoropropylene Films. In *Fluorinated Surfaces, Coatings, and Films*; Castner, D. G., Grainger, D. W., Eds., 2001.

5. Garcia, C. D.; Henry, C. S. *Anal. Chem.* **2003**, *75*, 4778.

6. Liu, Y.; Fanguy, J. C.; Bledsoe, J. M.; Henry, C. S. *Anal. Chem.* **2000**, *72*, 5939.

7. Pittman, J. L.; Henry, C. S.; Gilman, S. D. *Anal. Chem.* **2003**, *75*, 361.

8. Huang, X.; Gordon, M. J.; Zare, R. N. *Anal. Chem.* **1988**, *60*, 1837.

9. McCurdy, P. R.; Bogart, K. H. A.; Dalleska, N. F.; Fisher, E. R. *Rev. Sci. Instrum.* **1997**, *68*, 1684.

10. Bogart, K. H. A.; Cushing, J. P.; Fisher, E. R. *J. Phys. Chem. B* **1997**, *101*, 10016.

11. King, D. S.; Schenck, P. K.; Stephenson, J. C. *J. Molec. Spectrosc.* **1979**, *78*, 1.

12. *LIFBASE: Database and Spectral Simulation Program (Version 1.5)*; Luque, J.; Crosley, D. R., Eds.; SRI International Report MP 99-009, 1999.

13. Suzuki, C.; Kadota, K. *Appl. Phys. Lett.* **1995**, *67*, 2569.

CHAPTER 3

COMPARISON OF PULSED AND DOWNSTREAM DEPOSITION OF FLUOROCARBON MATERIALS FROM C_3F_8 AND *c*-C_4F_8 PLASMAS

Reprinted with permission from: I. T. Martin, G. Sh. Malkov, C. I. Butoi, and E. R. Fisher, Journal of Vacuum Science and Technology A **22 (2)**, 227 (2004).

This dissertation chapter contains results from a paper published in the *Journal of Vacuum Science and Technology A*. The manuscript was written by Ina T. Martin and edited by Ellen R. Fisher. This chapter describes the effects of pulsing plasmas and downstream depositions on fluorocarbon film compositions.

3.1. Introduction

Fluorocarbon (FC) plasmas are widely employed both in etch processes, and in the deposition of pinhole free, conformal thin films with useful properties such as low surface energies and low dielectric constants.[1] Recent studies have shown that C_3F_8/O_2 and C_4F_8/O_2 chamber cleans are more efficient, environmentally friendly, and cost effective than the previously used C_2F_6/O_2 processes.[2] C_3F_8/O_2 plasmas are also used in resist patterning that takes advantage of the selective etching of SiO_2 and Si_3N_4 over Si.[3-5] Inductively coupled high density C_4F_8 plasmas and C_4F_8/CO magnetron plasmas have been applied to the selective etching of SiO_2 over Si_3N_4, a critical step in the creation of contact holes as part of ultra-large-scale integrated circuit fabrication.[6-8]

In addition to etch processes, plasmas are used for the deposition of FC thin films that have numerous applications in the microelectronics and biomedical industries. Low dielectric constants (< 3.0) make these films potentially suitable as interlayer dielectrics in integrated circuit manufacturing,[9,10] and FC coatings on membranes have been employed to reduce methanol permeability in methanol fuel cell studies.[11] Plasma deposited FC films have unique protein retention capabilities and are of interest in the formation of thromboresistant coatings.[12] For example, films with high F/C ratios and high CF_2 and CF_3 content are considered potential substrates for biomolecule immobilization in surface linked assays.[12,13] Film properties depend on film composition and structure; control over these characteristics can be obtained through manipulation of plasma parameters such as the choice of feed gas, input power, input gas flow, reactor geometry, and whether the plasma is pulsed or continuous wave (CW).[1,12,14-17]

The goal of the work presented in this chapter is to examine and compare the structures of films deposited from C_3F_8 and C_4F_8 plasmas in both CW and pulsed systems, with the intent of optimizing the systems to produce high CF_2 and CF_3 content films. To this end, plasma parameters were chosen that minimize the exposure of the developing film to ions and other high energy species.[14,15,18] Pulsed plasmas and downstream depositions are common techniques for controlling film composition. In pulsed plasmas, the concentrations of high energy species decay during the plasma off-time, leading to a reduction in high energy ion bombardment and UV flux to the surface. Because of this, pulsed FC systems yield materials with greater monomer retention, higher F/C ratios and less crosslinking than their CW counterparts.[16,17,19] In CW plasmas, constant exposure to ions typically leads to deposition of more brittle materials. Additionally, radicals in CW plasmas are typically generated faster than they are consumed, so the concentration of trapped radicals within the film can become significant, increasing the probability of post-deposition atmospheric reactions.[15]

Use of downstream plasmas creates similar effects as with pulsed plasmas; substrates downstream from the plasma glow are exposed to long-lived precursors and energetic species, but not to ion bombardment.[20] In both pulsed and CW systems, this decreases crosslinking and slows deposition rates. Additionally, the concentration of trapped radicals in the film is significantly reduced. Both pulsed plasmas and downstream depositions can be effective in controlling film composition; this work has examined both experimental methods to determine which parameter has the greatest effect on the deposition of FC materials.

Previous work in our laboratories resulted in production of a wide variety of FC films, including the deposition of low dielectric constant, amorphous FC materials from pulsed C_2F_6/H_2 plasmas,[15] and highly ordered CF_2-rich films from downstream CW and pulsed hexafluoropropylene oxide (HFPO) plasmas.[14] The present work continues these studies by using C_3F_8 and C_4F_8 plasmas to produce FC materials. These monomers were chosen because, respectively, they are potentially good sources of CF_3 and CF_2. Although the deposition of materials from these plasmas has been a topic of interest in current literature,[9,21,22] they have not been compared directly and they have not been studied using pulsed plasmas.

3.2. Results

3.2.A. FTIR spectroscopy. The bulk composition of plasma-deposited films was analyzed using FTIR spectroscopy. The effects of source gas, *P* for CW plasmas, d.c. for pulsed plasmas, and the distance of the substrate from the plasma glow were examined. Figure 3.1 shows FTIR spectra of materials deposited on KBr pellets within the coil (position A), at 8 cm downstream (position B) and 28 cm downstream (position C) in CW and pulsed C_3F_8 plasmas. FC films are produced in both CW and pulsed plasmas at all three positions, with the exception of the 15 W CW system at position A. For the latter conditions, the most prominent spectral feature is the Si-F stretching mode (738 cm^{-1}). This is attributed to etching of the glass reactor followed by redeposition of the etched materials.[15] The spectra of materials deposited at position A in the CW systems do not change as a function of *P* (15-150 W), indicating that all CW C_3F_8 plasmas studied are dominated by etching within the coil region. Similar results were

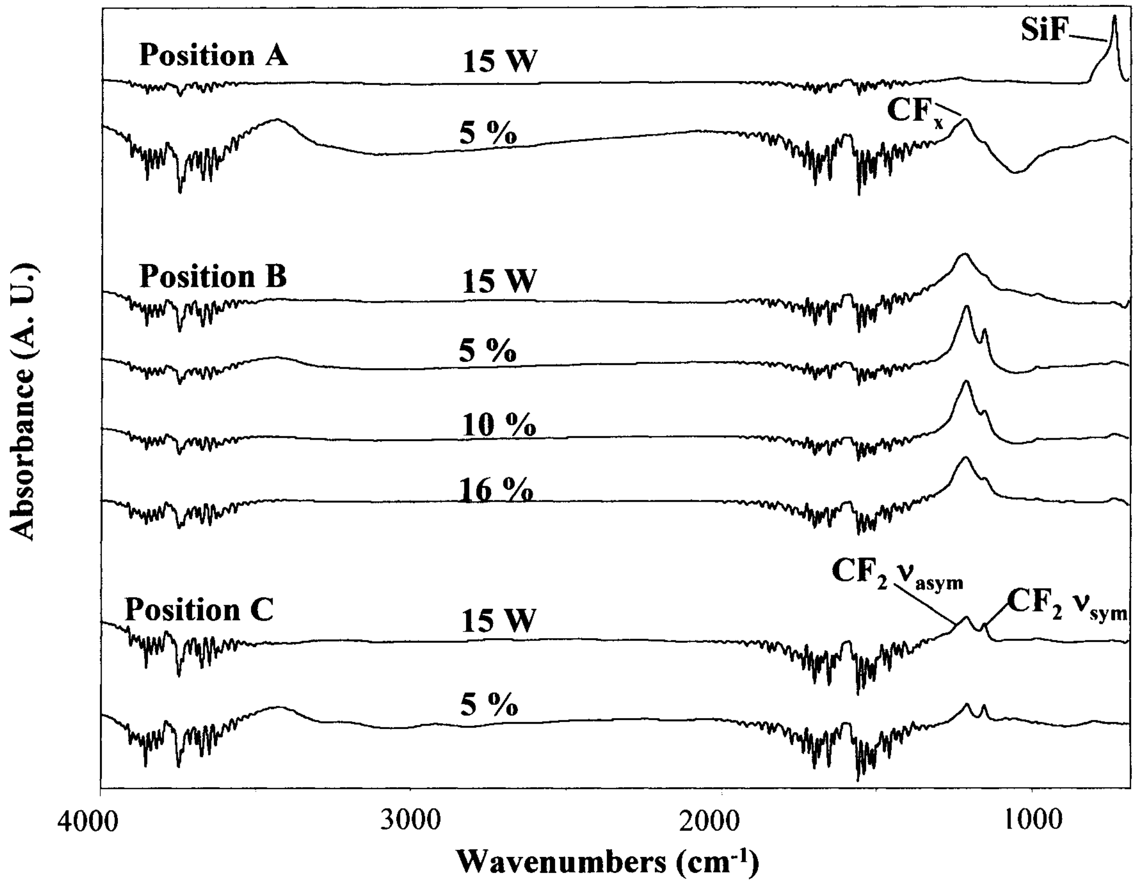

Figure 3.1 FTIR transmission spectra of materials deposited in C_3F_8 plasmas at positions A, B, and C (see Figure 2.1 for details on these designations) with a CW input power of 15 W, or a pulse sequence of 10/190 ms (5% d.c., positions A-C), 10/90 ms (10% d.c., position B), and 10/52 ms (16% d.c., position B).

obtained by Leezenberg et al. using C_3F_8 as a source gas in a parallel plate rf plasma at 840 W and 17 kHz.[21]

In contrast, the spectra of materials deposited in the coil from pulsed plasmas contain features consistent with amorphous crosslinked FC films, specifically the broad CF_x (x=1-3) stretching modes between 1100-1400 cm^{-1}.[1] This is shown in Figure 3.1 for the 5% d.c. (15 W equivalent power) system. As the substrate position moves downstream from the plasma coil region, the spectra of the deposited films change considerably. The spectrum for material deposited in a 15 W CW plasma displays the same broad amorphous CF_x absorption band at 1100-1400 cm^{-1}. The spectrum of material deposited at position B in a 5% d.c. pulsed plasma, however, has two distinct absorption bands at 1160 and 1220 cm^{-1} which are assigned to the CF_2 symmetric and asymmetric stretching modes, respectively.[1] The separation of these two bands is indicative of a more ordered, less amorphous material.[14] This establishes that materials deposited at position B in pulsed plasmas are less amorphous than those deposited in CW plasmas at equivalent input powers. At the farthest position downstream, position C, the spectra of materials deposited in pulsed and CW plasmas are very similar to each other, with distinct separation between the CF_2 stretching modes. This indicates that increasing the distance of the substrate from the coil also leads to a decrease in the amount of crosslinking in the bulk material.

The effect of increasing the d.c. of pulsed plasmas on film composition is also shown in Figure 3.1. At position B, increasing the d.c. leads to a loss of resolution between the CF_2 symmetric and asymmetric stretching modes, which indicates the deposition of a more crosslinked material. The same effect is observed in CW plasmas with increasing P at position B (spectra not shown). For both CW and pulsed plasmas, increasing P or d.c. does not noticeably change the spectra of materials deposited at position C, except at the highest powers, $P \geq 100$ W. Under these conditions, there is a decrease in the resolution of the CF_2 symmetric and asymmetric stretching modes.

Figure 3.2 shows the FTIR spectra of materials deposited at positions A, B, and C in CW and pulsed C_4F_8 plasmas. Many of the general trends observed in the C_3F_8 systems are repeated in the C_4F_8 systems. There are, however, some notable differences. First, there is clearly FC film deposition occurring at position A in the CW systems. Also, the film deposited at position A in the 5% d.c. pulsed plasma is more ordered than its counterpart in the C_3F_8 plasma, as evidenced by the more resolved CF_2 stretching bands. Second, there is indication of unsaturation in films deposited at position B. This is demonstrated in Figure 3.2 by the cluster of absorption peaks between 1630 and 1800 cm^{-1} in the spectra of materials deposited from CW and pulsed plasmas at position B. The small absorption band at 1633 cm^{-1} corresponds to C=C stretching; $C{=}CF_2$ groups appear between 1735-1755 cm^{-1}, and $-CF{=}CF_2$ stretching occurs between 1780-1800 cm^{-1}.[16,23] These peaks become more prominent when P or d.c. is increased. Note that the spectra of materials deposited at positions A and C did not change noticeably as a function of P (5-50 W) or d.c. (5-16%). The predominant trend seen in both pulsed and CW systems is that increasing the distance of the substrate from the plasma glow results in an increase in the resolution of the CF_2 ν_{sym} and ν_{asym} modes. A direct comparison of the spectra of materials deposited in a 15 W CW plasma, and a pulsed plasma with a 5% d.c. (15 W equivalent power) shows that materials deposited in pulsed plasmas are less crosslinked and have fewer unsaturated species than those

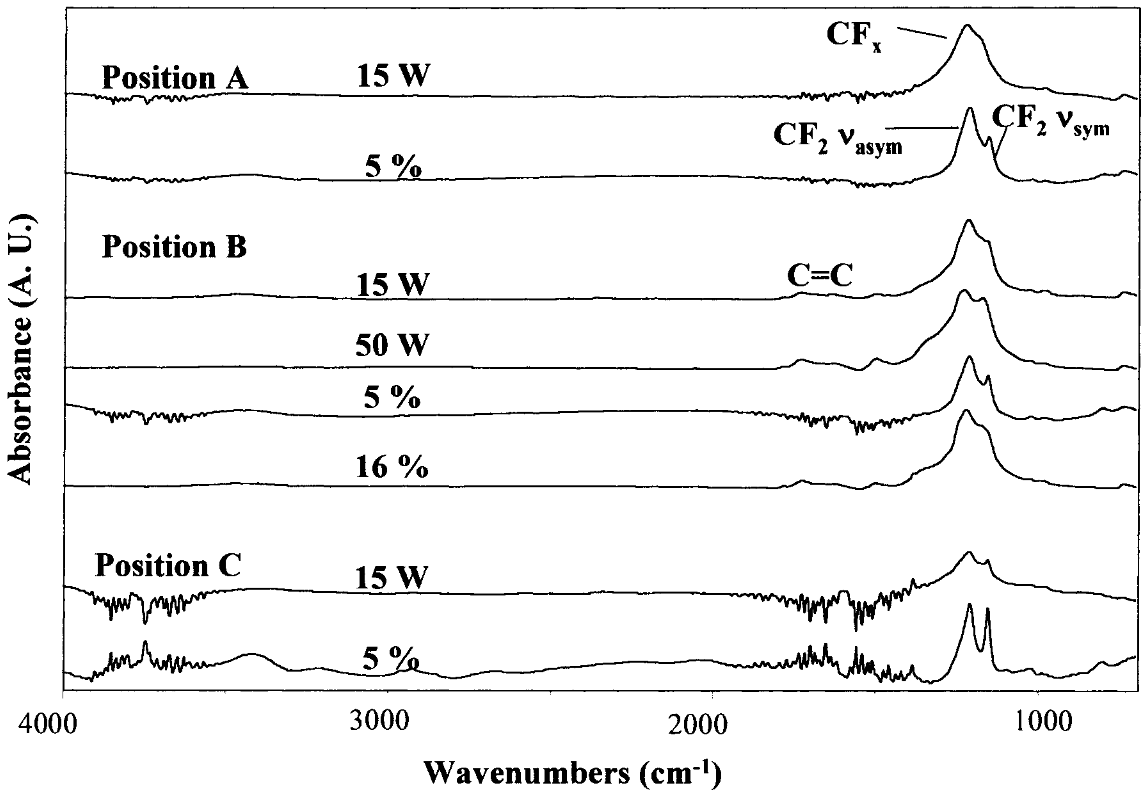

Figure 3.2 FTIR transmission spectra of films deposited at positions A, B, and C in CW C_4F_8 plasmas (P = 15, 50 W) and pulsed C_4F_8 plasmas (d.c. = 5% or 16%).

deposited in CW plasmas at each position.

3.2.B. Deposition rates. Figure 3.3 shows the deposition rates of materials deposited in CW and pulsed C_3F_8 and C_4F_8 plasmas at position B as a function of *P*. Data for the pulsed plasma systems are plotted using the equivalent CW power. For both systems, increasing *P* leads to an increase in deposition rate, presumably as a result of increased fragmentation of the monomer.[1] Deposition rates measured for C_3F_8 plasmas at position B (Figure 3.3a) are an order of magnitude lower than those measured for C_4F_8 plasmas (Figure 3.3b).

Previous work has shown that deposition rates decrease dramatically as the substrate position moves away from the coil region.[12,14,20] This is true for the systems studied here as well. Figure 3.4 shows that the deposition rates for films produced at position C in both systems have decreased considerably: they are all under ~12 Å/min, and C_4F_8 is still the more rapidly depositing system. At both positions B and C, materials deposited in CW plasmas have similar deposition rates to those formed in pulsed plasmas at equivalent powers, which suggests that the deposition rate is strongly tied to the equivalent power input. A closer examination of the pulsed plasma data reveals that the deposition rates are essentially constant when deposition per pulse is plotted as a function of pulse off-time. This indicates that the deposition is occurring primarily during the on-time, in contrast to other pulsed fluorocarbon deposition systems where deposition occurs primarily during the plasma off-time.[15-17,19]

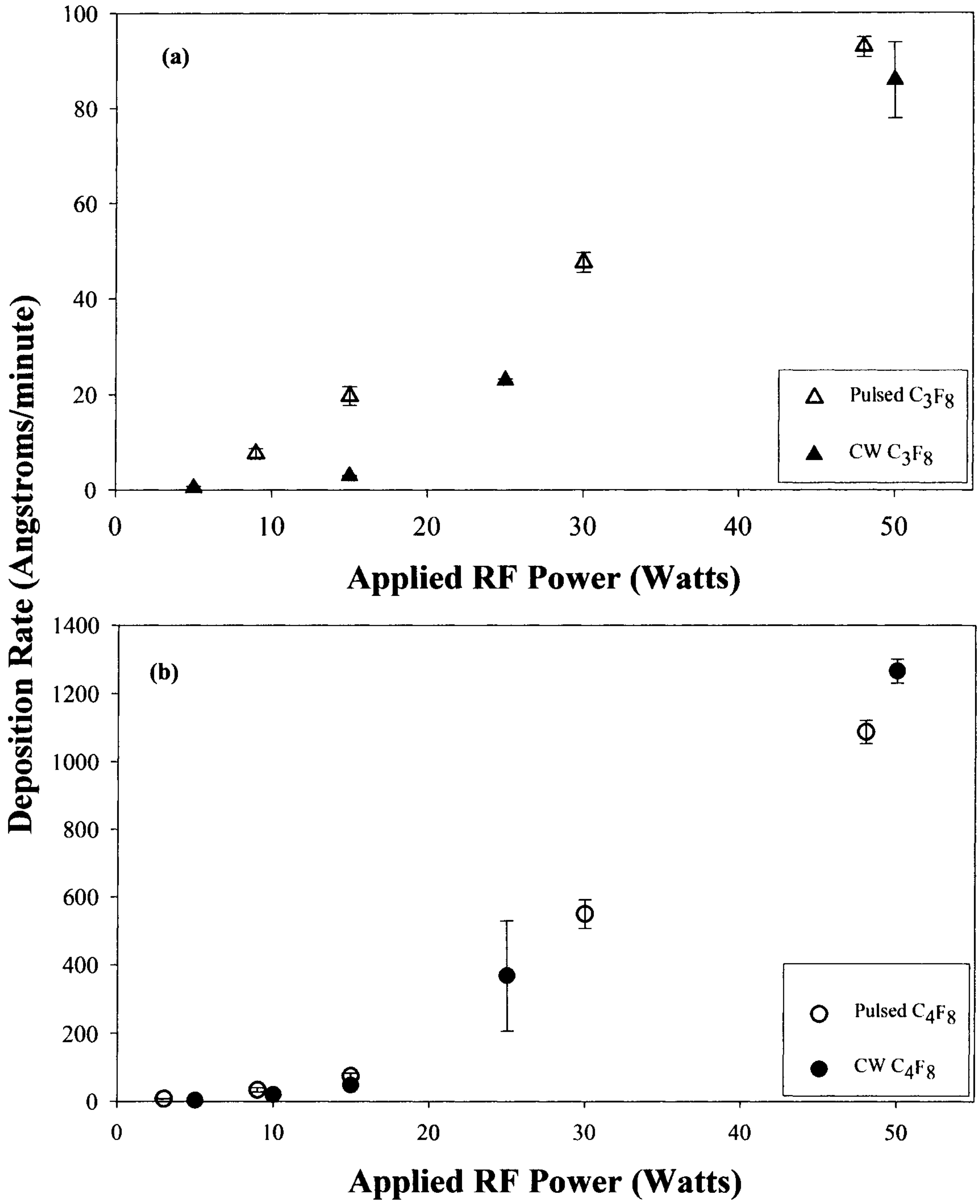

Figure 3.3 Deposition rates for films deposited at position B in CW and pulsed (a) C_3F_8 (triangles) and (b) C_4F_8 (circles) plasmas. Deposition rate is plotted as a function of applied rf power for CW plasmas (closed symbols) and of equivalent CW power for pulsed plasmas (open symbols).

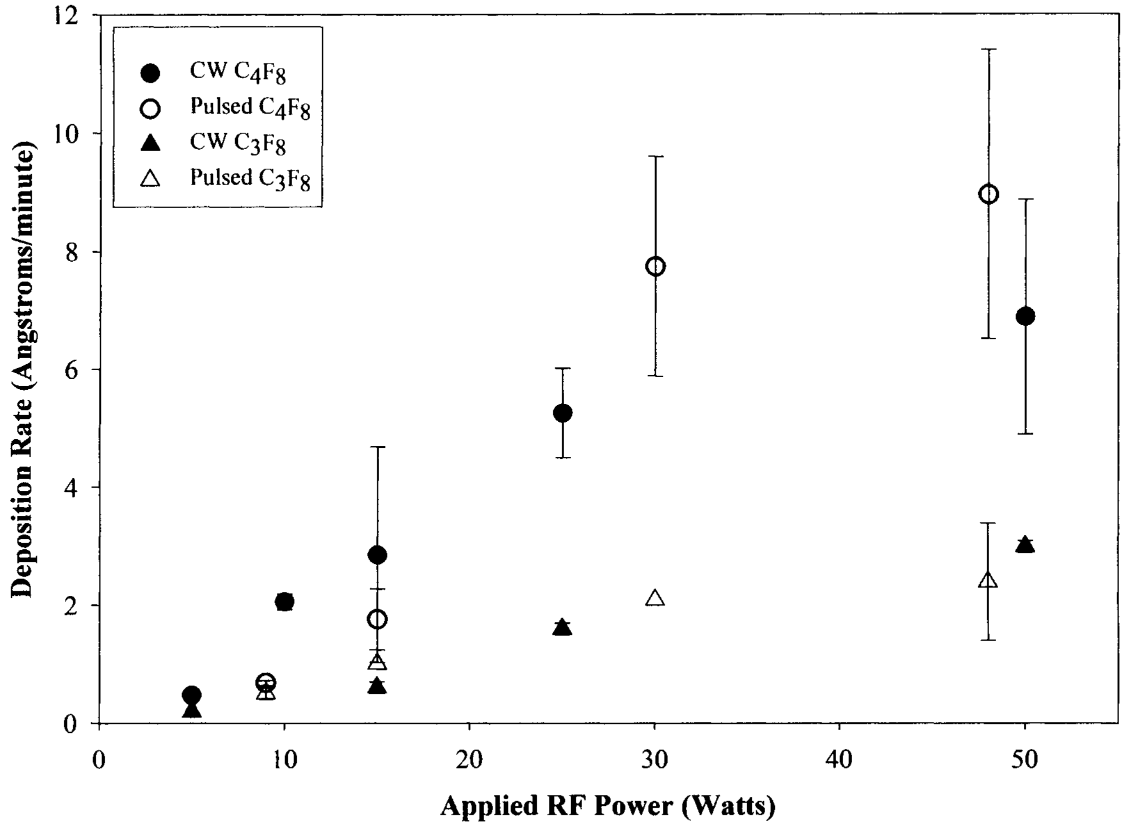

Figure 3.4 Deposition rates for films deposited at position C in CW and pulsed C_3F_8 (triangles) and C_4F_8 (circles) plasmas. Deposition rate is plotted as a function of applied rf power for CW plasmas (closed symbols) and of equivalent CW power for pulsed plasmas (open symbols).

3.2.C. XPS analysis. XPS was used for elemental and structural analyses of the FC materials deposited in C_3F_8 and C_4F_8 plasmas. High resolution C_{1s} spectra of materials deposited in C_3F_8 and C_4F_8 plasmas under different conditions are shown in Figures 3.5-3.7. Figure 3.5 and Table 3.1 provide detailed results of the XPS analysis of films deposited in C_3F_8 plasmas. Figure 3.5a is the spectrum of a film deposited in a 15 W CW plasma at position B. This film clearly contains a variety of CF_x moieties, with CF_3 and CF_2 dominating the spectrum. Increasing *P* to 50 W, Figure 3.5b, results in a film with a marked increase in the amount of crosslinking. In contrast, the spectrum of the film deposited in a 50 W CW plasma at position C (Figure 3.5c) shows a significant increase in CF_2 content and a concomitant decrease in CF_3 and crosslinking moieties. This corresponds directly with the FTIR data in Figure 3.1 and clearly demonstrates that increasing substrate distance from the glow and lowering *P* both result in higher CF_2 content, less crosslinked materials, indicating less fragmentation of the monomer.

The same trends are observed in materials deposited in pulsed plasmas, Figures 3.5d-3.5f. These spectra directly correlate (with respect to equivalent power and position) to the spectra for films deposited in CW plasmas shown in Figures 3.5a-3.5c. In comparison to materials deposited in CW plasmas, a significant increase in CF_2 content and a concomitant decrease in the amount of crosslinking species are observed for materials deposited at position B in the pulsed systems. For films deposited at position C, the spectra are very similar, with nearly equivalent amounts of CF_2 and % crosslinking. This supports the FTIR results and leads to the same conclusion: pulsed plasmas can be used to deposit higher CF_2 content films at position B, but they do not create a significant change in film composition farther downstream at position C.

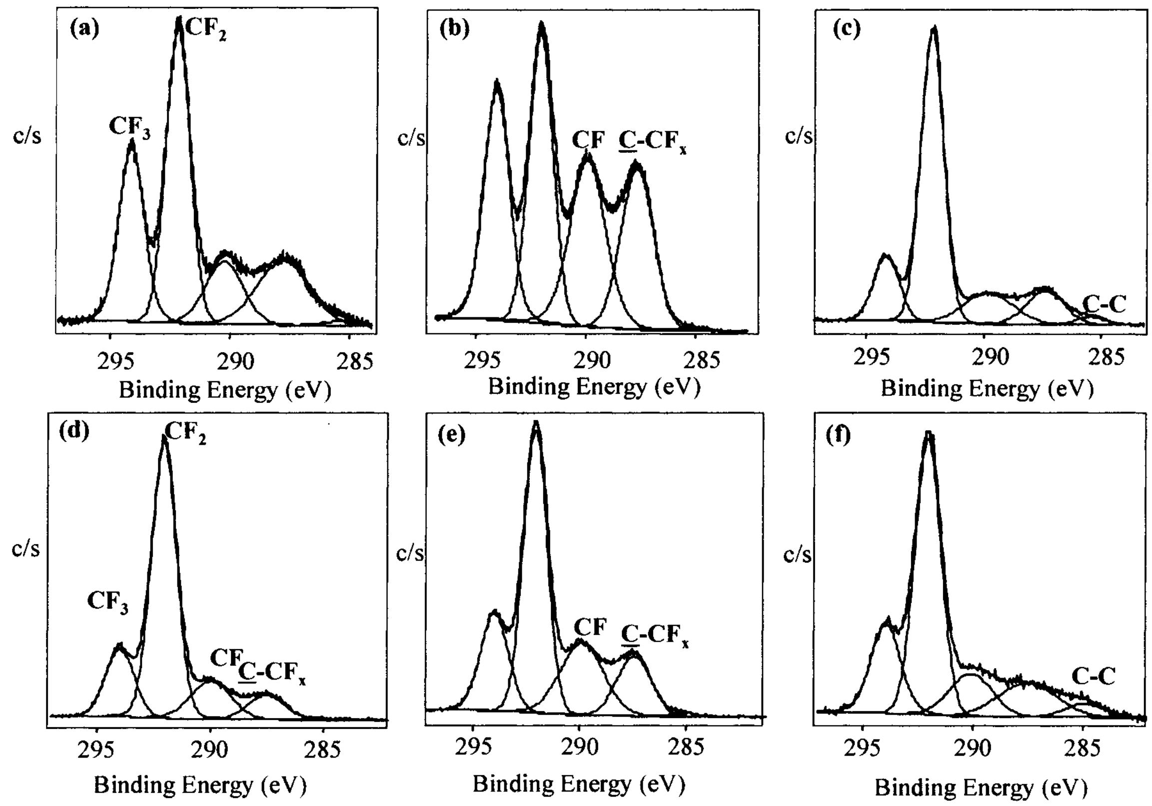

Figure 3.5 High resolution XPS C_{1s} spectra of films deposited in CW C_3F_8 plasmas at position B with applied powers of (a) 15 W and (b) 50 W, and at position C with an applied power of (c) 50 W, and in pulsed C_3F_8 plasmas at position B with d) a 5% d.c. and e) a 16% d.c., and at position C with f) a 5% d.c

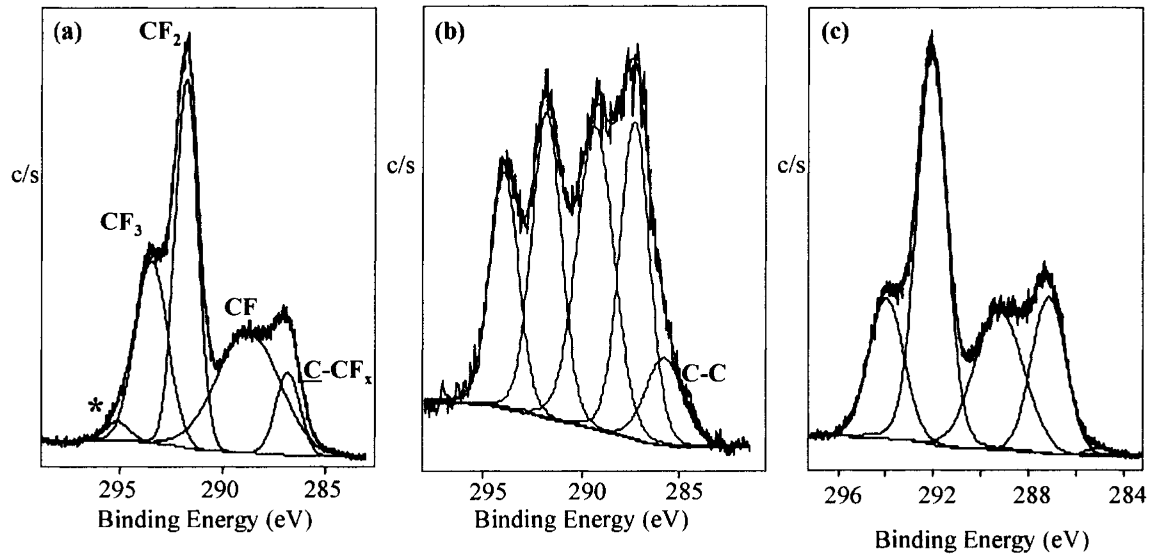

Figure 3.6 High resolution XPS C_{1s} spectra of films deposited in a CW C_4F_8 plasma at position B with input powers of (a) 15 W and (b) 50 W, and at position C with an input power of (c) 50 W. The peak marked with a * is due to potassium contamination of the sample.[24]

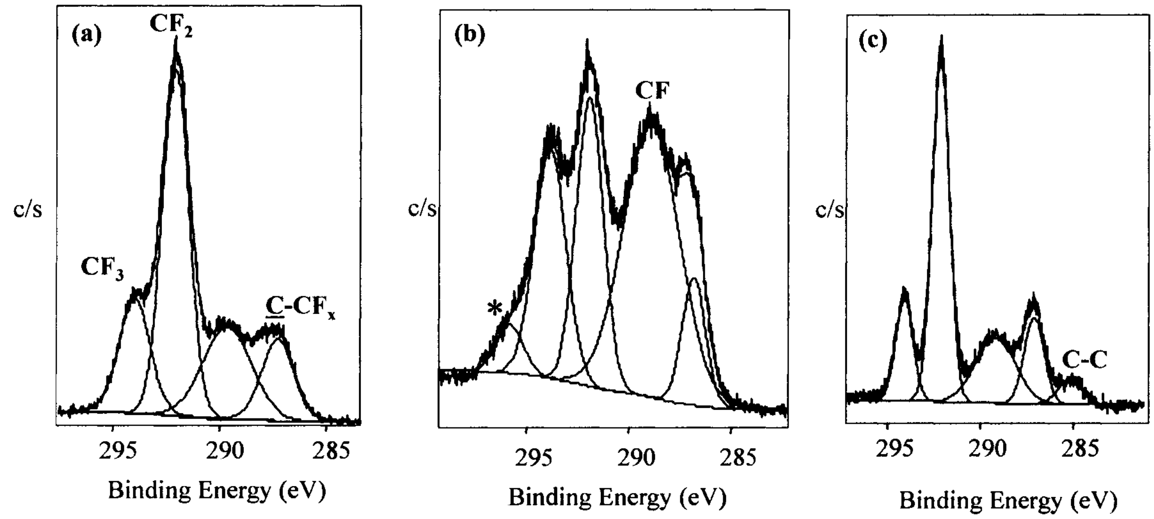

Figure 3.7 XPS C_{1s} spectra of films deposited in pulsed C_4F_8 plasmas at position B with a) a 3% d.c. and b) a 16% d.c.; and at position C with c) a 16% d.c. The peak marked with a * is due to potassium contamination of the sample.[24]

Table 3.1. Composition of FC materials deposited in CW and pulsed C_3F_8 plasmas.

Applied RF Power (W)[1]	Position	%CF_3	%CF_2	%Cross-linking	F/C
15	B	25.4 ± 1.3	40.3 ± 0.1	34.3 ± 1.9	1.66 ± 0.01
50	B	24.2 ± 1.2	28.7 ± 0.8	47.2 ± 1.6	1.39 ± 0.04
	C	16.7 ± 1.7	53.3 ± 5.7	30.0 ± 4.1	1.67 ± 0.04
100	B	22.6 ± 0.6	27.5 ± 0.3	50.5 ± 0.1	1.36 ± 0.01
	C	19.7 ± 3.1	35.7 ± 8.6	44.6 ± 5.5	1.66 ± 0.20
9 (3%)	B	18.9 ± 1.5	56.4 ± 3.1	24.7 ± 7.7	1.69 ± 0.04
30 (10%)	B	27.6 ± 5.0	46.7 ± 3.9	27.3 ± 3.3	1.65 ± 0.07
	C	17.0 ± 3.7	56.0 ± 2.5	27.0 ± 1.2	1.69 ± 0.01
48 (16%)	B	30.7 ± 9.5	34.5 ± 9.9	33.9 ± 3.7	1.57 ± 0.03
	C	24.6 ± 11.8	46.3 ± 16.8	27.3 ± 4.9	1.61 ± 0.09

[1] For pulsed systems, corresponds to equivalent CW power. Duty cycle is given in the parentheses.

Table 3.1 also lists the F/C ratios for our films. The lowest F/C ratio materials are deposited using $P \geq 50$ W at position B. The highest F/C ratio achieved with the C_3F_8 system is only 1.69 ± 0.04, which was obtained with a 3% d.c. plasma at position B. These results are similar to those found in another C_3F_8 PECVD study where a F/C ratio of 1.5 ± 0.13 was measured for materials deposited in a parallel plate reactor.[25] Note that elemental analysis of the films shows that all materials contain < 2% O and Si.

Materials deposited in C_4F_8 plasmas are more crosslinked than those deposited in C_3F_8 plasmas under the same conditions (Figures 3.6 and 3.7 and Tables 3.2 and 3.3). Figure 3.6 shows the high resolution XPS C_{1s} spectra of films deposited in a CW C_4F_8 plasma under identical experimental conditions as those shown in Figures 3.5a-c. All three spectra show a greater % crosslinking than their C_3F_8 counterparts. Similar to the C_3F_8 systems, lower CW input powers yield higher CF_2 content films. For $P > 15$ W, moving the substrate farther downstream also results in higher CF_2 content films.

Figure 3.7 shows the high resolution C_{1s} spectra of films deposited in pulsed C_4F_8 plasmas at position B with a 3% d.c. (9 W equivalent power) and a 16% d.c. (48 W equivalent power); and at position C with a 16% d.c. (Figure 3.7c). Using a lower d.c., or positioning the substrate farther from the glow results in spectra with higher CF_2 content and lower concentrations of crosslinking moieties. The composition of materials deposited in pulsed C_4F_8 plasmas changes as a function of deposition time and film thickness, whereas no dependence on these parameters is observed in the C_3F_8 plasmas. This is illustrated by the Table 3.3 data for materials deposited at position B with a 3% d.c. C_4F_8 plasma. As deposition time is increased from 1 to 30 minutes, there is a concomitant increase in CF_3 content, a decrease in CF_2 content, and a decrease in %

Table 3.2. Composition of FC materials deposited in CW C_4F_8 plasmas.[1]

Applied RF Power (W)	Position	%CF_3	%CF_2	%Cross-linking	F/C
5	B	14.7 ± 1.1	74.7 ± 2.0	10.7 ± 3.1	1.87 ± 0.09
15	B	26.7 ± 4.7	38.1 ± 3.6	36.6 ± 3.8	1.51 ± 0.03
	C	13.6 ± 1.8	34.2 ± 4.8	52.3 ± 6.5	1.37 ± 0.03
25	B	22.0 ± 1.6	25.5 ± 2.7	52.5 ± 2.0	1.27 ± 0.05
	C	16.6 ± 2.7	39.1 ± 1.0	44.4 ± 3.6	1.37 ± 0.06
50	B	15.5 ± 1.2	23.2 ± 1.4	61.2 ± 1.6	1.13 ± 0.17
	C	17.9 ± 0.9	40.4 ± 1.3	41.7 ± 1.3	1.37 ± 0.04

[1] Data averaged from high resolution XPS spectra taken using a 45° take-off angle.

Table 3.3. Composition of films deposited at position B in pulsed C_4F_8 plasmas (3% d. c.).[1]

Deposition Time (min)	%CF_3	%CF_2	%Cross-linking	F/C	Film Thickness (Å)
1	16.6	45.4	38.0	1.58	34 – 41
5	18.0	48.0	34.1	1.57	170 – 205
10	19.1	46.3	34.6	1.53	340 – 410
15	37.0	32.8	30.2	1.53	510 – 615
30	38.2	31.4	30.4	1.58	1020 - 1230

[1] Data averaged from high resolution XPS spectra taken using a 45° take-off angle.

crosslinking. Changes in film composition with deposition time are not observed in materials deposited in CW C_4F_8 plasmas or in materials deposited at position C in pulsed C_4F_8 plasmas.

3.2.D. Contact angle measurements. Static contact angle measurements for films deposited at positions B and C in CW and pulsed C_3F_8 and C_4F_8 plasmas are listed in Table 3.4. All deposited materials are hydrophobic, with contact angles between 101 and 122°. There is no obvious dependence of contact angle on substrate position or plasma power. Figure 3.8 shows the Table 3.4 contact angle data plotted as a function of the F/C ratio of the films. As fluorine content increases, the contact angles increase, similar to what is seen by Favia et al. for FC materials deposited from C_2F_6/H_2 plasmas.[12]

3.2.E. SEM. Figure 3.9 shows SEM images of films deposited on Si from C_3F_8 and C_4F_8 plasmas. Figure 3.9a shows a typical SEM image of a film deposited in a C_3F_8 plasma at position B (deposition conditions: 10% d.c. C_3F_8, position B, 40 min., thickness ~ 2000 Å). It is smooth and featureless on a micron scale, which suggests that polymerization takes place on the substrate instead of in the gas phase.[9] Figure 3.9b contains the SEM image of a film deposited in a 25 W CW C_4F_8 plasma at position B for 2 minutes (~740 Å). Similar to Figure 3.9a, the film is smooth and featureless. However, increased deposition time in the C_4F_8 system leads to a significant change in surface morphology. Figures 3.9c and 3.9d show micrographs of materials deposited in a 10% d.c. C_4F_8 plasma at position B for 5 and 60 minutes, respectively. A higher magnification of the film deposited for 5 minutes, shown in the inset of Figure 3.9c, reveals the presence of numerous ~200 nm wide spherical particles. The film shown in

Table 3.4. Static contact angles for films deposited in CW and pulsed C_3F_8 and C_4F_8 plasmas.

Applied RF Power (W)[1]	Position	C_3F_8	C_4F_8
5	B	109 ± 1	117 ± 3
	C	106 ± 1	109 ± 2
15	B	110 ± 2	116 ± 1
	C	104 ± 1	112 ± 3
25	B	111 ± 2	107 ± 1
	C	105 ± 1	112 ± 1
50	B	110 ± 2	102 ± 1
	C	109 ± 1	112 ± 2
10 (3%)	B	112 ± 1	112 ± 2
	C	109 ± 2	110 ± 3
15 (5%)	B	114 ± 2	110 ± 2
	C	115 ± 1	112 ± 3
30 (10%)	B	112 ± 2	110 ± 1
	C	117 ± 1	115 ± 4
48 (16%)	B	110 ± 1	112 ± 1
	C	115 ± 1	109 ± 1

[1] For pulsed systems, the power corresponds to the equivalent CW power, with duty cycle in parentheses.

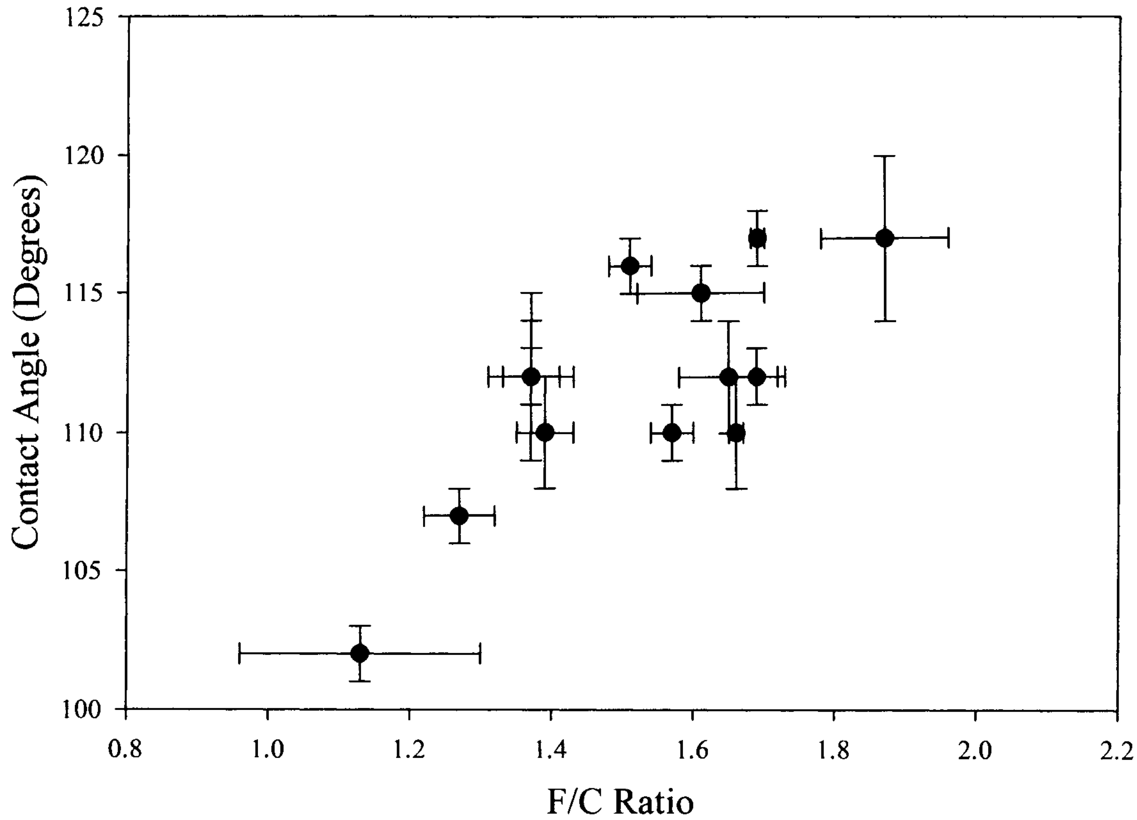

Figure 3.8 Contact angles from Table 3.4 plotted as a function of the F/C ratio of the films on which they are measured.

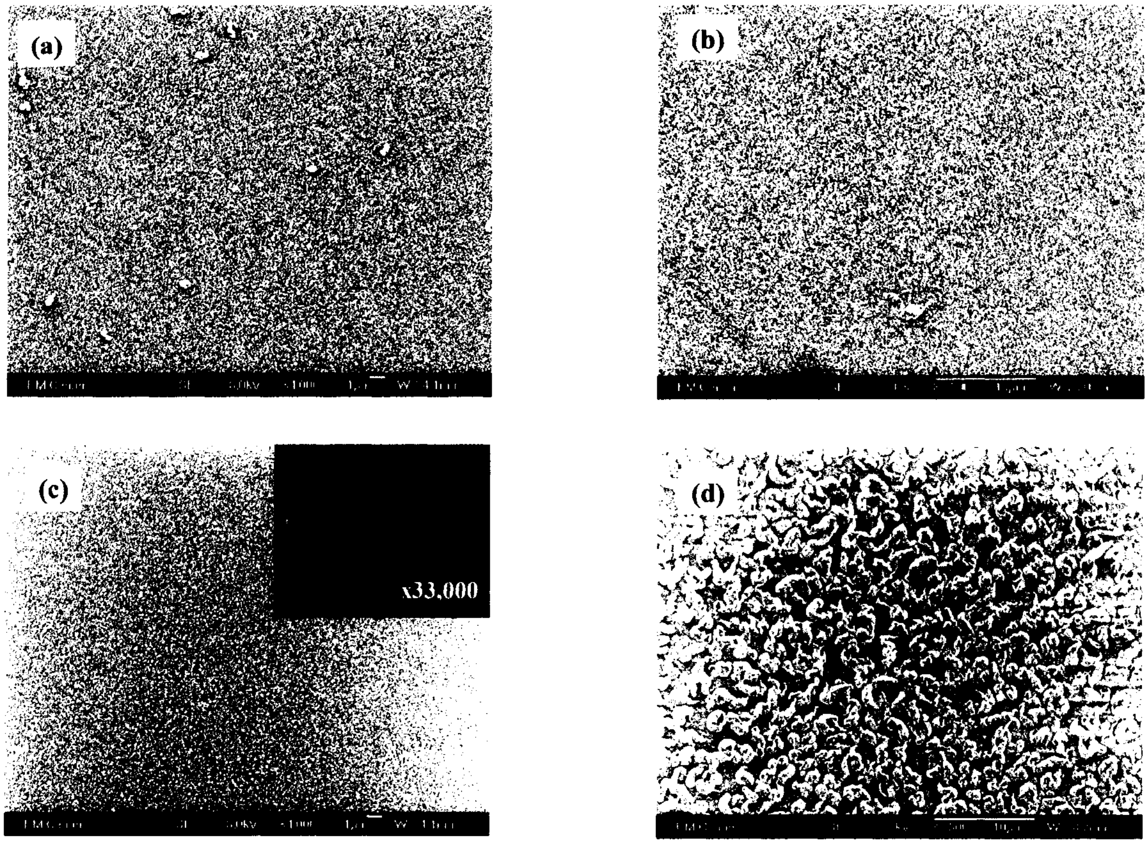

Figure 3.9 SEM images of films deposited on Si substrates at position B using the following parameters: a) pulsed C_3F_8, 10% d.c., 40 min deposition (~2000 Å thick, x4000); b) CW C_4F_8, P = 25 W, 2 min deposition (~740 Å thick, x2500); c) pulsed C_4F_8, 10% d.c., 5 min deposition (~2700 Å, x4000); and d) pulsed C_4F_8, 10% d.c., 60 min deposition. The inset in c) shows a high magnification of this film (x33,000).

Figure 3.9d (>5000 Å) has a very rough surface covered with micron size particles. This suggests that longer exposure to the plasma results in particulate formation that can be incorporated into the growing film.

To explore the flexibility of these materials, films of similar thicknesses were deposited on Cu wires from pulsed and CW C_3F_8 and C_4F_8 plasmas. The wire was twisted into a loop after the deposition of the film, Figure 3.10. The material deposited from the pulsed C_3F_8 plasma (Figure 3.10a) is smooth, with no visible cracking, which indicates a good degree of flexibility. In contrast, the materials deposited at all other conditions (Figures 3.10b-d) are cracked. In the case of Figure 3.10b, the film has nearly completely delaminated. As expected, the most flexible material is the film with the lowest % crosslinking in XPS measurements.

3.3. Discussion

3.3.A. C_3F_8. Octafluoropropane is a linear molecule (global warming potential, gwp =7000) whose use in chamber clean processes results in lower PFC emissions than CF_4 and C_2F_6 based procedures.[2,26] The etch properties of C_3F_8 plasmas have been studied extensively, but film deposition studies involving this monomer are limited. Given the structure of the molecule, however, the potential for creating CF_3 rich films is high. Indeed, we were able to find conditions that produced materials with ~25% CF_3, similar to the results of Hoffman and coworkers.[25] Interestingly, the effects of pulsing the plasma are strongly dependent on the substrate position in the C_3F_8 system. Films deposited in the coil are most affected by pulsing the plasma, as demonstrated by their FTIR spectra, Figure 3.1. Under CW conditions (15 W), no deposition occurs, and

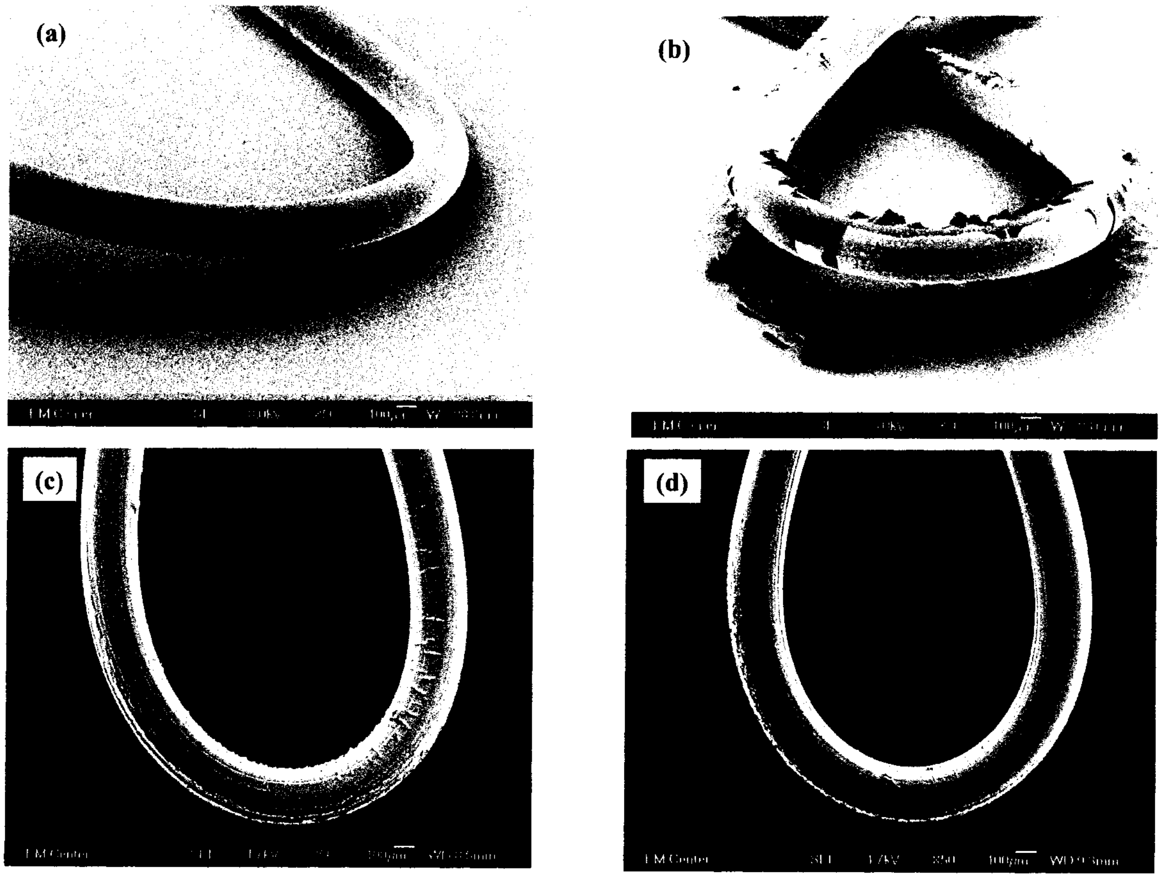

Figure 3.10 SEM images of 2000-2700 Å films deposited on Cu wire from a 10 % d.c. pulsed a) C_3F_8 and b) C_4F_8 plasma, and 25 W CW c) C_3F_8 and d) C_4F_8 plasmas.

etching of the reactor predominates; under pulsed conditions (5% d.c.), an amorphous, highly crosslinked film is produced. At positions B and C, both pulsed and CW C_3F_8 plasmas are primarily depositing systems. FTIR and XPS data, however, demonstrate that pulsed plasmas deposit less crosslinked, higher F/C ratio materials at position B. At position C, there is little difference between materials deposited under pulsed or CW conditions. This is likely because substrates are far enough downstream to negate the benefits associated with pulsing the plasma system. This type of behavior has been seen previously in our laboratories with HFPO plasmas.[14] Overall, the films with the highest F/C ratios were deposited at position B using low *P* or low d.c. and at position C with higher d.c. or *P*.

Although the etching properties of C_3F_8 plasmas have been studied for applications in the microelectronics industry, materials deposited in these systems have a variety of potential uses. Ji et al. used $Ar/C_2H_2/C_3F_8$ plasmas to deposit hydrophobic FC coatings for porcelain insulators and Al conductors.[27] For this purpose, a F/C ratio of <1 yielded the best mechanical (high hardness) and surface properties (rough, hydrophobic). Although our films have considerably higher F/C ratios, the ones deposited from pulsed C_3F_8 plasmas at position B show good overall mechanical properties by the absence of delamination, even under stress, Figure 3.10a. Additional applications for these materials include surface modification for biomaterials and the insulation of electrodes and scanning tunneling microscope (STM) tips.[28] Requirements for these materials include good insulating properties and chemical and physical inertness, along with selective binding of proteins. Hoffman and coworkers have shown selective binding of albumin to FC materials with F/C ratios of 1.1-1.5 and high CF_3 content.[25] Their results demonstrated that the biological reactivity of FC films may be a function of specific surface groups as well as the F/C ratio. Favia et al. also found greater fibrinogen retention for FC films with high F/C ratios and high CF_3 content.[12] F/C ratios for materials deposited from our C_3F_8 plasmas ranged from 1.35-1.70 and the highest CF_3 content materials were produced at position B in both pulsed and CW systems. We are currently assessing the suitability of these materials for biological sensor applications.[29]

3.3.B. C_4F_8. Similar to C_3F_8, octafluorocyclobutane (gwp = 8700) is used industrially for chamber clean processes and has lower PFC emissions than CF_4 and C_2F_6.[2] C_4F_8 was chosen as a deposition monomer because it has a highly strained ring structure composed of -CF_2- units making it an ideal precursor for CF_2-rich films. Indeed, we found we could deposit materials containing up to 75% CF_2 from low *P* CW C_4F_8 plasmas, see Table 3.2. FTIR and XPS data show that pulsed C_4F_8 plasmas result in the deposition of higher CF_2 content, less crosslinked materials at positions A and B, similar to what was observed in the C_3F_8 systems. Unlike C_3F_8 plasmas, however, this is also true at position C, Figures 3.6 and 3.7, where we still observe differences in composition between films deposited under pulsed and CW conditions. This suggests that fragmentation and ionization of the C_4F_8 monomer is extensive, as the effects of high-energy species are detected at position C, 28 cm downstream from the coil. The high deposition rate (Figures 3.3 - 3.4) that is typical of depositing C_4F_8 plasmas[9] and the extensive fragmentation of the C_4F_8 monomer seen in the C_4F_8 PI-MS data[18] lend further support to the high fragmentation and ionization of the monomer in the plasma system. Ultimately, these data demonstrate that individually, pulsing or using remote systems does not afford the highest level of control over film composition that a combination of the two methods provides.

Similar to C_3F_8, films produced from C_4F_8 plasmas have enormous potential in a number of applications. Most studies of these materials have focused on their dielectric properties as these materials are potential replacements for low k interlevel dielectrics in integrated circuit manufacturing. For example, Endo et al. measured a dielectric constants of 2.3 for films deposited from C_4F_8 helicon wave plasmas.[30] Likewise, Agraharam et al. used high pressure capacitively coupled C_4F_8/Ar plasmas to produce FC films with dielectric constants ranging from 2.29-2.55 with F/C = 1.1-1.2.[31] A more direct comparison can be made to the work of Sandrin et al. who used low power inductively-coupled rf C_4F_8 plasmas with similar conditions to ours employed here for CW systems (i.e. pressure ~ 200 mTorr, P = 7 W).[9] They found films with an average F/C ratio of 1.5, containing ~33% CF_2 and 24% CF_3. For comparison, films produced in our system at position B (pressure ~240 mT, P = 5 W) contain up to 75% CF_2 and 15% CF_3 with F/C = 1.87. Clearly, the use of downstream processing results in higher retention of the C_4F_8 monomer structure. Similar to our results, Sandrin et al. found that the F/C ratio decreases as P increases. Using a variety of plasma conditions we can create films with a wide range of F/C ratios (1.13 to 1.87) and CF_2 contents (25 to 75%). This monomer is extremely versatile and could be exploited to produce materials suitable for a wide range of applications.

3.3.C. Comparison of monomers. A direct comparison between monomers with obvious differences in structures and F/C ratios affords insight into the chemistry that occurs within the plasmas. It is well know that FC monomers with higher F/C ratios promote etching processes.[1] C_3F_8 (F/C = 2.67) plasmas are predominantly etching in the coil region, whereas C_4F_8 (F/C = 2) plasmas are predominantly depositing. Our C_4F_8 plasmas have higher deposition rates than the C_3F_8 plasmas, at all positions. Although this can be partially attributed to the lower F/C ratio of the C_4F_8 monomer, it is more likely a result of the ring strain inherent to the molecule's geometry, which makes it highly reactive within the plasma system.

Previous mass spectral analyses[18] illustrate the differences in the reactivity of the two monomers studied. PI-MS data show that CF_3^+ and CF^+ are the predominant ions formed in C_3F_8 and C_4F_8 plasmas respectively, indicating that the fragmentation of the original monomer is more extensive within the C_4F_8 system. Furthermore, under identical experimental conditions, C_4F_8 plasmas have greater concentrations of higher molecular weight ions than C_3F_8 plasmas do.[18] This correlates to the XPS data, which show that materials deposited in C_4F_8 plasmas are more crosslinked than those deposited in C_3F_8 plasmas under the same conditions (Figures 3.5-3.7). The bombardment of the surface by heavier ions may contribute to the deposition of more amorphous films in the C_4F_8 systems.

The high reactivity of the C_4F_8 monomer is key to its versatility. In addition to higher deposition rates, it allows film formation at very low *P* (5 W). Downstream film formation under these conditions results in minimally crosslinked, CF_2 rich materials that are in contrast to the highly crosslinked, amorphous materials deposited at higher *P*. As a final note, an additional feature of materials deposited in both pulsed and CW C_3F_8 and C_4F_8 plasmas is that they easily passed the "scotch tape" test for adherence, and are harder to scratch than the relatively soft materials deposited in HFPO plasmas.[14] This suggests these materials may be useful in applications requiring more mechanically robust FC films.

3.4. Summary

We have explored various plasma parameters for plasma deposition of FC films from C_3F_8 and C_4F_8 monomers, and demonstrated that a wide range of FC materials can be deposited within a large parameter space. Of the two monomers studied here, C_4F_8 is more reactive, which also makes it more versatile for materials fabrication. By varying plasma parameters or substrate position, C_4F_8 plasmas can produce materials that are either more crosslinked, or that are more CF_2/CF_3 rich than those deposited in C_3F_8 plasmas. Additionally, in this system, pulsed plasmas result in less fragmentation of the original monomer structure in films deposited at all positions. In the C_3F_8 systems, the effects of pulsing the plasma are strongly dependent on the substrate position and film chemistry does not change appreciably with plasma parameters. Overall, careful choice of monomer chemistry and structure as well as plasma parameters can lead to control of the deposited FC materials. This ability to control the film content is critical for creating materials designed for specific applications.

References

1. d'Agostino, R.; Cramarossa, F.; Fracassi, F. Plasma Deposition, Treatment, and Etching of Polymers. In *Plasma Deposition, Treatment, and Etching of Polymers*; d'Agostino, R., Ed.; Academic Press, Inc.: San Diego, 1990; pp 95-143.

2. Allgood, C.; Hsu, S.; Mocella, M. *Comparison of PECVD chamber cleaning processes (environmental, productivity and economic considerations)*, Proceedings of the Electrochemical Society (2001), 2001-6 (Environmental Issues with Materials and Processes for the Electronics and Semiconductor Industries), pp 9-14.

3. Shiba, S.; Fukuyama, S.; Yoneda, Y.; Saito, K.; Kawasaki, Y. (Fujitsu Ltd., Japan), Patent No. JP 63118739 (23 May 1988).

4. Shiba, S.; Saito, K.; Kawasaki, Y.; Watabe, K.; Yoneda, Y. (Fujitsu Ltd., Japan), Patent No. JP 02059753 (28 February 1988).

5. Nippon Electric Co., Ltd., Japan, Patent No. JP 58184147 (27 October 1983).

6. Lee, H. J.; Kim, J. K.; Kim, J. H.; Whang, K. *J. Vac. Sci. Technol. B* **1997**, *16*, 500.

7. Hayashi, H.; Sekine, M. *Jpn. J. Appl. Phys.* **1999**, *38*, 4910.

8. Kinoshita, H. (Cho LSI Gijutsu Kenkyu Kumiai, Japan), Patent No. JP 55002719 (10 January 1980).

9. Sandrin, L.; Silverstein, M. S.; Sacher, E. *Polymer* **2001**, *42*, 3761.

10. Lee, W. W.; Ho, P. S. *MRS Bulletin* **1997**, 19.

11. Feichtinger, J.; Galm, R.; Walker, M.; Baumgartner, K.-M.; Schulz, A.; Rauchle, E.; Schumacher, U. *Surf. Coat. Technol.* **2001**, *142-144*, 181.

12. Favia, P.; Perez-Luna, V. H.; Boland, T.; Castner, D. G.; Ratner, B. D. *Plasmas Polym.* **1996**, *1*, 299.

13. Garrison, M. D.; Luginbuhl, R.; Overney, R. M.; Ratner, B. D. *Thin Solid Films* **1999**, *352*, 13.

14. Butoi, C. I.; Mackie, N. M.; Gamble, L. J.; Castner, D. G.; Barnd, J.; Miller, A. M.; Fisher, E. R. *Chem. Mater.* **2000**, *12*, 2014.

15. Mackie, N. M.; Dalleska, N. F.; Castner, D. G.; Fisher, E. R. *Chem. Mater.* **1997**, *9*, 349.

16. Mackie, N. M.; Castner, D. G.; Fisher, E. R. *Langmuir* **1998**, *14*, 1227.

17. Panchalingam, V.; Chen, X.; Savage, C. R.; Timmons, R. B.; Eberhart, R. C. *J. Appl. Polym. Sci.: Appl. Polym. Symp.* **1994**, 123.

18. Williams, K. L.; Martin, I. T.; Fisher, E. R. *J. Am. Soc. Mass Spectrom.* **2002**, *13*, 518.

19. Han, L. M.; Timmons, R. B.; Lee, W. W. *J. Vac. Sci. Technol. B* **2000**, *18*, 799.

20. Castner, D. G. *NATO ASI Series, Series E: Applied Sciences* **1997**, *346*, 221.

21. Leezenberg, P. B.; Reiley, T. C.; Tyndall, G. W. *J. Vac. Sci. Technol. A.* **1999**, *17*, 275.

22. Takada, N.; Shibagaki, K.; Sasaki, K.; Kadota, K. *J. Vac. Sci. Technol. A* **2001**, *19*, 689.

23. Leich, M. A.; Mackie, N. M.; Williams, K. L.; Fisher, E. R. *Macromolecules* **1998**, *31*, 7618.

24. Haque, Y.; Ratner, B. D. *J. Appl. Polym. Sci.* **1986**, *32*, 4369.

25. Bohnert, J. L.; Fowler, B. C.; Horbett, T. A.; Hoffman, A. S. *J. Biomater. Sci. Polymer Edn.* **1990**, *4*, 279.

26. Van San, R.; Zazera, L. *Solid State Phenomena* **1999**, *65-66*, 261.

27. Ji, H.; Cote, A.; Koshel, D.; Terreault, B.; Abel, G.; Ducharme, P.; Ross, G.; Savoie, S.; Gagne, M. *Thin solid films* **2002**, *405*, 104.

28. Lewis, K. B.; Ratner, B. D. *J. Vac. Sci. Technol. B* **1992**, *10*, 2331.

29. Godek, M. L.; Malkov, G. S.; Fisher, E. R.; W., G. D. *J. Biomed. Mater. Res.* **2005**, *To be submitted.*

30. Endo, K.; Tatsumi, T. *Appl. Phys. Lett.* **1997**, *70*, 1078.

31. Agraharam, S.; Hess, D. W.; Kohl, P. A.; Bidstrup Allen, S. A. *J. Vac. Sci. Technol. B* **2001**, *19*, 439.

CHAPTER 4

PLASMA MODIFICATION OF PDMS MICROFLUIDIC DEVICES FOR CONTROL OF ELECTROOSMOTIC FLOW

This dissertation chapter describes the modification of polydimethylsiloxane (PDMS) capillary electrophoresis microchips using plasma-enhanced chemical vapor deposition (PECVD). Treatments with C_3F_8 and acrylic acid plasmas deposited thin films within the devices, resulting in modified electroosmotic flow (EOF) values.

4.1 Introduction

Capillary electrophoresis (CE) microchips have been constructed from both hard materials, including silicon and glass, and soft materials, such as polydimethylsiloxane (PDMS).[1,2] In comparison to soft materials, silicon and glass device construction is costly, labor intensive, and requires a clean room environment. The material rigidity also makes the creation of moving parts a challenge.[1,2] Consequently, construction of microfluidic devices from soft materials such as PDMS has become increasingly popular. In addition to the straightforward fabrication, PDMS is inexpensive and has good optical properties, which allows for optical detection.[1-3] Furthermore, many devices can be constructed from a single molding master.[4] In spite of these desirable properties, there are several unresolved issues with PDMS. The primary disadvantage of PDMS is its hydrophobicity, which leads to the adsorption and absorption of hydrophobic analytes and makes the channels difficult to fill with aqueous solutions.

Several methods for the chemical modification of PDMS surfaces have been demonstrated in an effort to address this issue. In the literature, there are three general approaches for modifying the surface chemistry: dynamic coatings with surfactants, adsorbed polymer coatings, and covalent modification. Dynamic coatings provide good EOF stability but require the continuous presence of a surfactant in the mobile phase.[5] Adsorbed polymer coatings also stabilize the EOF and do not require the presence of the polymer in the mobile phase.[6] Both of these techniques have minimal impact on analyte adsorption and absorption. Covalent coatings, including plasma deposited films have shown the best performance with regards to analyte absorption.[4,7]

There are several examples of PDMS modification via polymer grafting in the literature. Hu et al. have modified PDMS microfluidic devices by UV grafting monomer mixtures (poly(ethylene glycol), poly(ethylene glycol) diacrylate, and AA) onto the surfaces. Their cross-linked, mixed monomer grafted PDMS resulted in more hydrophilic surfaces, considerably larger EOF values, and highly efficient separations of biologically relevant peptides.[4] Wirth and coworkers demonstrated the separation of proteins using PDMS microchips modified with grafted polyacrylamide. The multistep deposition process involved surface oxidation of the PDMS channels, the formation of a self-assembled monolayer of benzyl chloride initiators, and atom-transfer radical polymerization.[7] The modified devices were hydrophilic and had considerably greater resistance to protein adsorption when compared to absorbed or dynamic coatings.

We propose plasma modification of preassembled PDMS microfluidic devices as a straightforward method to tailor the surface chemistry of chips for a variety of applications in microfluidics and lab-on-a-chip systems. Low pressure plasmas are widely used both to create polymers and to chemically alter the surface properties of polymeric materials.[8-15] Experimentally, these plasma treatments involve simple, one or two step dry processes, which result in minimal waste. Non-depositing plasma treatments can result in both functional group implantation and crosslinking of the polymer. Previous work in our laboratories involves the use of H_2O and CO_2 plasmas to permanently modify various polymeric membranes.[9-11] Alternatively, plasma enhanced chemical vapor deposition (PECVD) can be used to modify polymers by creating new organic or inorganic materials covalently bound to the original polymer. Plasma deposited thin films are typically conformal, pinhole free, can provide stable and sterile surfaces, and are able to adhere to a wide variety of substrates.[8] Previous work in our laboratories has demonstrated the efficacy of PECVD in coating diverse sample geometries.[16]

Another advantage of PECVD is the virtually unlimited range of plasma monomers available. As a result, an expansive collection of potential materials can be created via plasma polymerization. Plasma polymerized fluorocarbon (FC) films have a wide range of utility, because of their inertness, hydrophobicity, biocompatibility, low dielectric constants, and low friction coefficients.[8,17,18] We are interested in FC thin films as they could potentially be resistant to organic solvents, and a fluorocarbon surface should not be ionizable in the buffers typically used in microchip separations, giving rise to low EOF. Plasma polymerized AA (p-AA) is another material with interesting properties: p-AA films are typically hydrophilic in comparison to FC materials and contain carboxylic acid groups. p-AA films are attractive for microchip modification as a hydrophilic surface should result in decreased protein adsorption compared to bare PDMS, and the carboxylic acid functionalities could lead to improved channel wetting capacity.

This chapter contains results for microfluidic devices modified by PECVD. PDMS microdevices were assembled, and then coated with either FC or p-AA films. Effectiveness of the surface modification was determined by x-ray photoelectron spectroscopy (XPS), contact angle measurements and scanning Auger microscopy (SAM). Subsequently, the EOF was measured at various pHs and aging stages. In general, FC films proved to be more stable, and reduced both the EOF magnitude and pH dependence. AA films were less stable, and gave a greater variation in EOF with pH than native PDMS. Including an Ar plasma treatment before the deposition step reduced the absorption of a hydrophobic fluorescent dye into the PDMS and improved the adhesion of the plasma deposited thin films.

4.2 Results and Discussion

4.2.A Plasma deposited materials analyses. Table 4.1 lists the static water contact angles measured on untreated and treated PDMS. Air plasma treatments were performed in the commercial cleaner; all other plasma treatments were performed in our inductively coupled rf plasma reactor. The air plasma treatment used to seal the PDMS chips initially results in a 0° contact angle, with some hydrophobic recovery within 60 min. After 24 h, contact angles increase to 30 - 60°. This broad range of values is the result of the marginal parameter control available in the plasma cleaner; the increase in contact angle arises from the well-known hydrophobic recovery that PDMS exhibits after plasma oxidation.[2] The extent of modification via the sealing process does not affect the surface properties of the deposited films.

To better adhere our plasma deposited material to the PDMS, we included an Ar plasma pretreatment step before the deposition.[13] The following materials analysis results pertain to samples subjected to both an air plasma treatment and an Ar plasma pretreatment before the film deposition step. The contact angle of the FC film deposited from the C_3F_8 plasma on PDMS is 115 ± 5°. This measurement is within the combined experimental error of that for the material deposited on Si wafers using the same deposition parameters (110 ± 2°).[14] The average contact angle measured for the p-AA sample is 65 ± 9°, lower than that of p-AA deposited on Si using the same deposition

Table 4.1. Contact angles and elemental analysis of plasma treated PDMS.[a]

Plasma Source[b]	Buffer[c]	Contact angle	% C	% O	% Si	%F	% N	F/C
None	None	113 (3)	47.6 (0.3)	27.3 (0.1)	25.2 (0.4)	0	0	---
Air	None	30-60	20.1 (1.2)	51.8 (0.9)	28.2 (0.3)	0	0	---
Ar	None	---	13.1 (0.5)	53.9 (0.8)	31.1 (0.9)	0	1.9 (1.0)	---
Ar/C_3F_8	None	115 (5)	41.7 (0.5)	2.5 (0.8)	1.3 (0.6)	53.0 (1.4)	1.6 (0.2)	1.27 (0.04)
Ar/C_3F_8	1 x	---	45.7 (0.2)	7.4 (0.4)	4.0 (0.1)	41.1 (0.1)	1.9 (0.1)	0.90 (0.00)
Ar/C_3F_8	4 x	---	46.8 (0.7)	23.0 (2.8)	14.9 (1.4)	12.4 (4.1)	2.9 (0.4)	0.26 (0.08)
Ar/AA	None	65 (9)	65.3 (0.7)	25.9 (2.5)	8.8 (1.9)	0	0	---
Ar/AA	1 x	---	48.3 (8.3)	31.7 (4.8)	18.0 (3.3)	0	2.0 (0.5)	---

[a]Values in parentheses for selected measurements represent the standard deviation of the mean of several measurements.
[b]Plasma parameters are detailed in Section 2.1.
[c]The value in this column indicates if and how often the sample was exposed to buffer before the measurement was taken. 1 x denotes the sample was soaked once in buffer for 30 min; 4 x denotes the sample was soaked in buffer 4 times, in 30 min increments.

parameters (85 ± 2°).[19] The p-AA sample is much more hydrophilic than both the untreated and FC plasma treated PDMS. The FC film appeared smooth and featureless to the naked eye, whereas the AA film appeared to have small cracks on the surface.

The elemental surface composition of plasma treated PDMS was quantified via XPS, Table 4.1. The experimentally measured composition of PDMS (47.6% C, 27.3% O, 25.2% Si) is in good agreement with the stoichiometric composition of the polymer (50% C, 25% O, 25% Si). The air plasma treatment leads to a significant increase in O content (51.8%) and a concomitant decrease in C (20.1%), these values do not change significantly 5 days after treatment. Compositionally, Ar plasma treated PDMS that is exposed to atmosphere resembles air plasma treated PDMS: a standard Ar treatment results in an increase in O content to 53.9%, a decrease in C content to 13.1%, and a slight increase in Si to 31.1%. Additionally, a small amount of N (1.9%) is incorporated into the PDMS. The incorporation of both the N and additional O are attributed to post deposition atmospheric reactions. Thus, the Ar plasma successfully creates active sites on the PDMS surface, as expected, which improves the adhesion of the plasma deposited films. Note that the elemental compositions of air and Ar plasma treated PDMS correspond well to literature results that demonstrate that non-depositing plasma treatment of PDMS leads to the formation of a thin silica-like layer on the polymer surface.[12,20]

The elemental composition of the FC film deposited from the C_3F_8 plasma is primarily F and C, Table 4.1, consistent with our prior film deposition work.[14] The trace N (1.6%) is likely from post deposition atmospheric reactions, as neither the PDMS substrate nor the FC monomer contain N. Si, however, is present exclusively in the

PDMS, which makes Si content a good gauge of substrate coverage. The trace Si (1.3%) present in the FC film indicates good initial coverage of the underlying PDMS (Table 4.1).

High resolution XPS spectra yield information on the bonding environments of the deposited films. Figure 4.1a shows the high resolution C_{1s} spectrum of untreated PDMS. It was fit with one peak (FWHM=1.5 eV), representing the single molecular environment of C in the polymer (Si-$\underline{C}$-H, 284.8 eV).[12] Figure 4.1b is the high resolution C_{1s} spectrum of a FC film deposited on Si using a C_3F_8 plasma with the same deposition parameters discussed earlier; this C envelope is considerably more complex, and has been decomposed into four chemical environments: CF_3 (294.0 eV), CF_2 (292.1 eV), CF (290.0 eV), and $\underline{C}$-CF_x (287.3 eV). The spectrum for the C_3F_8 plasma treated PDMS, Figure 4.1c, is decomposed into five chemical environments, the first four correspond to those seen in Figure 4.2b, and the fifth, located at 284.8 eV, could have contributions from $\underline{C}$-C, $\underline{C}$-H, and/or $\underline{C}$-Si bonds. The underlying PDMS is most likely the main contributor to this peak, as it is not present in the spectrum of the FC film on Si (Figure 4.2b). Note that the assignment for CF includes contributions from both $\underline{C}$F-C and $\underline{C}$F-CF_x, making the FWHM (2.16 eV) slightly greater than those of the other peaks.

One of the issues with generating stable surface modifications of PDMS is the presence of low molecular weight mobile oligomers in the polymer.[20] These oligomers tend to rearrange on the surface, resulting in hydrophobic recovery for non-depositing plasma treated PDMS.[21] To determine if this surface rearrangement occurs on a PDMS sample with a film deposited on it, XPS analysis was performed on FC plasma treated PDMS that was aged in air over a 5 day period. Results show a slight increase in the

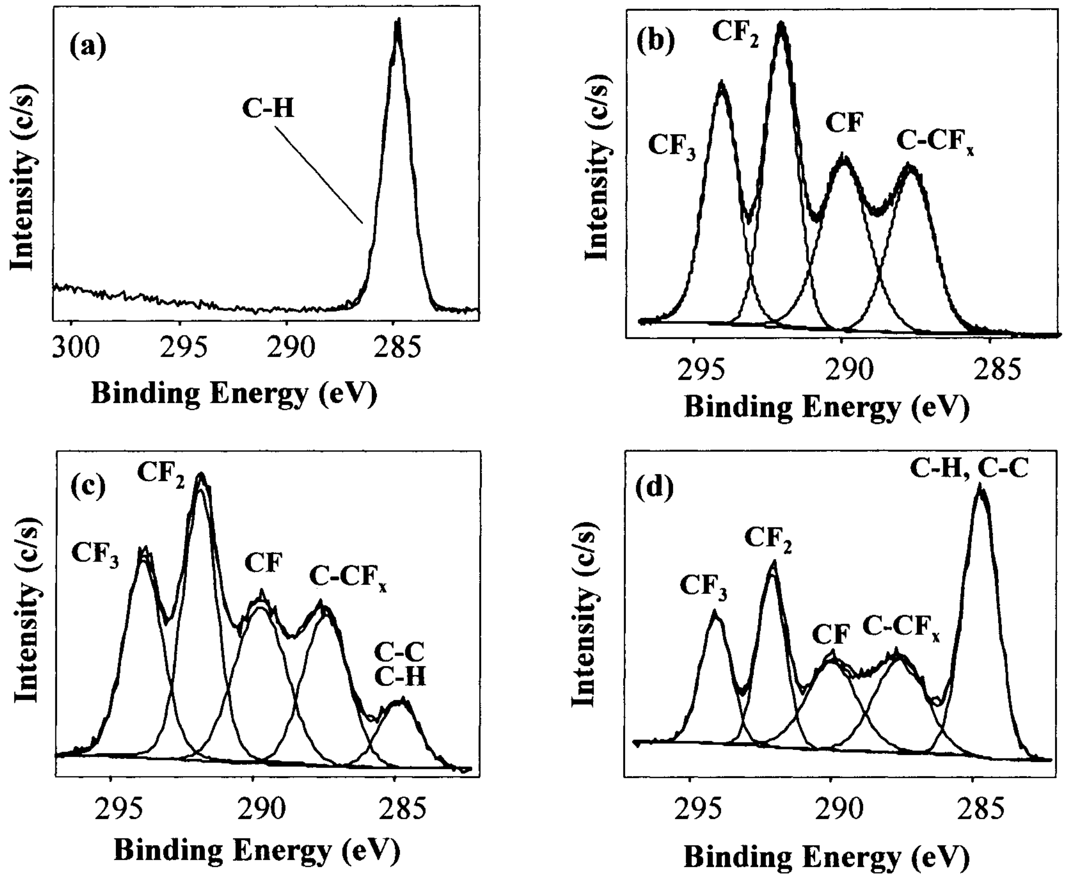

Figure 4.1 High resolution XPS C_{1s} spectra of (a) untreated PDMS, (b) p-C_3F_8 on Si, (c) p-C_3F_8 on PDMS, and (d) p-C_3F_8 on PDMS after exposure to buffer for 30 minutes.

intensity of the peak at 284.8 eV in the high resolution C_{1s} data. Additionally, during a typical set of EOF measurements, the plasma treated microfluidic device is exposed to buffer for ~ 30 min. To determine the effect this has on film composition, a sample of C_3F_8 plasma treated PDMS was soaked in buffer, and XPS analysis was then performed. The Table 4.1 values indicate an increase in both O and Si content, to 7.4% and 4.0% respectively, and a decrease in F content to 41.1% after exposure to buffer. After repeated exposure to the buffer, the O and Si components are even greater, 23.0% and 14.9% respectively, and the F is decreased to 12.4%. The high resolution C_{1s} spectrum of FC plasma treated PDMS after a 30 min exposure to buffer (Figure 4.2d), shows both a significant reduction in the intensity of the CF_x peaks attributed to the FC film, and an increase in the intensity of the PDMS substrate peak located at 284.8 eV. This combined with the increase in Si and O content is attributed to an increase in the signal from the underlying PDMS substrate, which suggests either rearrangement of the PDMS over the FC film or removal of the FC film in the buffer.

Initially, the elemental composition of our p-AA film is primarily O and C, Table 4.1, Figure 4.2a. The Si content is 8.8%, slightly higher than that measured for the FC film. After exposure to buffer, the Si increases to 18.0%, which suggests that the p-AA film is less robust than the FC material. The fitting used for the high resolution C_{1s} spectra of our p-AA films, Figure 4.2b, uses five peaks and closely matches that found in the literature.[22] The most significant deviation from p-AA spectra in the literature is the FWHM of the C-H/C-H peak (2.58 eV), wider than that typically found in this type of plasma polymer. We attribute this to contributions from C-C/C-H in the film, and C-H in the underlying PDMS substrate: variations in the molecular environments of identical

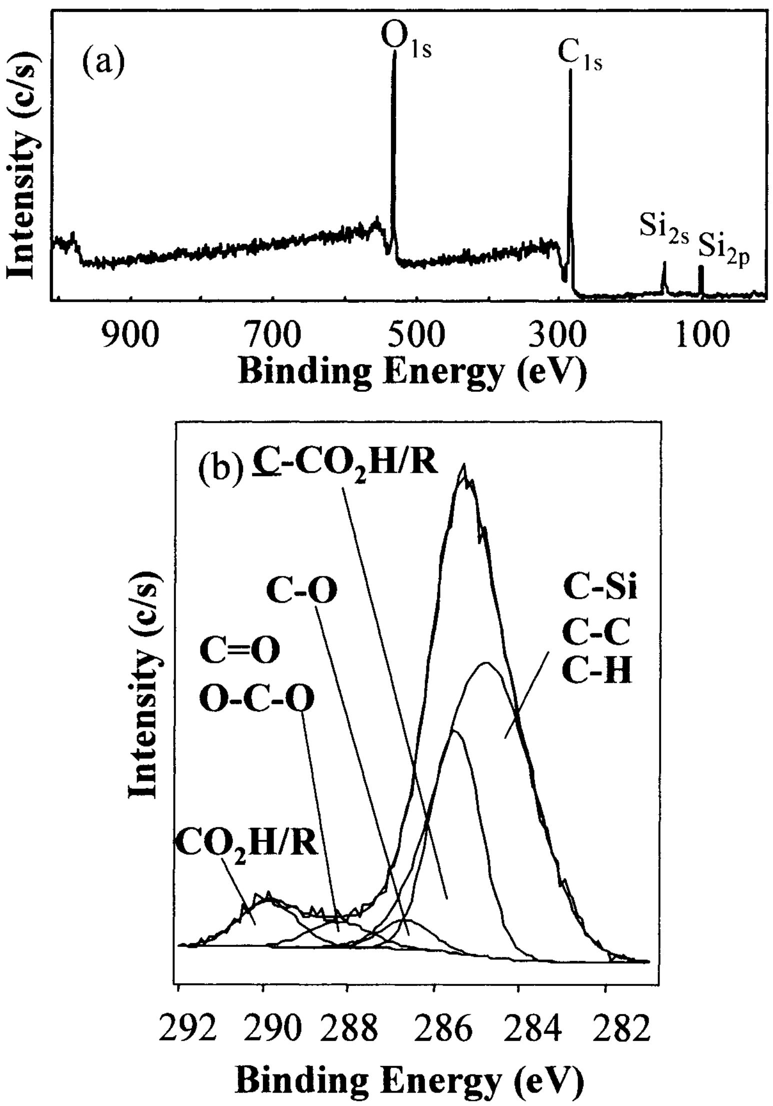

Figure 4.2 (a) Survey and (b) high resolution XPS C_{1s} spectra of PDMS coated with p-AA.

groups contribute to broader FWHMs.[17] The most interesting feature in the high resolution spectrum of p-AA is the COOH/R peak at 289.88 eV, as this is the ionizable functionality of interest in electrophoresis applications. The contribution of this moiety to the total area is 6% which indicates extensive cross-linking of the p-AA film.[22] Films deposited under less energetic conditions that result in higher retention of the AA monomer are typically water soluble, and are therefore not useful for our applications.

4.2.B Chip coatings. The surface analysis data presented above pertain to pieces of PDMS treated with different plasmas. The microfluidic devices were irreversibly sealed before plasma treatment, so a series of experiments were carried out to determine the extent of plasma modification within the reservoirs and channels. For the plasma to treat the interior of the device, the gas phase species must enter the channel via the reservoirs, or through the porous PDMS. To ascertain the extent of coverage in the channel, we performed SAM imaging of the blank of a microfluidic device. For this particular experiment, we used a Si wafer as the blank instead of PDMS to improve our imaging capabilities. The Si blank was reversibly sealed to the PDMS replica and treated with an C_3F_8 plasma. The blank was then removed and imaged using SAM; Figure 4.3 shows the F_{KLL} maps taken of the Si. F is apparent in both the reservoirs and the channel, but not outside the channel area. As the Si blank does not contain F prior to treatment, the F_{KLL} signal should exclusively appear on the area treated by the FC plasma. The presence of F in restricted areas confirms that the plasma enters the channels through the reservoirs, not through the porous PDMS. Figure 4.3a is the F_{KLL} map of the reservoir located closest to the rf coil in the reactor during the deposition. Clearly there is good coverage of the underlying Si, and the F is limited to the channel and reservoir areas that

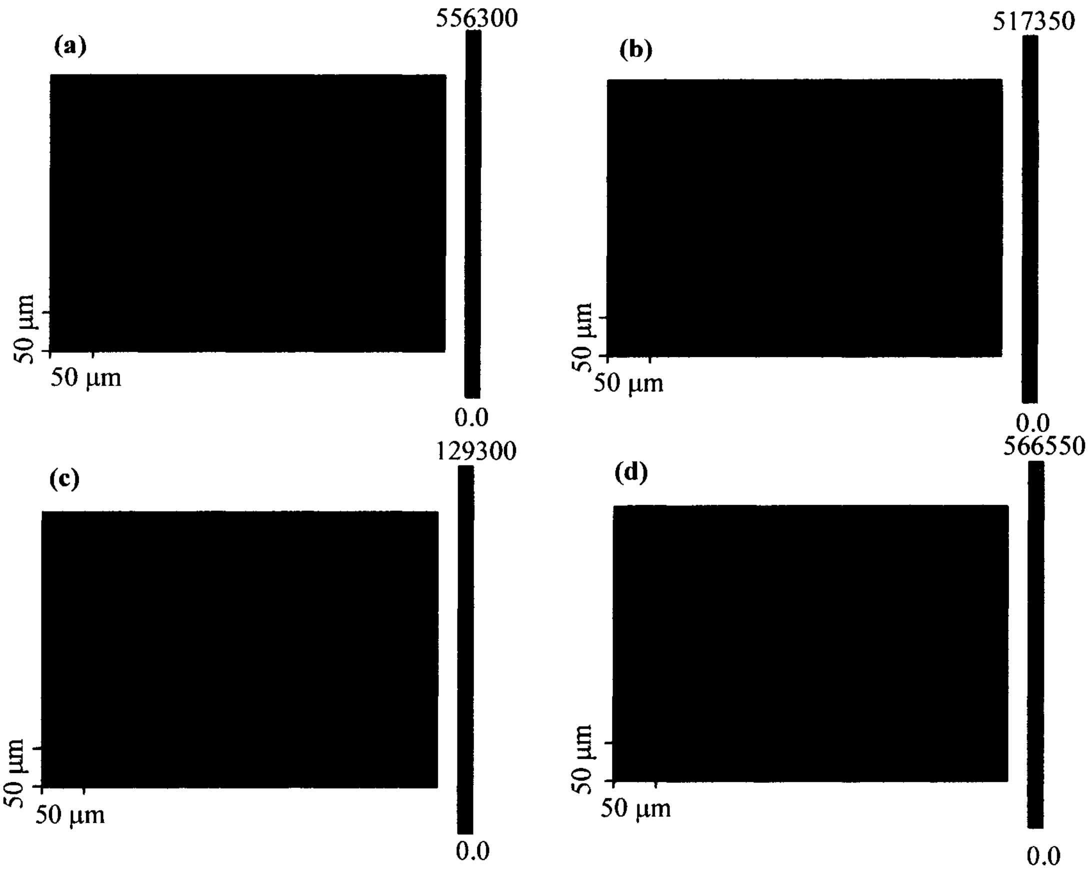

Figure 4.3 XPS maps of F_{KLL} signal of the Si base of a PDMS microchip; (a) shows the upstream reservoir and beginning of the channel; (b) and (c) are images of the channel farther downstream; and (d) is the downstream reservoir and channel.

were exposed to the plasma. Figure 4.3b is the map of the channel further downstream; full coverage of the Si is still apparent. Farther downstream, Figure 4.3c, the F_{KLL} signal becomes less intense, and there are areas without any signal. This is also true at the reservoir located downstream from the plasma source (Figure 4.3d). The areas where F is not detected suggest incomplete coverage of the channel.

Another method of determining the extent that the plasmas treat the channels in sealed devices is via dye absorption measurements. A solution of rhodamine dye was introduced into untreated and treated chips, and the width of the fluorescence across the channel was measured as a function of time (Figure 4.4). An increase in width indicates the absorption of the rhodamine dye into the PDMS. The kinetics of dye absorption for the untreated chip were sufficiently rapid that we could not obtain fluorescent images of the channel without some degree of rhodamine absorption into the channel walls. Initially, there was a rapid increase in the width (27 pixels) of the signal, which was followed by a plateau wherein the width no longer increased. After 60 minutes, the extent of absorption remained constant, Figure 4.4. The error calculated for the untreated chip was 3%; we estimate it to be similar for the plasma treated devices.
Fluorescence width measurements for a sealed chip treated only with an Ar plasma show a drastic decrease in the absorption of dye into the channel, Figure 4.4. The fluorescence width increases only slightly over time; this ability to inhibit dye absorption lasts for a minimum of five days after Ar plasma treatment. Fluorescence measurements for devices coated with FC and p-AA films that included an Ar plasma pretreatment were within error of the results for devices treated only with an Ar plasma. Samples coated with p-AA contain small cracks in the surface. These cracks are the only parts of the

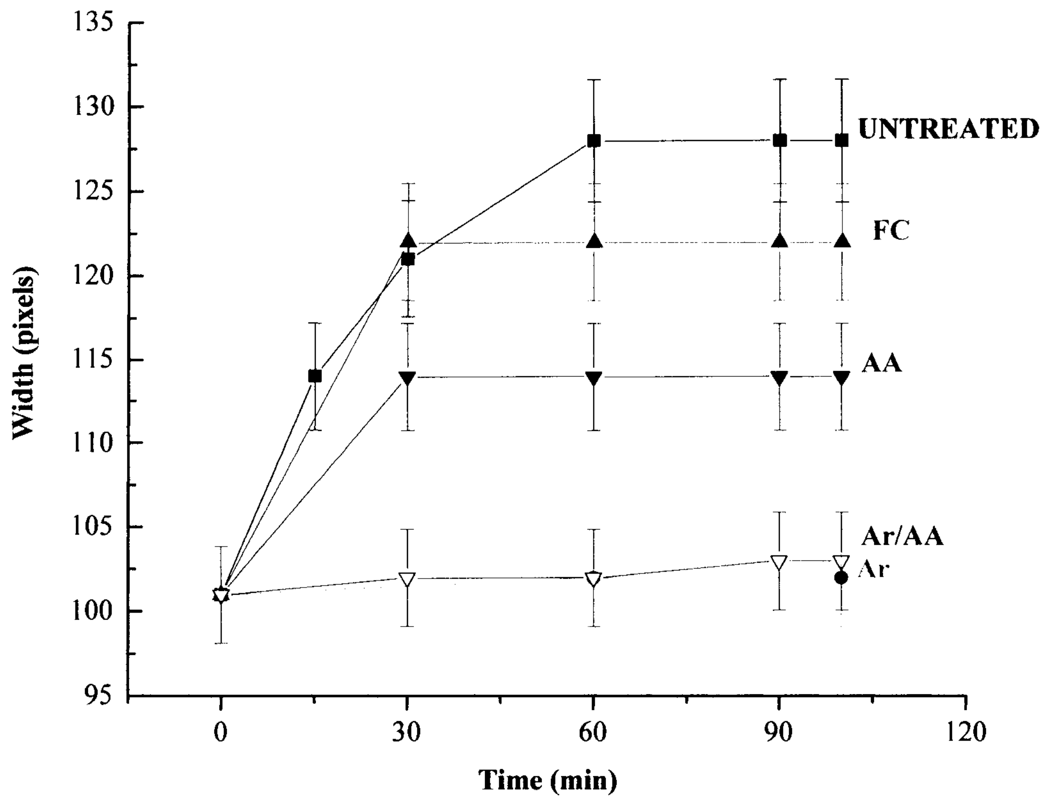

Figure 4.4 The width of the fluorescent signal of rhodamine containing buffer across the channel as a function of time for unmodified and Ar, Ar/AA, AA, and C_3F_8 plasma treated devices.

channel that fluoresce after the rhodamine solution is rinsed out, indicating that the dye absorbed into the PDMS through the cracks but did not absorb into the surface of the AA film.

Fluorescence measurements were also obtained for chips treated with either AA or FC plasmas, without an Ar plasma pretreatment. The AA treatment alone has some capacity to lower dye absorption, whereas results for the FC film resemble the untreated device, Figure 4.4. These data demonstrate that the Ar plasma pretreatment step is the critical factor for inhibiting dye absorption.

XPS data show that an Ar plasma treatment followed by exposure to atmosphere changes the surface elemental composition of PDMS by decreasing C and increasing O content, Table 4.1. This is consistent with literature results for Ar plasma treated PDMS membranes.[15] Plasma treatments based on inert gases such as Ar typically result in the formation of free radicals on the surface that recombine to cross-link the surface, and react with O_2 and N_2 after exposure to the atmosphere.[15] SEM images of Ar plasma treated PDMS (not shown) reveal surface damage (pitting, cracking) that is typical of a cross-linked polymer. Cross-linking of the PDMS surface makes it less porous, thereby limiting dye absorption. As this is a physical effect, Ar plasma treatment followed by a film deposition step also inhibits dye absorption, even when the deposited material is hydrophobic, such as the FC film. The ability of the Ar plasma treated samples to minimize absorption of a hydrophobic dye is promising in that it may also inhibit the absorption of other hydrophobic analytes, such as proteins and DNA, which would allow for their separation and detection in PDMS microchips. Further work is underway to characterize the effect of coatings on separations of proteins and peptides.

In summary, the SAM images suggest that the FC coating within the channel is incomplete; however, all of the dye absorption data show conformal treatment throughout the length of the channel. If the plasma treatment did not extend throughout the channel, there would be a broadening of the fluorescent signal where the dye solution was in direct contact with unmodified PDMS. The inhibition of dye absorption throughout the chip suggests we are able to treat the entire length of a sealed channel; however, we may not be able to image the channel with high enough resolution to verify this hypothesis completely.

4.2.C. EOF measurements. The generation of EOF in a capillary depends on the net charge density on the surface of the capillary that is in contact with the aqueous solution. This gives rise to an electrical double layer, which results in the generation of EOF in the presence of an electrical field.[21] The potential at the liquid-surface interface is known as the zeta potential, ζ, and changes affecting the zeta potential will have an effect on the EOF. For example, in PDMS chips, higher pH creates an increase in the zeta potential and therefore the EOF.[5,6] The ability to generate reproducible and controllable EOF would improve the reproducibility of analyses.

EOF of plasma treated samples was measured as a function of pH, over a 5 day period. EOF measurements of Ar plasma treated chips were within error of untreated devices up to 48 h after treatment. Figure 4.5 contains the EOF values measured in the Ar/C_3F_8 plasma treated PDMS. EOF is lowest for a newly coated chip; on day 1, there is ~ 30% reduction in EOF at all pH values. On Day 2 and beyond, EOF values are ~10% lower than untreated channels for pH 5 and pH 7, and ~21% lower at pH 9. The variation in EOF for untreated devices is 32.3% between pH 5 and 9. The change in EOF in

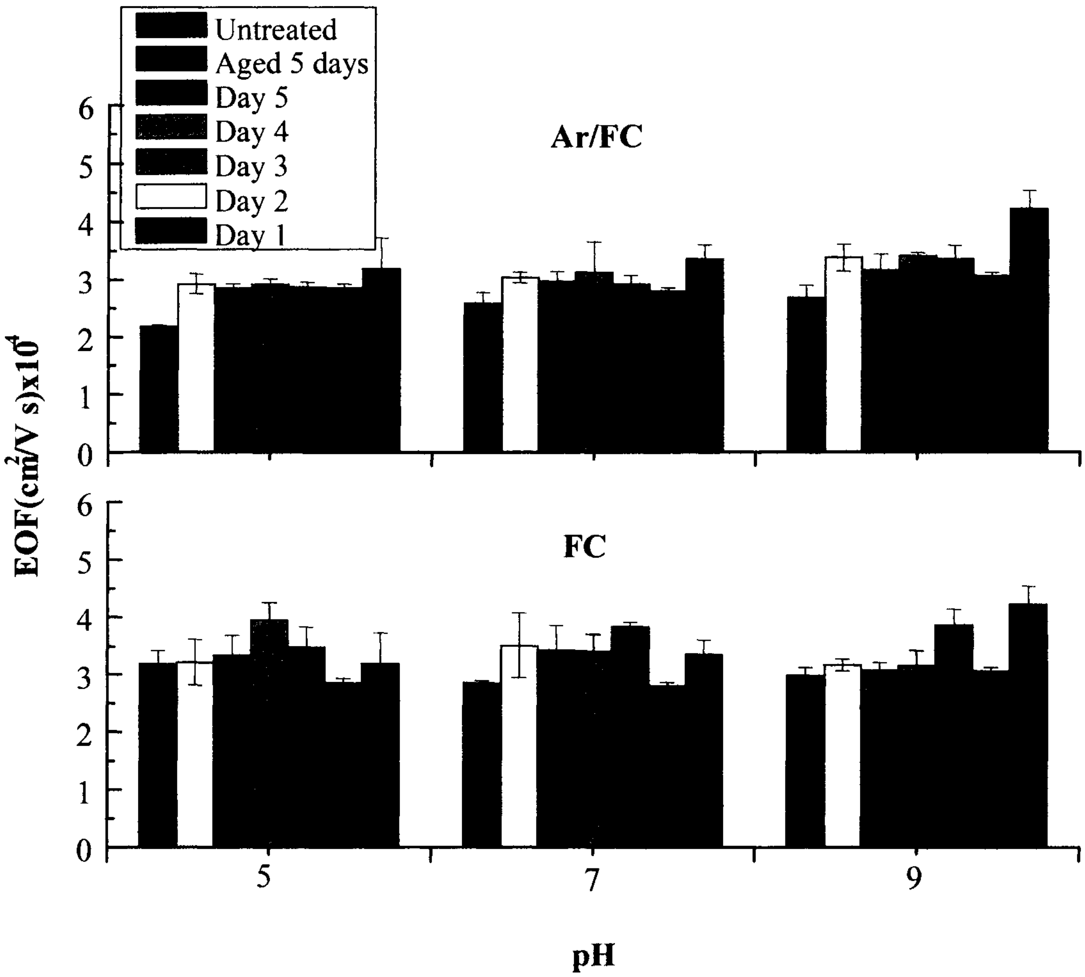

Figure 4.5 EOF values for C_3F_8 plasma treated microchips as a function of pH and age of sample. The EOF of an unmodified device is shown for comparison.

treated devices, however, is less than that observed in the uncoated channel: the variation between pH 5 and 9 is 23% on Day 1, but decreases to less than 17% after this. The aged chip had a 7.4% variance in EOF for this pH range. Note that the EOF measured on an aged Ar/C_3F_8 treated chip is within error of devices used multiple times, which suggests that some stabilization of the surface occurs within the first 24 h of treatment. Additionally, twelve consecutive runs of the chip yielded a constant EOF, indicating the coating is quite robust. EOF values for a microchip treated only with an C_3F_8 plasma have greater daily fluctuations, and are ~13 % higher than those measured in the Ar/C_3F_8 plasma treated device, Figure 4.5. This shows that the Ar plasma pretreatment increases the stability of the FC coating.

Overall, these data show that the Ar/FC treatment leads to a decrease in EOF, and an increase in the stability of the EOF with respect to pH. In comparison to previous work involving dynamic coatings, the Ar/FC plasma treatment is on par with anionic polybrene (PB-) coated devices (variation of 17.7 % between pH 5 and 10), but less effective than the cationic polybrene/dextran sulfate (PB/DS) coated devices (1.6% between pH 6 and 10).[23]

The reduction in EOF seen in FC plasma treated microchips indicates that the treatment reduces the zeta potential across the pH range tested. The source of EOF in both native and oxidized PDMS is a subject of interest in the literature.[24] For plasma oxidized PDMS, silanol groups are suggested as the source of the charge for EOF.[4] The change in EOF with pH is well characterized with higher pH buffer resulting in higher EOF. The FC coating should not have any SiO_x ionizable groups. Although the EOF is reduced with FC coatings, it is still supported, which could be caused by incomplete coverage of the surface. Alternatively, the underlying negative charges from the PDMS may be exerting their influence on the solution through the thin film. This behavior has been seen before for polyelectrolyte coatings on fused silica capillaries.[25] The stability of the EOF with changing pH suggests that the coating is complete enough to control the surface charge along the channel. Greater EOF stability with changing pH is a benefit to analysis, as changes in migration time with pH would not occur. The exact mechanism involved in generation of the zeta potential is not known at this time but is under investigation in the Henry group.

Figure 4.6 shows the EOF for Ar/AA treated chips at different pH. This treatment produces a 17% increase in EOF compared to untreated PDMS at pH 9. At pH 7, the EOF remains unchanged (0.003%) and there is a reduction in EOF at both pH 4 (37%) and pH 5 (31%). The largest decrease in EOF occurs at pH 4, the value where the buffer pH is lower than the pKa of AA (pKa = 4.25).[26] Both this result and the pH dependence of the EOF suggest some retention of the acid functionality in the p-AA film, consistent with XPS results (Figure 4.3b). When a weak acid is at a pH below its pKa, most sites are protonated, which reduces the negative surface charge, resulting in a low EOF. At pH 5 only partial deprotonation occurs and the surface charge will be dominated by the neutral acrylic acid, resulting in a lower EOF than untreated. The EOF at pH 7 is almost identical to that of an untreated chip, which may be due to equivalent charged sites being created both from deprotonation of the acid and charging of silanol groups within the PDMS. An increased EOF at pH 9 may be due to the large number of deprotonated sites of the AA and the charging of silanol groups in the PDMS, resulting in a higher EOF than the native PDMS. The variability of the EOF across the pH range may provide the

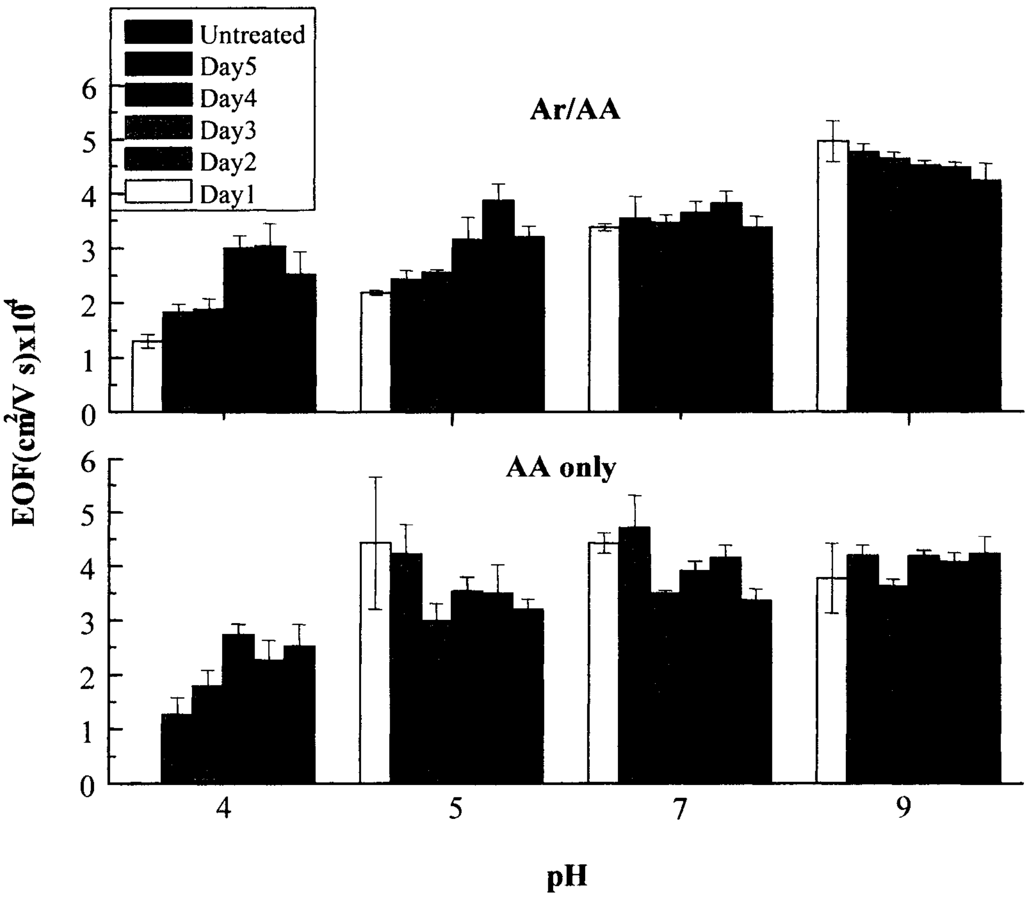

Figure 4.6 EOF values for AA plasma treated microchips as a function of pH and age of sample. The EOF of an unmodified device is shown for comparison.

possibility for tuned EOF.

The durability of the AA coating is inferior to the FC coating and required the use of an Ar pretreatment to obtain a usable stability (Figure 4.6). After 3 days, for Ar/AA treated devices, EOF values return to that of an untreated chip, indicating loss of coating. This agrees with the XPS data (Table 4.1) that revealed a substantial loss of film after exposure to buffer. However, loss of EOF control occurs regardless of use of the chip: EOF measured for the first time on a device 5 days after plasma treatment had a similar EOF to an untreated device, which demonstrates a lack of film stability in air. EOF values were also measured for chips treated with an AA plasma, without the Ar plasma pretreatment, Figure 4.6. These values have the greatest variance over the pH range studied in this work. The same general trend for EOF vs. pH was seen as for the Ar/AA coating, but with more significant daily changes. Note that the addition of the Ar pretreatment resulted in only 3 days of stability; further efforts are being directed towards developing a more stable AA coating.

4.3. Conclusions

We have demonstrated that PECVD can be used to treat preassembled polymer microfluidic devices, resulting in modified EOF. An Ar plasma pretreatment was used to increase the stability of both the FC and p-AA coatings. The Ar plasma treatment was also found to be important for reducing dye absorption. Experiments currently underway in our laboratories are exploring separations within these systems, alternate coatings, and non-depositing plasmas as a way to alter the hydrophobicity of the PDMS.

References

1. Quake, S. R.; Scherer, A. *Science* **2000**, *290*, 1536.
2. Duffy, D. C.; McDonald, J. C.; Schueller, O. J. A.; Whitesides, G. M. *Anal. Chem.* **1998**, *70*, 4974.
3. Martin, S. R.; Gawron, A. J.; Lunte, S. M.; Henry, C. S. *Anal. Chem.* **2000**, *72*, 3196.
4. Hu, S.; Ren, X.; Bachman, M.; Sims, C. E.; Li, G. P.; Allbritton, N. *Electrophoresis* **2003**, *24*, 3679.
5. Harrison, D. J. *Electrophoresis* **2000**, *25*, 107.
6. Henry, C. S.; Liu, Y.; Bledsoe, J. M.; Hopkins, C. D. *Abstracts of Papers - American Chemical Society* **2001**, *221st*, ANYL.
7. Xiao, D.; Le, T. V.; Wirth, M. J. *Anal. Chem.* **2004**, *76*, 2055.
8. d'Agostino, R.; Cramarossa, F.; Fracassi, F. Plasma Polymerization of Fluorocarbons. In *Plasma Deposition, Treatment, and Etching of Fluorocarbons*; d'Agostino, R., Ed.; Academic Press, Inc.: San Diego, 1990; pp 95.
9. Steen, M. S.; Hymas, L.; Havey, E. D.; Capps, N. E.; Castner, D. G.; Fisher, E. R. *J. Membr. Sci.* **2001**, *188*, 97.
10. Steen, M. S.; Jordan, A. C.; Fisher, E. R. *J. Membr. Sci.* **2002**, *204*, 341.
11. Wavhal, D. S.; Fisher, E. R. *J. Polym. Sci., Part B: Polym. Phys.* **2002**, *40*, 2473.
12. Williams, R. L.; Wilson, D. J.; Rhodes, N. P. *Biomaterials* **2004**, *25*, 4659.
13. Egitto, F. D.; Matienzo, L. J. *IBM J. Res. Develop.* **1994**, *38*, 423.
14. Martin, I. T.; Malkov, G. S.; Butoi, C. I.; Fisher, E. R. *J. Vac. Sci. Technol. A* **2004**, *22*, 227.
15. Matsuyama, H.; Teramoto, M.; Hirai, K. *J. Membr. Sci.* **1995**, *99*, 139.

16. Steen, M. L.; Flory, W. C.; Capps, N. E.; Fisher, E. R. *Chem. Mater.* **2001**, *13*, 2749.

17. Sandrin, L.; Silverstein, M. S.; Sacher, E. *Polymer* **2001**, *42*, 3761.

18. Lee, W. W.; Ho, P. S. *MRS Bulletin* **1997**, 19.

19. Malkov, G. S.; Martin, I. T.; Schwisow, W. B.; Chandler, J. P.; Fisher, E. R. *Chem. Mater.* **2004**, *submitted.*

20. Delacorte, A.; Befahy, S.; Poleunis, C.; Troosters, M.; Bertrand, P. *Adhesion Aspects of Thin Films* **2004**, *2*, 1.

21. Kirby, B. J.; Hasselbrink Jr., E. F. *Electrophoresis* **2004**, *25*, 187.

22. Candan, S.; Beck, A. J.; O'Toole, L.; Short, R. D. *J. Vac. Sci. Technol. A* **1998**, *16*, 1702.

23. Liu, Y.; Fanguy, J. C.; Bledsoe, J. M.; Henry, C. S. *Anal. Chem.* **2000**, *72*, 5939.

24. Wheeler, A. R.; Trapp, G.; Trapp, O.; Zare, R. N. *Electrophoresis* **2004**, *25*, 1120.

25. Sui, Z.; Schlenoff, J. B. *Langmuir* **2003**, *19*, 7829.

26. Harris, D. C. *Quantitative Chemical Analysis*, 6th ed.; Freeman and Company: New York, 2003.

CHAPTER 5

ION EFFECTS ON CF_2 SURFACE INTERACTIONS DURING C_3F_8 AND C_4F_8 PLASMA PROCESSING OF SILICON

Reprinted with permission from: I. T. Martin and E. R. Fisher, Journal of Vacuum Science and Technology A **22 (5)**, 2168 (2004).

This dissertation chapter contains results from a full paper cited above. The manuscript was written by Ina T. Martin and edited by Ellen R. Fisher. This chapter describes the effect of ions on CF_2 surface production during C_3F_8 and C_4F_8 plasma processing of Si substrates. Additionally, it describes a positive correlation found between CF_2 surface production and the composition of FC films deposited in both the IRIS apparatus and independent reactors.

5.1. Introduction

Fluorocarbon (FC) plasmas are widely used industrially for both etching and deposition schemes. Recently, FC plasma etch processes have moved from smaller monomers such as CF_4 and C_2F_6 to larger monomers such as C_3F_8 and C_4F_8.[1] The etch procedures that use these larger FC monomers have an increased efficiency, which makes them both more environmentally friendly and more cost effective. Etch selectivity between materials frequently depends on the different film deposition rates that occur on different substrates.[2] Multiple studies of materials deposited from C_3F_8 and C_4F_8 plasmas are available in the literature,[3-9] focusing on film composition and properties. C_4F_8 plasma polymerization processes are of particular interest due to the use of C_4F_8 plasmas in the polymerization step of the Bosch process.[10] As plasma monomer sizes increase, so do the types of gas phase species created and the number of possible surface interactions. As a result, understanding the underlying chemistry of both etch and deposition processes becomes more complicated.

One species that is often studied in FC systems is CF_2 because its role as an etch product or deposition precursor appears to change, depending on the plasma system and type of substrate being processed. For example, both CF_x (including CF_2) and C_xF_y radicals have been cited as FC polymer deposition precursors in rf and ultra high frequency FC plasmas.[11,12] In other systems, however, evidence indicates that CF_2 is not a deposition precursor. Measurements of the spatial distribution of absolute CF_2 radical densities in C_4F_6 and C_3F_6 ECR (electron cyclotron resonance) plasmas demonstrated that CF_2 radicals do not contribute directly to FC film growth.[13] These results are in good agreement with calculations by Goto and coworkers for C_4F_8 ECR plasmas, which revealed that C_xF_y ($x \geq 2$) molecules are important polymer precursors over CF_x ($x = 1$-3) species.[14] This ambiguity in the literature makes it important to study the behavior of CF_2 in each type of FC system.

We have previously used our IRIS technique to investigate CF_2 surface interactions in predominantly etching vs. depositing FC plasma systems. In general, IRIS measures the fraction of molecules scattering off of a surface, relative to those impacting the surface in the molecular beam for a particular species. This ratio, the scattering coefficient, S, is related to the surface reactivity, R, by $R = 1\text{-}S$. Thus, IRIS measurements allow the determination of a net surface loss, ($S < 1$), net surface production ($S > 1$), or unit scattering ($S = 1$) for an individual species during plasma processing. Surface scattering coefficients for CF_2 molecules, $S(CF_2)$, have been measured in our laboratory for a range of FC plasma systems [CF_4, C_2F_6, C_2F_6/H_2, CHF_3, and hexafluoropropylene oxide (HFPO)] during the plasma processing of a variety of substrates (Si, SiO_2, Si_3N_4, polyimide, photoresist, and stainless steel).[15-18] Several generalizations can be made about the results obtained for these systems. Slowly depositing systems such as HFPO have $S(CF_2) \sim 1$, a lower value than that measured in etch systems such as 100% C_2F_6. Highly depositing systems such as 50/50 C_2F_6/H_2 had $S(CF_2) < 1$, suggesting that CF_2 is a deposition precursor in these systems. Etching FC systems not only had S (CF_2) >> 1, but the S values are substrate dependent, most likely because the plasma is interacting directly with the substrate, unlike depositing systems, wherein the plasma is interacting with the deposited films, the composition of which is independent of the substrate. Additionally, ions have been shown to contribute to CF_2

surface production during HFPO plasma processing of Si, Cu, and polytetrafluoroethylene (PTFE), and during C_2F_6 plasma processing of Si.[17]

This work focuses on IRIS studies of CF_2 in C_3F_8 and C_4F_8 plasmas, which are part of the current generation of industrially relevant plasma monomers. We have two primary foci, the first of which is to determine if $S(CF_2)$ values can be used as an overall gauge for the predominant plasma regime, etching vs. deposition, in these larger FC systems. The second is to determine the effects of ions on S (CF_2) in these systems. Earlier work has shown that ions are key contributors to CF_2 surface production in both HFPO and C_2F_6 plasma systems,[17] but this is the first FC system in which we have been able to identify the ions created in the plasmas, and relate them to our $S(CF_2)$ values.

5.2. Results

5.2.A. Gas phase analysis. Both LIF and plasma ion mass spectrometry were used to study the gas phase composition of 100% C_3F_8 and C_4F_8 plasmas. Figure 5.1 shows the LIF excitation spectrum collected from 230.000 – 238.000 nm in 0.025 nm increments from a 50 W C_3F_8 plasma. Comparison to the literature verifies that the fluorescing species is indeed CF_2.[19,20] The predominant feature in this spectrum is the $(0,11,0)\rightarrow(0,0,0)$ band of the A^1B_1-X^1A_1 transition, which was used to collect the CF_2 density and reactivity data. Similar excitation spectra have been collected for C_4F_8 plasma molecular beams in the IRIS apparatus.

Figure 5.2a shows the relative density of CF_2 in C_3F_8 and C_4F_8 plasmas as a function of P with and without a grounded mesh in the path of the molecular beam. For all systems, increasing P leads to greater CF_2 production in both plasmas; this is

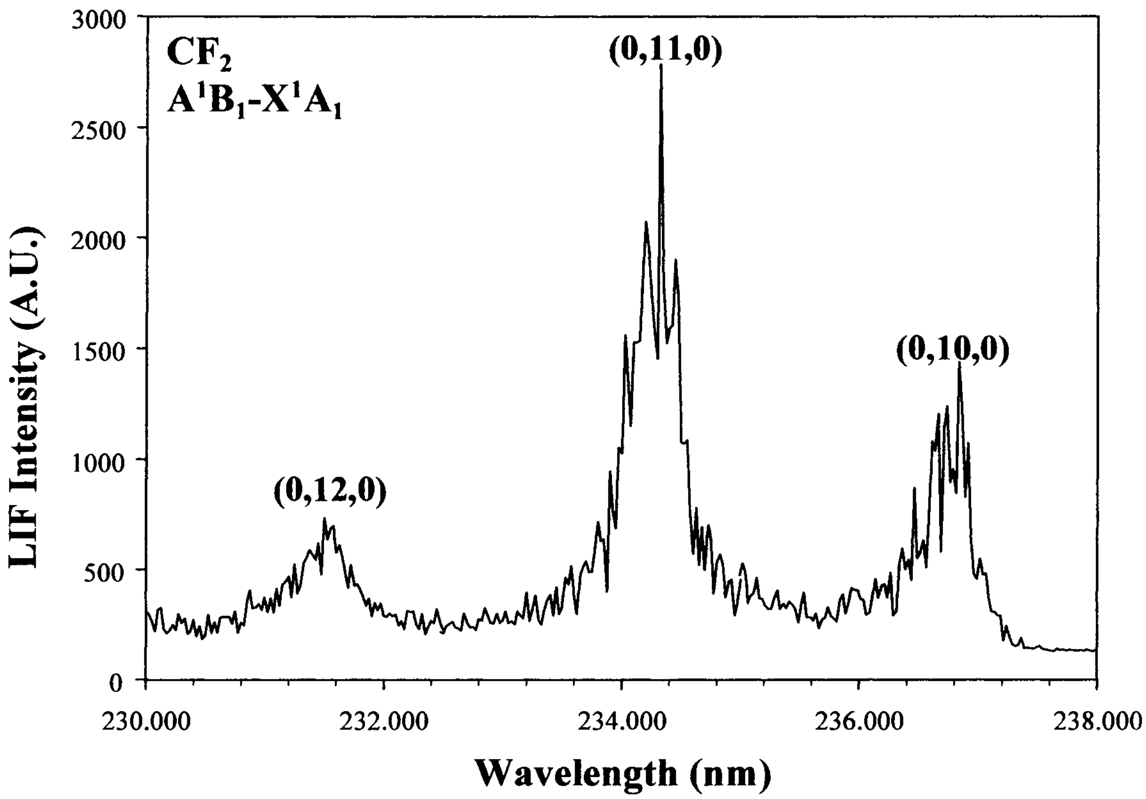

Figure 5.1 Experimental fluorescence excitation spectrum of CF_2 in the molecular beam formed from a 50 W C_3F_8 plasma. The transition used for all density and reactivity meaurements was the (0,11,0)→(0,0,0) vibronic band of the A^1B_1-X^1A_1 transition.

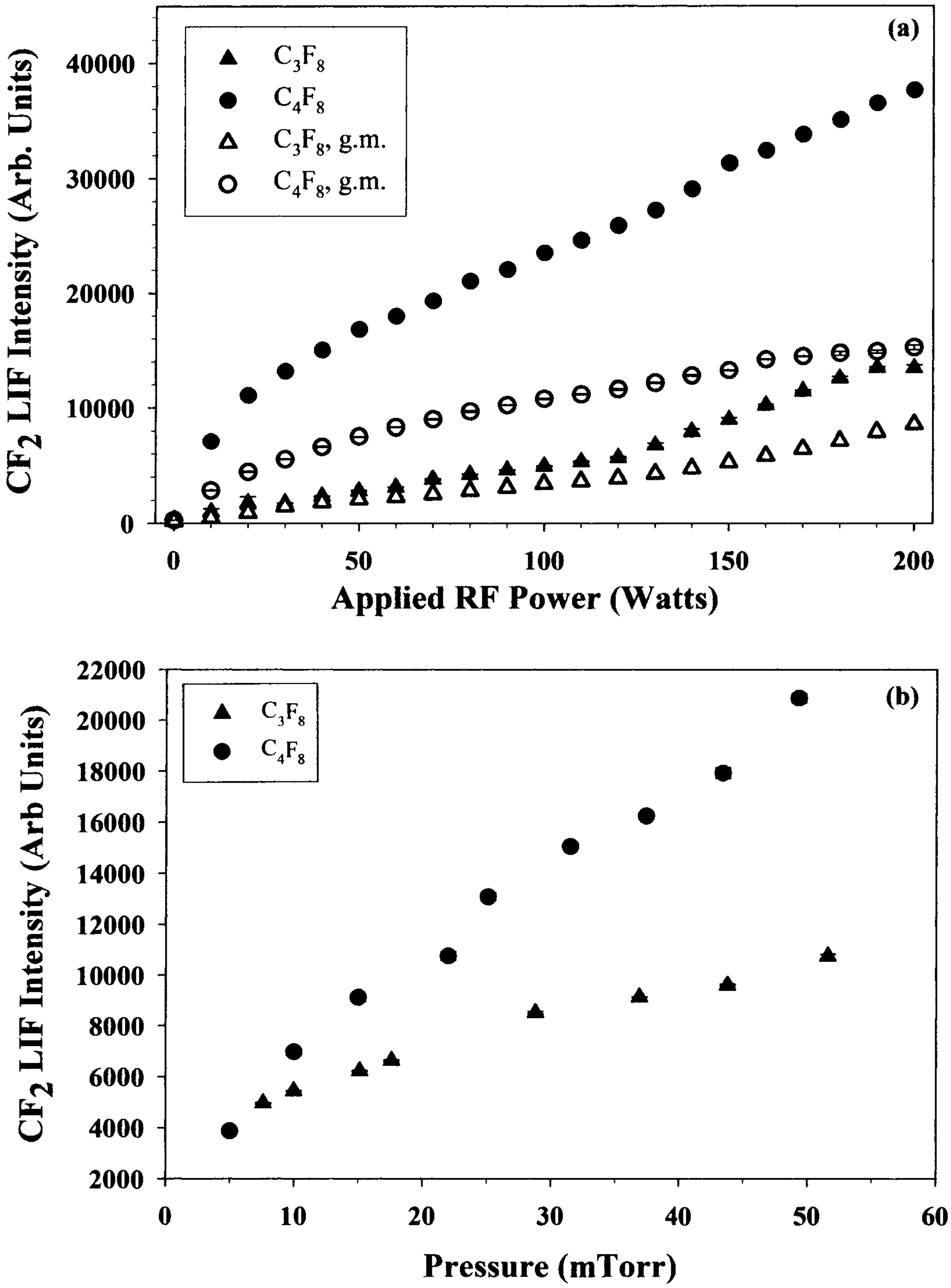

Figure 5.2 Relative LIF intensities of CF_2 radicals in C_4F_8 (circles) and C_3F_8 plasmas (triangles) as a function of (a) applied rf power and (b) pressure. Open symbols indicate data taken with a grounded mesh (g.m.) in the path of the molecular beam.

attributed to increased fragmentation of the monomer. Similar trends were also observed for 100% C_2F_6 and HFPO plasmas in our IRIS experiments.[16,17] Overall, C_4F_8 plasmas produce more CF_2 than C_3F_8 plasmas, most likely because the structure of C_4F_8 consists of a cycle of four CF_2 units. Earlier work has shown that the cyclic structure of the C_4F_8 monomer allows for more extensive fragmentation within the plasma than what occurs with the linear C_3F_8 monomer.[9] CF_2 densities measured with a grounded mesh in the path of the molecular beam are lower at all P in both systems, as shown in Figure 5.2a. We attribute this to the grounded mesh acting as a partial physical barrier to plasma species, in addition to being a barrier to charged species. Figure 5.2b shows the relative CF_2 densities in 25 W C_3F_8 and C_4F_8 plasmas as a function of pressure. In both systems, increased CF_2 production occurs with increasing pressure, and C_4F_8 plasmas produce more CF_2 than the C_3F_8 plasmas do at all pressures.

5.2.B. Surface interactions of CF_2. Figure 5.3 shows a series of ICCD images of CF_2 LIF from a 75 W C_3F_8 plasma. Figure 5.3a contains the LIF signal from CF_2 molecules present only in the molecular beam. For Figure 5.3b, a Si substrate was rotated into the path of the molecular beam, so the LIF signal imaged is from CF_2 molecules present in both the molecular beam and those scattered off the surface. Figure 5.3c is the difference between Figures 5.3b and 5.3a, and shows only the CF_2 molecules scattered off the substrate surface. Clearly, there is some surface production of CF_2. To quantify the amount of CF_2 scatter, 20 columns of pixels were averaged and this was plotted as a function of distance along the laser axis to yield the plots shown in Figure 5.4. The dashed lines in Figure 5.4 are the simulated curves for the incident beam and scattered molecules, assuming an adsorption-desorption mechanism, with $S = 1.33$.

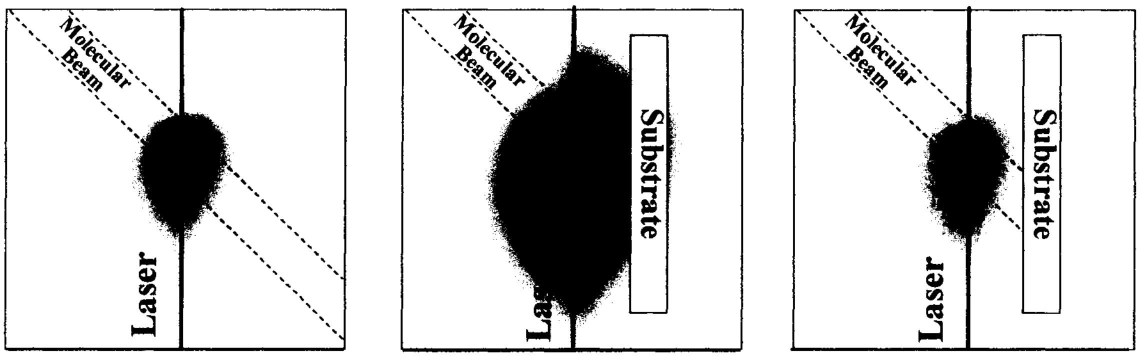

(a) (b) (c)

Figure 5.3 Spatially resolved 2D ICCD images of the LIF signal for the CF_2 A^1B_1 (0,11,0)→(0,0,0) state (a) in the 75 W C_3F_8 molecular beam and (b) with a Si substrate rotated into the path of the molecular beam (laser-surface distance = 3.1 mm). The image in (c) is the difference between (a) and (b) and shows only the CF_2 molecules scattering from the surface. LIF signals with the highest intensity appear as the darkest regions, and lines indicate the location of the molecular and laser beams. All images are on the same intensity scale.

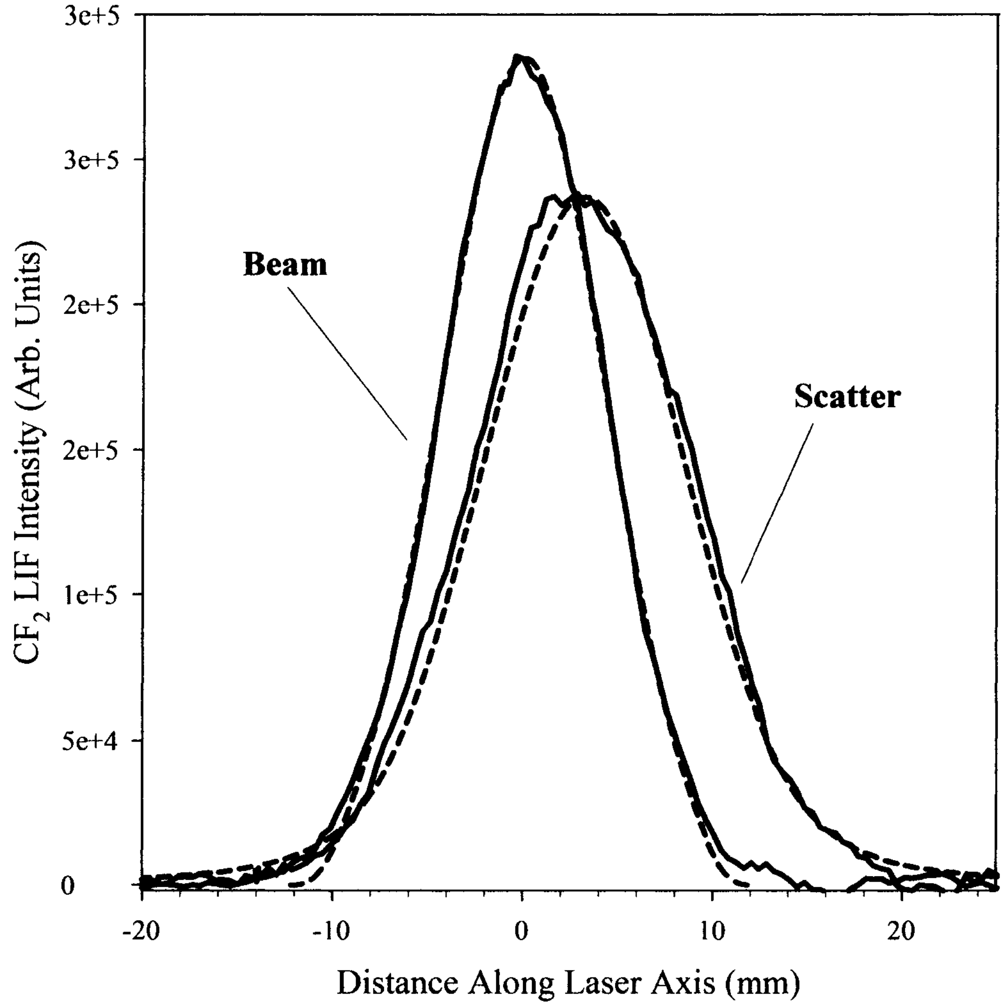

Figure 5.4 Cross-sections of the CF_2 LIF images shown in Figures 5.3a and c (solid lines). Dashed lines represent the simulation results for $S = 1.33$ with a laser-surface distance of 3.1 mm.

Averaging multiple data sets taken over a five month period yields $S = 1.34 \pm 0.11$ for this set of parameters.

Figure 5.5a is a plot of *S* values measured for CF_2 during C_3F_8 plasma processing of Si as a function of *P* with and without the grounded mesh in the path of the molecular beam. For the unperturbed system, $S(CF_2)$ clearly increases at higher *P*. Placing the grounded mesh into the path of the molecular beam leads to a decrease in $S(CF_2)$ at all *P*, and $S(CF_2) \sim 1$ for $P \leq 100$ W. This unmistakably demonstrates that ions make a significant contribution to CF_2 surface production.

Figure 5.5b shows *S* values measured for CF_2 during C_4F_8 processing of Si as a function of *P* with and without the grounded mesh in the path of the molecular beam. Trends similar to those in the C_3F_8 system are observed with C_4F_8: $S(CF_2)$ increases with *P* for the unperturbed system, and there is a significant reduction in *S* values measured under ion-limited conditions. Note that the power dependence of $S(CF_2)$ is less clear in the C_4F_8 system, the $S(CF_2)$ values appear to level off at higher *P*. Overall, $S(CF_2)$ for C_4F_8 plasmas are higher than those for C_3F_8 plasmas under the same experimental conditions. Additionally, $S(CF_2)$ for a 50 W C_4F_8 plasma with a lower input gas pressure (~15 mTorr) is considerably higher than that measured at higher pressures (~45 mTorr), Table 5.1. For discussion purposes, the S (CF_2) values from Figure 5.5, as well as those previously measured from other FC plasma systems,[15,17] are also listed in Table 5.1.

5.2.C PI-MS data. Plasma ion-mass spectrometry (PI-MS) involves the identification of nascent ions created in the plasma systems. In this work, ions created in C_3F_8 and C_4F_8 plasmas were identified by collecting MS data with the ionizer off. In this setting, the MS functions solely as a detector, thereby allowing the identification of

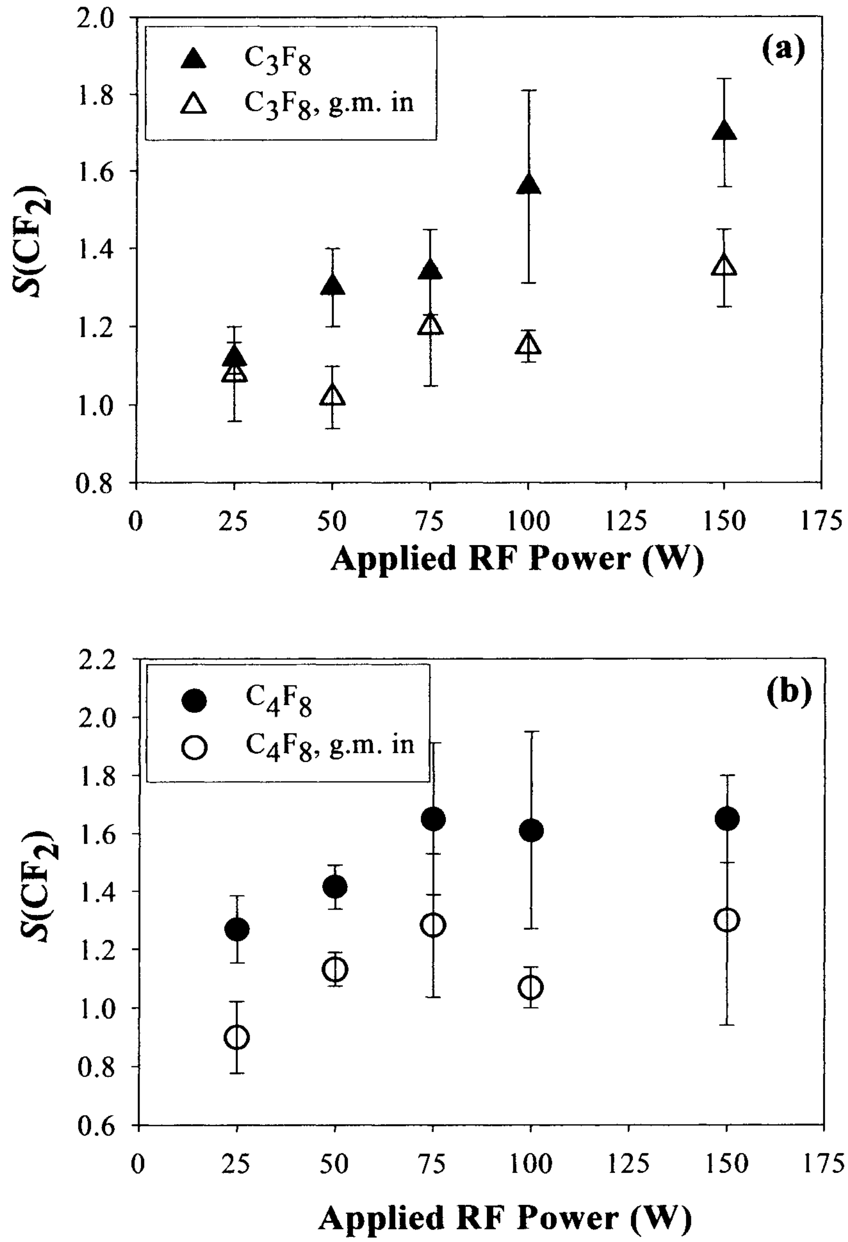

Figure 5.5 Scatter coefficients (*S*) for CF_2 during (a) C_3F_8 and (b) C_4F_8 plasma processing of Si. Open symbols represent measurements taken with a grounded mesh in the path of the molecular beam. Values are the averages of multiple data sets taken over a 2 year time period.

Table 5.1. CF_2 scatter coefficients for FC plasma processing of Si.[a,b]

Plasma	Pressure (mTorr)	25 W	50 W	75 W	100 W	150 W	200 W
CHF_3 [15]	25	----	1.65 (0.03)	----	1.83 (0.05)	----	----
C_2F_6 [17]	25	----	1.44 (0.03)	----	----	----	----
C_2F_6, g.m. [17]	30	----	1.07	----	----	----	
50/50 C_2F_6/H_2 [17]	30	----	0.84 (0.02)	----	----	----	----
HFPO [17]	45	0.97 (0.03)	----	----	1.15 (0.03)	----	1.29 (0.05)
C_3F_8	45	1.12 (0.04)	1.30 (0.10)	1.34 (0.11)	1.56 (0.25)	1.70 (0.14)	
C_3F_8, g.m.	45	1.08 (0.12)	1.02 (0.08)	1.20 (0.15)	1.15 (0.04)	1.35 (0.10)	
C_4F_8	45	1.27 (0.12)	1.42 (0.08)	1.65 (0.26)	1.61 (0.34)	1.65(0.15)	----
C_4F_8, g.m.	45	0.90 (0.12)	1.13 (0.06)	1.28 (0.25)	1.07 (0.07)	1.3 (0.36)	----
C_4F_8	15	----	1.90 (0.14)	----	----	----	----

[a]Values for C_3F_8 and C_4F_8 are averages for 2-8 data sets, with each data set being the average of multiple images. One standard deviation from the mean is shown in parentheses after the *S* values.
[b]Reference numbers for previously published data are located in brackets after plasma source.
*$S(CF_2)$ for HFPO were collected at 35 W and 135 W instead of at 25 W and 100 W

nascent ions. Previous work in our group examined the effect of ions on CF_2 surface production for C_2F_6 and HFPO plasmas.[17] Ion-limiting techniques have included placing a grounded mesh in the path of the plasma molecular beam to remove charged species, using pulsed plasma sources to minimize ion production in the beam source, and biasing the substrate (negatively or positively) to deflect positive or negative ions.[17] C_3F_8 and C_4F_8 are the first FC plasma systems wherein we have also been able to identify the ions created within the plasma, which allows us to more specifically explore their role in CF_2 surface production.

The distributions of ions within the plasma systems are clearly dependent on the feed gas, Figure 5.6. Figure 5.6a contains the mass spectrum of ions in a 100 W C_4F_8 plasma molecular beam: the predominant ionic species is CF^+. Figure 5.6b shows the mass spectra of ions in a 100 W C_3F_8 plasma molecular beam collected with and without a grounded mesh in the path of the molecular beam. The predominant ion under both conditions is CF_3^+. Note that there is a significant reduction in plasma ion transmission with the grounded mesh, demonstrating the effectiveness of this method for reducing ion bombardment of the surface. Despite the lower signals, relative peak intensities do not change significantly, suggesting that higher mass ions are transmitted at the same rate as lower mass ions. Previous work identified ions in both C_3F_8 and C_4F_8 plasma molecular beams as a function of P.[21] For both systems, as P increases, the relative intensities of CF_x^+ species increase, and the relative intensities of $C_xF_y^+$ species decrease, indicating greater fragmentation of the monomer gas.

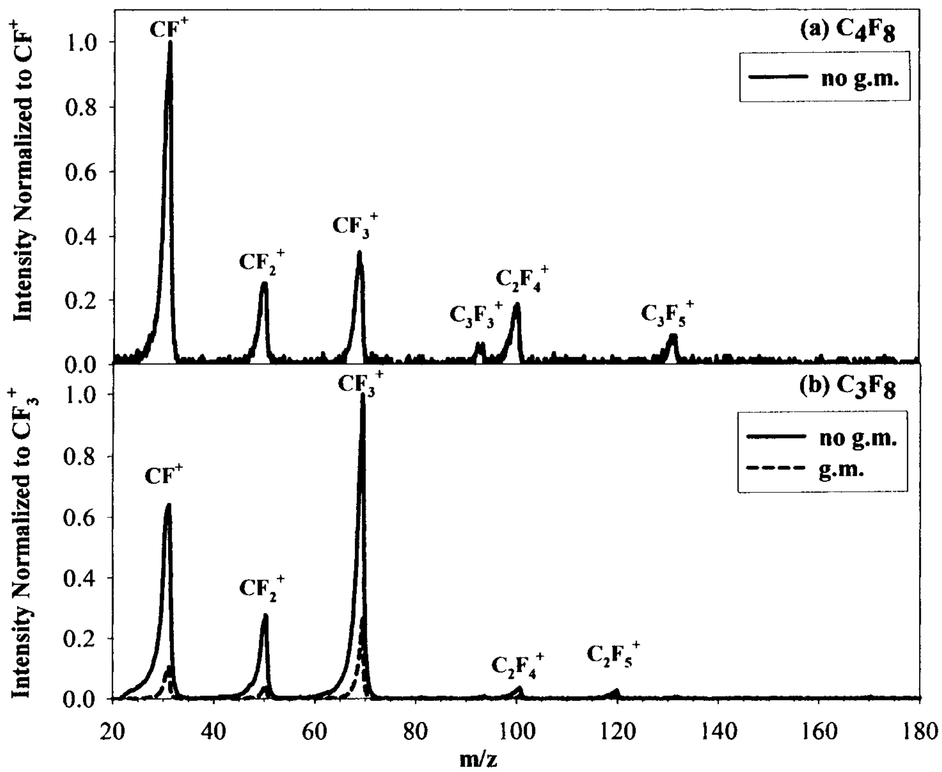

Figure 5.6 Plasma-ion mass spectra of ions from (a) a 100 W C_4F_8 plasma molecular beam, and (b) a 100 W C_3F_8 plasma molecular beam under normal (solid line) and ion-limited conditions (dashed line). Data are normalized to the most intense ion in the spectrum taken without a grounded mesh in the path of the molecular beam.

5.2.D. Surface analysis. To determine the effects of plasma treatment on the surface, XPS analysis was performed on Si samples treated in the IRIS chamber. After treatment, the IRIS chamber was purged with N_2 and the samples were transferred to the XPS chamber within five minutes. Figure 5.7 shows the high resolution C_{1s} XPS spectra of materials deposited from 50 and 150 W C_4F_8 plasma molecular beams. Both systems deposit crosslinked, amorphous fluorocarbon films. Table 5.2 shows the elemental composition of materials deposited on IRIS substrates with C_4F_8 plasma molecular beams. All materials have F/C ratios of 0.9 – 1.0. The essentially trace levels of Si indicate that the substrate is completely covered, suggesting that the plasma is interacting only with the deposited FC material.

Ideally, we should be able to directly compare films deposited in our plasma reactors to those deposited in the IRIS apparatus. Indeed, in other systems, we have explicitly shown this to be true. In the C_3F_8 and C_4F_8 systems, however, there are some minor differences in film composition between IRIS substrates and materials deposited 8 cm downstream from the coil in our cylindrical glass plasma reactor.[9] In general, the materials deposited in the IRIS chamber have lower F/C ratios and are more crosslinked than those deposited directly in the plasma reactor. This is attributed to the difference in pressure regimes between the two apparatuses, which is caused by different pumping capabilities.* The plasma source for the IRIS has a pressure of ~45 mTorr with a flow rate of 10 sccm, whereas the plasma reactor used for downstream depositions operates at a pressure of ~200 mT under the same flow conditions. Lower plasma pressures

* This point is supported in Chapter 6, which discusses ion energy data collected after publishing this work. Briefly, ion energies were shown to be inversely proportional to the pressure of the FC plasmas. Higher ion energy measurements result in the deposition of more crosslinked materials, therefore lower plasma pressures result in the deposition of more crosslinked materials.

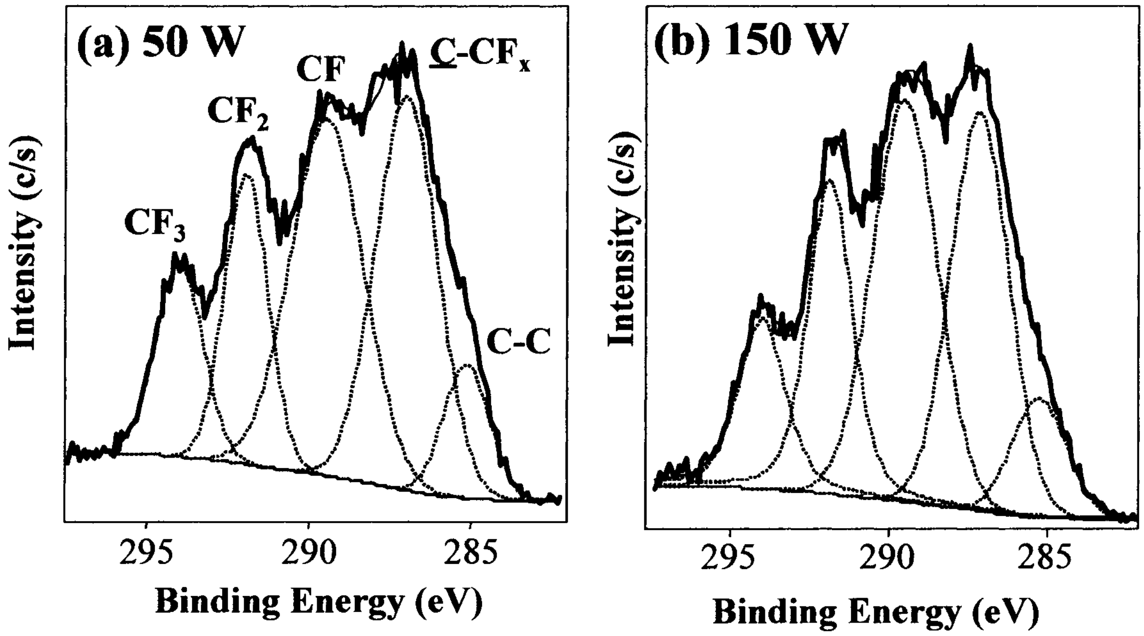

Figure 5.7 High resolution XPS C_{1s} spectra of materials deposited on Si wafers in the IRIS chamber from (a) 50W and (b) 150 W C_4F_8 plasmas.

Table 5.2. Composition of fluorocarbon materials deposited on IRIS substrates.[a]

P (W), source gas	%C	%F	%O	%Si	F/C
25, C_4F_8	50.6 (2.0)	43.7 (2.0)	3.4 (0.1)	1.8 (0.7)	0.87 (0.07)
50, C_4F_8	49.6 (0.4)	47.4 (0.3)	2.65 (2.4)	0.1	0.96 (0.01)
150, C_4F_8	49.0 (1.1)	47.8 (1.1)	3.2 (0.2)	< 0.2	0.98 (0.04)

[a]Numbers in parentheses represent one standard deviation of the mean.

typically contribute to higher ion densities, which result in more crosslinked materials. The relationship between ion densities, deposited films and scatter coefficients is discussed in detail below.

5.3. Discussion

Plasma-processing of materials involves a complex mix of molecule-surface interactions that are difficult to fully characterize. It has only been recently that researchers have attempted to delineate the roles of individual species during plasma processing. With fluorocarbon plasmas, this becomes even more difficult because of the dual nature of these systems, which is well documented in the literature.[13,14,22,23] Etching of Si-based materials is nearly always accompanied by deposition of FC materials, which aids etch selectivity.[2,23] Characterization of these materials and knowledge of specific plasma-surface interactions during FC plasma processing can provide control over the two regimes. The ultimate goal for such studies is premeditated, rational design of plasma methods to fulfill demands for new materials and etch processes.

One of the most characterized molecules in traditional FC plasmas (CF_4, C_2F_6) is CF_2. Just as FC plasmas have a dual nature, CF_2 has a dual role within these systems, sometimes acting as a film deposition precursor, and sometimes as an etch product. C_4F_8 plasmas are of particular interest because they are used for both the selective etching of SiO_2 over Si, and for the deposition step providing sidewall passivation in the Bosch process.[10] Despite the widespread interest in larger FC systems, characterization of CF_2 and other gas phase species in C_3F_8 and C_4F_8 systems is limited. We have measured the relative densities of CF_2 in C_3F_8 and C_4F_8 plasma molecular beams, and quantified the overall surface production of CF_2 during plasma processing of Si. The spectral selectivity of LIF has allowed us to make these CF_2 specific measurements in the presence of all the other plasma species. Measurements were taken under conditions that limit ion-surface interactions, and that enhance ion production in the plasma, thereby increasing ion bombardment of the surface. Such manipulations of the ion population in the plasma beam allow us to determine the effect of ions on CF_2 surface production.

In this work, we performed three different experiments that served to alter the ion chemistry in the plasma molecular beams. First, increasing P leads to higher $S(CF_2)$ values in both C_3F_8 and C_4F_8 systems. Increasing applied rf power in a plasma typically leads to an increase in both ion density and ion energy.[24] As a result, the substrate surface is bombarded by a larger number of energetic species, leading to an increased degree of ion-assisted CF_2 surface production, Table 5.1. This is supported by mass spectral data of our plasma molecular beams, which reveal that for both systems, increased P leads to an increase in relative ion density.[21] There also appears to be more production of monocarbon species, as opposed to $C_2F_x^+$ and higher order fragments.

Second, decreasing the source pressure for 50 W C_4F_8 plasmas results in significantly higher CF_2 surface production, Table 5.1. Increased pressure in a plasma results in both decreased electron energy, and shorter particle mean free paths.[11,25] Goyette, et al. measured the relative ion composition of c-C_4F_8 rf plasmas as a function of pressure and found the magnitude of the total ion flux decreases with increasing pressure between 5 and 20 mTorr.[26] As electron energy decreases, not only are fewer ions formed, but the ions created via electron impact dissociation tend to have lower energies than those formed in lower pressure systems. This likely leads to less ion-induced CF_2 surface production in the higher pressure system. The third experiment used a grounded mesh screen to create an ion-limited molecular beam, resulting in a decrease in CF_2 surface production under all conditions studied. As expected, limiting ion bombardment of the surface has the smallest effect on the system that produces the fewest ions, the 25 W C_3F_8 plasma, Table 5.1. All three of these experimental results reveal that ions have a distinct influence on the surface production of CF_2.

Overall, *S*(CF_2) values measured for the C_3F_8 system are lower than those in the C_4F_8 system. Under ion-limited conditions, however, *S*(CF_2) is approximately the same for both systems. Therefore, the higher *S*(CF_2) values measured in unperturbed C_4F_8 systems are due to greater ion induced CF_2 surface production. This could be a result of more energetic ions in the C_4F_8 system, or it could be due to differences in the CF_x^+ and $C_xF_y^+$ distributions. The ion energy data for these systems are discussed in Chapter 6. This chapter discusses differences in ionic compositions of the plasmas. There are two notable differences in the ionic compositions of 100 W C_3F_8 and C_4F_8 plasma molecular beams, Figure 5.6. First, C_4F_8 plasmas produce a greater relative intensity of heavier ions than C_3F_8 plasmas. Physical processes such as sputtering are more efficient with higher mass ions, as the rate of etching is related to momentum transfer to the surface.[27] Thus, if sputtering contributes to the observed surface production of CF_2, surface bombardment by heavier ions helps explain the higher *S*(CF_2) values measured for C_4F_8 plasmas.

The second difference is that the identity of the predominant ions is different in the two systems. CF^+ dominates the ion spectrum in the C_4F_8 plasma, whereas CF_3^+ is the major ion formed in the C_3F_8 system. Results in the literature can help determine whether this difference in predominant ion distribution can lead to different net CF_2

production rates. In general, CF_x^+ (x=1-3) ions are neutralized at the surface of FC films, either reacting to contribute to film formation, producing neutral $CF_x(g)$ species, or sputtering the deposited film layer. As demonstrated by Toyoda and coworkers, few CF_x^+ ions survive intact when interacting with thin FC films on Al under conditions similar to those found in our IRIS experiments.[28] Over a wide range of incident energies (30 – 150 eV), the ion survival rate for CF_x^+ (x=1-3) was < 6%, indicating that the majority of the CF_x^+ ions were neutralized and either adsorbed to the surface, or scattered as neutral species. The neutral products of these surface reactions, however, were not monitored. Thus, the individual contributions of CF^+ and CF_3^+ to CF_2 surface production are not discernable from these experiments.

Three possible surface reactions that lead to CF_2 generation from CF_x^+ neutralization are given in equations 5.1-5.3, where * represents an active surface site:

$$CF_2^+ (g) + * \rightarrow CF_2 (ads) \rightarrow CF_2 (g) \qquad (5.1)$$

$$CF_3^+ (g) + 2* \rightarrow CF_2 (ads) + F (ads) \rightarrow CF_2 (g) + F (ads) \qquad (5.2)$$

$$CF^+ (g) + F (ads) \rightarrow CF_2 (g) + * \qquad (5.3)$$

Reaction (5.1) is a simple neutralization/desorption reaction; process (5.2) represents the adsorption and dissociation of CF_3^+ to form CF_2(ads), followed by desorption; and (5.3) is the neutralization of CF^+ followed by the reaction with adsorbed F to form CF_2 (g). The ionic compositions of the plasma systems might suggest that reactions (5.2) and (5.3) are more important than reaction (5.1) as relative ion intensities are $CF^+ > CF_3^+ > CF_2^+$ in C_4F_8 plasmas and $CF_3^+ > CF^+ > CF_2^+$ in C_3F_8 plasmas. To know if differences in relative CF_x^+ distributions contribute to the differences in CF_2 surface production in the two plasma systems, however, detailed information on reaction rates for processes (5.1)-(5.3) is required.

Perusal of the literature finds that both experimental and theoretical work has examined the question of ion-surface interactions in fluorocarbon plasmas. Booth and coworkers investigated CF_x radical production and loss in CF_4 plasmas under both fluorine rich and fluorine poor conditions,[29-32] and found that ions contribute to CF_2 surface production in both cases. Under fluorine rich conditions (i.e. using a reactive ion etching plasma), ion-bombardment of the powered electrode determines whether the electrode is a net source or sink of CF and CF_2.[30] The mechanism proposed for radical formation was the conversion of highly energetic CF_x^+ ions to neutral radicals at the powered electrode. The sum of the absolute CF and CF_2 neutral fluxes from the surface was always less than or equal to the incident ion flux, making this a plausible mechanism. The surface acted as a net sink for CF and CF_2 under conditions that limited or removed ion bombardment (i.e. lower applied rf powers and measurements made after the discharge was extinguished). Under fluorine poor conditions wherein polymerization dominates, every surface in the reactor acted as a net source of CF_2. In this case, the incident ion flux was less than the combined CF and CF_2 flux, suggesting that simple conversion of CF_x^+ ions to radicals, as in reactions (5.1)-(5.3), cannot entirely explain the CF_2 surface production. The two possible explanations presented for surface production of CF_2 in this case are (a) neutralization and decomposition of multicarbon ions, $C_xF_y^+$, and (b) ion induced decomposition of the depositing polymer layer, with the primary polymerization precursor being C_xF_y ions or molecules.[29] In our systems, either of these explanations are plausible sources of CF_2 surface production. Indeed, they suggest that surface reactions/bombardment involving larger ions are more important to CF_2 surface production than reactions (5.1)-(5.3).

Theoretical work by Zhang and Kushner also investigated mechanisms for CF_2 radical generation and loss in a CF_4 rf discharge.[33] They used an integrated kinetics and plasma equipment model, which was validated by direct comparison to Booth's work under F rich conditions.[30] The model results demonstrate that ion-surface interactions lead to CF_2 surface production, and that increasing ion energies result in increasing CF_2 yields. Specifically, CF_3^+ and larger FC ions contribute to CF_2 formation by dissociation on the surface (reaction 5.4) or through ion sputtering of the deposited FC film (reaction 5.5),[33] where P_s and W_s represent polymer passivated surface sites and bare surface sites respectively.

$$C_xF_y^+ + P_s \rightarrow CF_2(g) + C_{x-1}F_{y-2}(g) + P_s \qquad (5.4)$$

$$C_xF_y^+ + P_s \rightarrow C_xF_y(g) + CF_2(g) + W_s \qquad (5.5)$$

Zhang and Kushner's calculations also show that dissociation and sputtering reaction probabilities are nearly the same, with that for process (5.4) being slightly higher depending on process conditions.[33] In accordance with Booth's experimental results, this suggests that the presence of larger FC ions significantly influences CF_2 surface production. Their results also show that ion-surface reaction probabilities increase with increasing incident ion energy, which supports the increase in CF_2 production observed in our systems at both higher powers and lower pressures.

One additional piece of supporting theoretical work comes from molecular dynamics (MD) simulations by Graves and coworkers. Results for CF^+, CF_2^+, and CF_3^+ bombardment of Si show that a significant fraction of the incident CF_3^+ ions leave the surface as CF_2 over a wide range of incident ion energies (E_i). The yield of CF_2 per impacting CF_3^+ ranged from 0.085 ± 0.008 for $E_i = 25$ eV to 0.484 ± 0.010 for $E_i = 50$ eV. Higher E_is resulted in lower CF_2 production.[34] In addition, MD simulations of CF^+ and CF_2^+ found net FC film deposition over a wide range of E_i. CF^+ bombardment of this FC layer resulted in significant F and C atom deposition per ion impact, suggesting CF_2 production via reaction (3) is unlikely.

As noted in Section 5.1, this discussion has focused on two possible explanations for the observed differences in $S(CF_2)$ measured in the two FC systems studied here. The experimental and theoretical work presented above establishes that larger ions have a greater influence on CF_2 surface production than do smaller ions. The C_4F_8 plasma clearly contains a greater concentration of larger ions, thus $S(CF_2)$ values measured in the C_4F_8 systems are higher than those measured in the C_3F_8 systems under comparable conditions. Indeed, the highest scatter coefficient measured for CF_2 in 50 W FC plasmas arises from the low pressure C_4F_8 plasma system, Table 5.1, which is the system most likely to produce the highest concentration of high molecular weight ions.

As noted in the Introduction, previous IRIS studies have explored the contributions of ions to CF_2 surface production. For example, ions increased CF_2 surface production during both etching (100% C_2F_6 plasmas) and depositing (50:50 C_2F_6/H_2 and HFPO plasmas) processes.[17] Table 5.1 summarizes many of the $S(CF_2)$ values measured in these systems. Briefly, C_2F_6 plasmas are etching systems, C_2F_6/H_2 plasmas were strong depositors, and HFPO plasmas were slow depositing systems. Systems with high deposition rates had $S(CF_2)<1$, suggesting that CF_2 is a polymer precursor. Systems with much lower deposition rates display scatter values around unity, Table 5.1. These earlier studies suggested that CF_2 surface interactions could be exploited as a method of predicting whether net etching or net deposition occur. The results presented here for C_3F_8 and C_4F_8 plasmas, however, indicate surface interactions may be more complicated with larger FC monomers. For 50 W plasmas, $S(CF_2)$ in $C_3F_8 < S(CF_2)$ in C_2F_6, as expected for a depositing system vs. an etching system. In contrast, $S(CF_2)$ for C_4F_8 is comparable to $S(CF_2)$ for C_2F_6, even though C_4F_8 is a depositing system (~1 Å/minute for a 25 W C_4F_8 plasma molecular beam). Interestingly, data collected under ion-limited conditions yield S~1 for both C_4F_8 and C_2F_6 systems, indicating ions make similar contributions to CF_2 surface production under very different processing conditions. Thus, CF_2 surface interactions alone cannot predict the global processes occurring in larger FC systems.

As a final note, one of the overarching goals of our IRIS work is to correlate gas-phase and surface analysis data with plasma-surface interactions. For the fluorocarbon systems, there is a correlation between our reactivity measurements and the films deposited either directly in a reactor (similar to that used as the IRIS beam source) or on the substrates used in IRIS experiments. Earlier, we noted that films deposited in our plasma reactors are not identical to those deposited in the IRIS instrument. In drawing a correlation, however, we choose to compare scatter values measured under particular plasma source conditions with films deposited under those same conditions in our plasma reactor. In other words, $S(CF_2)$ measured for C_4F_8 (P = 25 W) was paired with the % crosslinking measured in films deposited in a 25 W C_4F_8 plasma, 8 cm downstream from the coil. Here, we define % crosslinking as the sum of %CF, %$\underline{C}$-CF_x, and %CH as measured by XPS. Figure 5.8 shows the relationship between $S(CF_2)$ and % crosslinking

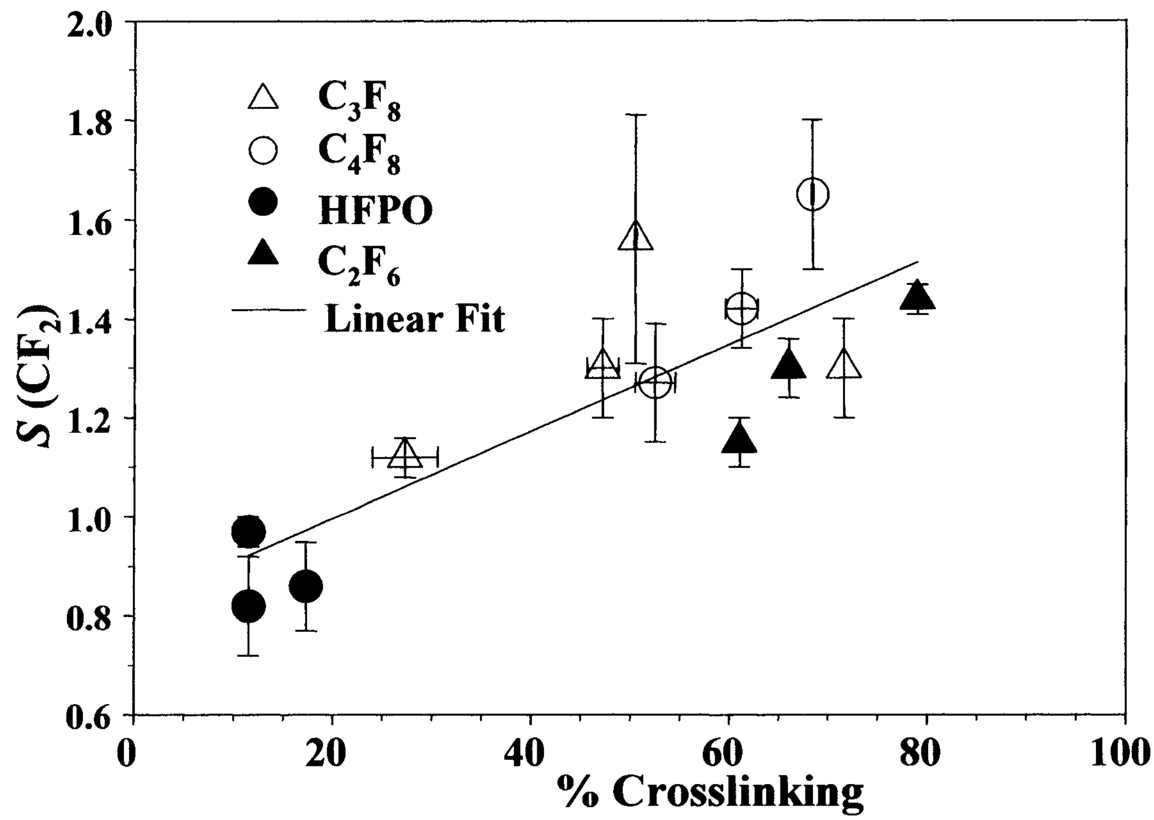

Figure 5.8 Relationship between $S(CF_2)$ and % crosslinking in materials deposited during FC plasma processing of Si. Data shown are for films deposited 8 cm downstream from the coil in independent plasma reactors and on IRIS substrates using (Δ) C_3F_8, (O) C_4F_8, (●)HFPO, and (▲) C_2F_6 plasmas. The line is a linear regression fit to all of the data ($R^2 = 0.7$).

in materials deposited from a wide range of FC plasmas using data presented in Table 5.1 This figure was first published in its present form in a review article written by Ellen Fisher.[35] Overall, CF_2 surface production shows a positive correlation with % crosslinking in the deposited films. Moreover, as discussed in our previous paper, conditions which lead to higher crosslinking occur under conditions with higher ion bombardment.[9] Thus, the correlation shown in Figure 5.8 is reasonable as both $S(CF_2)$ and % crosslinking are sensitive to ion bombardment. This positive correlation represents the first demonstration of the relationship between surface scattering coefficients measured with the IRIS technique and resulting film characteristics. What makes this especially noteworthy is that the correlation transcends several different plasma systems studied over a period of seven years by multiple Fisher group members.

As noted above in section 5.2.D, the materials deposited on IRIS substrates are more crosslinked than those deposited directly in the reactor, which can be clearly seen in Figure 5.8. One possible explanation for these differences is that the films deposited on IRIS substrates are exposed to a different pressure regime, including different possible sources of outgassing. This could result in different relative contributions of the C-H peak in the high resolution C_{1s} envelope, thereby changing the % crosslinking measured for the IRIS films. Nonetheless, the positive correlation shown in Figure 5.8 represents the first direct demonstration of the relationship between surface scattering coefficients and resulting film characteristics.

5.4. Summary

CF_2 surface interactions were investigated during C_3F_8 and C_4F_8 plasma processing of Si using our IRIS instrument. $S(CF_2)$ values >1 show that there is net production of CF_2 at the Si surface during C_3F_8 and C_4F_8 plasma processing. This suggests that CF_2 is not a deposition precursor in these larger FC systems. This is the first example of significant CF_2 surface production measured during deposition of FC materials in the IRIS system. Manipulation of ions reaching the plasma-surface interface shows that charged species are critical to CF_2 surface production. This is further demonstrated by the higher $S(CF_2)$ values measured under conditions that create higher ion densities and energies. PI-MS data also suggest that the contribution of $C_xF_y^+$ to CF_2 surface production may be more significant than the contribution of smaller CF_x^+ ions. The most noteworthy result of this work is that we have shown a positive correlation between scatter coefficient values and film characteristics, demonstrating the unique contributions IRIS experiments can make to the understanding of underlying chemical mechanisms.

References

1. Allgood, C.; Hsu, S.; Mocella, M., *Comparison of PECVD chamber cleaning processes (environmental, productivity and economic considerations)*, Proceedings of the Electrochemical Society (2001), 2001-6 (Environmental Issues with Materials and Processes for the Electronics and Semiconductor Industries), (2001), pp 9-14.

2. Standaert, T. E. F. M.; Schaepkens, M.; Rueger, N. R.; Sebel, P. G. M.; Oehrlein, G. S.; Cook, J. M. *J. Vac. Sci. Technol. A* **1998**, *16*, 239.

3. Agraharam, S.; Hess, D. W.; Kohl, P. A.; Bidstrup Allen, S. A. *J. V. Sci. Technol. B* **2001**, *19*, 439.

4. Bohnert, J. L.; Fowler, B. C.; Horbett, T. A.; Hoffman, A. S. J. *Biomater. Sci., Polym. Ed.* **1990**, *4*, 279.

5. Ji, H.; Cote, A.; Koshel, D.; Terreault, B.; Abel, G.; Ducharme, P.; Ross, G.; Savoie, S.; Gagne, M. *Thin Solid Films* **2002**, *405*, 104.

6. Lewis, K. B.; Ratner, B. D. *J. V. Sci. Technol. B* **1992**, *10*, 2331.

7. Endo, K.; Tatsumi, T. *Appl. Phys. Lett.* **1997**, *70*, 1078.

8. Sandrin, L.; Silverstein, M. S.; Sacher, E. *Polymer* **2001**, *42*, 3761.

9. Martin, I. T.; Malkov, G. S.; Butoi, C. I.; Fisher, E. R. *J. Vac. Sci. Technol. A* **2004**, *22*, 227.

10. Craigie, C. J. D.; Sheehan, T.; Johnson, V. N.; Burkett, S. L.; Moll, A. J.; Knowlton, W. B. *J. Vac. Sci. Technol. B* **2002**, *20*, 2229.

11. d'Agostino, R.; Cramarossa, F.; Fracassi, F. Plasma Polymerization of Fluorocarbons. In *Plasma Deposition, Treatment, and Etching of Fluorocarbons*; d'Agostino, R., Ed.; Academic Press, Inc.: San Diego, 1990; pp 95.

12. Samukawa, S. "New Gas Chemistry for High-Performance SiO_2 Patterning in Sub-0.1 μm ULSIs"; AIP Conference Proceedings: Atomic and Molecular Data and Their Applications, 2002.

13. Nakamura, M.; Hori, M.; Goto, T.; Ito, M.; Ishii, N. *J. Vac. Sci. Technol. A* **2001**, *19*, 2134.

14. Miyata, K.; Hori, M.; Goto, T. *Jpn. J. Appl. Phys. Part 1* **1997**, *36*, 5340.

15. Capps, N. E.; Mackie, N. M.; Fisher, E. R. *J. Appl. Phys.* **1998**, *84*, 4736.

16. Butoi, C. I.; Mackie, N. M.; McCurdy, P. R.; Peers, J. R. D.; Fisher, E. R. *Plasmas Polym.* **1999**, *4*, 77.

17. Butoi, C. I.; Mackie, N. M.; Williams, K. L.; Capps, N. E.; Fisher, E. R. *J. Vac. Sci. Technol. A* **2000**, *18*, 2685.

18. Mackie, N. M.; Capps, N. E.; Butoi, C. I.; Fisher, E. R. *ACS Symposium Series* **2001**, *787*, 168.

19. Matthews, N. M. *Can. J. Phys.* **1967**, *45*, 2355.

20. King, D. S.; Schenck, P. K.; Stephenson, J. C. *J. Mol. Spectrosc.* **1979**, *78*, 1.

21. Williams, K. L.; Martin, I. T.; Fisher, E. R. *J. Am. Soc. Mass Spectrom.* **2002**, *13*, 518.

22. Nakamura, M.; Masaru, H.; Goto, T. *J. Appl. Phys.* **2000**, *90*, 580.

23. Li, X.; Schaepkens, M.; Oehrlein, G. S.; Ellfson, R. E.; Frees, L. C.; Mueller, N.; Korner, N. *J. Vac. Sci. Technol. A* **1999**, *17*, 2438.

24. Lieberman, M. A.; Lichtenberg, A. J. *Principles of Plasma Discharges and Material Processing*; Wiley and Sons: New York, 1994.

25. Samukawa, S.; Donnelly, V. M.; Malyshev, M. B. *Jpn. J. Appl. Phys. Part 1* **2000**, *39*, 1583.

26. Goyette, A. N.; Wang, Y.; Misakian, M.; Olthoff, J. K. *J. Vac. Sci. Technol. A* **2000**, *18*, 2785.

27. Moss, S. J. Polymers in plasmas. In *The Chemistry of the Semiconductor Industry*; Ledwith, A., Ed.; Chapman and Hall: New York, 1987; pp 391.

28. Sugai, H.; Mitsuoka, Y.; Toyoda, H. *J. Vac. Sci. Technol. A* **1997**, *16*, 290.

29. Cunge, G.; Booth, J. P. *J. Appl. Phys.* **1999**, *85*, 3952.

30. Booth, J. P.; Cunge, G.; Chabert, P.; Sadeghi, N. *J. Appl. Phys.* **1998**, *85*, 3097.

31. Booth, J. P. *Plasma Sources Sci. Technol.* **1999**, *8*, 249.

32. Booth, J. P.; Hancock, G.; Perry, N. D.; Toogood, M. J. *J. Appl. Phys.* **1989**, *66*, 5251.

33. Zhang, D.; Kushner, M. J. *J. Vac. Sci. Technol. A* **2000**, *18*, 2661.

34. Abrams, C. F.; Graves, D. B. *Thin Solid Films* **2000**, *374*, 150.

35. Fisher, E. R. *Plasma Process. Polym.* **2004**, *1*, 13.

CHAPTER 6

RELATIONSHIP BETWEEN ION ENERGIES AND CF_2 SURFACE INTERACTIONS DURING FLUOROCARBON PLASMA PROCESSING OF SILICON

This chapter characterizes nascent ions in C_3F_8 and C_4F_8 plasma molecular beams. The effect of applied rf power and source pressure on relative ion densities, mean ion energies, and ion energy distributions are discussed. A strong linear correlation exists between mean ion energies and the CF_2 surface production measurements discussed in Chapter 5.

6.1. Introduction

Ions are critical contributors to numerous plasma processes, including the etching of Si and SiO_2, and the deposition of FC films. Complete characterization of plasma ions requires investigation of the identity, flux, and ion energy distributions (IEDs) of the ions bombarding the surface during plasma processing of a substrate. Ion energies are of particular importance as literature studies demonstrate that they impact both etch efficiency and film properties.[1-3] For example, molecular dynamics simulations by Smirnov et al. show that Si and O etch yields increase with ion energy during simulated CF_x^+ ion bombardment of SiO_2.[1] Fuoco and Hanley examined in depth the use of $C_2F_4^+$ and $C_3F_5^+$ ion beams to grow thin FC films on Si; the ion energies (5-200 eV) control the film morphology and the thickness of the interface layer, which in turn affect the resulting etch process.[2] Recent work in the Fisher group has shown that ion energies critically influence the structure and mechanical properties of plasma deposited diamond like carbon (DLC) films.[3]

Chapter 5 discussed ions detected in C_3F_8 and C_4F_8 plasma molecular beams using a Dycor LC200S residual gas analyzer (RGA). In those studies, the plasma molecular beam was interacting with a depositing FC film, and ions were found to enhance CF_2 surface production. This chapter completes the characterization of ions in these systems through the use of a Hiden PSM003 mass spectrometer (MS). In contrast to the RGA, the Hiden MS has energy analysis capabilities, which were used to measure the IEDs and relative ion intensities in the plasma molecular beams. IEDs for C_xF_y ions were characterized at various applied rf plasma powers (*P*) and gas pressures. This work has two important results. First, the IEDs measured in the plasma molecular beams used in

IRIS experiments resemble those sampled directly from plasma sources in the literature. Second, there is a positive correlation between the mean ion energies present in the plasma molecular beam and the CF_2 surface production data presented in Chapter 5. In the last decade, numerous publications have characterized ion energies in plasmas as part of full gas-phase analyses.[4-6] Modeling work by Kushner and coworkers discusses the effect of ion energy on the surface production of molecules such as CF_2.[7] The effects of ion energies on resulting surface effects, such as topography, and etch and deposition rates of films have also been studied.[2,8,9] Work presented in this chapter shows the first experimental example of a direct relationship between these gas-phase measurements and modeled gas-surface interactions data.

6.2. Experimental Details for the Hiden Mass Spectrometer

The MS was mounted onto the IRIS main chamber using the flange that typically houses the substrate holder used in reactivity measurements. As a result, the detector was placed directly in line with the plasma molecular beam, which allowed the analysis of the ions that bombard the substrate surface during reactivity measurements. The data presented here are the first IEDs measured directly on the IRIS chamber.

It is important that the MS is operated using conditions that eliminate modification of the ion energies by the instrument. The PSM003 consists of a combination of ion extractor, electron-impact ion source, Bessel box energy filter, triple-section quadrupole mass filter (QMF) and secondary electron multiplier. The probe is surrounded by an aluminum cylindrical cover with a 5 mm diameter hole on the center of the top surface. The distance between the slits that define the molecular beam and the top surface of the probe cover is ~5 cm, which is much less than the mean free path (> 100 cm) in the main chamber under the present operation conditions (main chamber pressure < $5x10^{-5}$ Torr). To sample ions, a vacuum sealed 300 μm diameter skimmer located 2 mm below the orifice in the probe cover was attached to the end of the mass spectrometer. Ions created in the plasma sequentially pass through the reactor orifice, grid, probe cover orifice, and sampling orifice, and eventually enter the ion energy analyzer of the mass spectrometer.

A base pressure of ~ 8×10^{-8} Torr inside the probe is achieved by using a 60 l/s turbo molecular pump backed by a 400 l/min mechanical pump. With the 300 μm sampling orifice, the pressure in the mass spectrometer probe was maintained at < 1×10^{-6} Torr during experiments, lower than the minimum required pressure (5×10^{-6} Torr) for operating the ion detector. Moreover, the low pressure environment in the mass spectrometer probe increases the mean free path of the sampled species to prevent gas-phase ion-molecule collisions and ensures that no disturbance of ion energy occurs inside the probe. For ion analysis, the internal ionization source is switched off and the front lenses are used to extract ions and focus them into the mass filter. The source region is held at the mid axis potential of the gauge. The QMF identifies various ions according to their mass-to-charge ratio and the IED is measured individually for each m/q selected ion.

6.3. Results

Figure 6.1 shows mass spectra of the ions present in 50 W C_3F_8 and C_4F_8 plasma molecular beams (gas pressure ~ 45 mTorr). These data are consistent with our published spectra for these systems collected with the Dycor RGA, Figure 5.6.[10,11] The Hiden data has a higher upper limit of the m/z ratio: 300, vs. 200 for the RGA data.

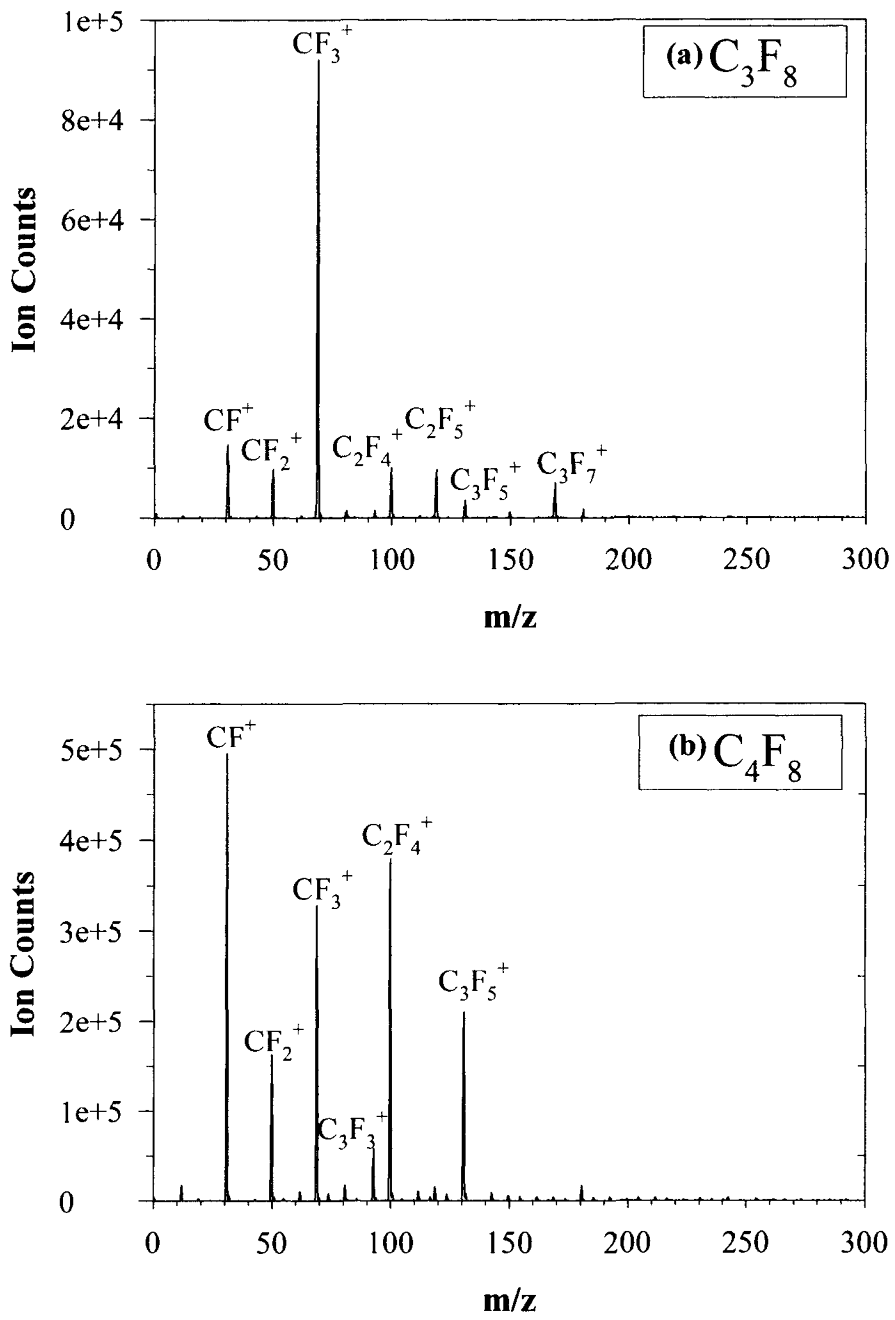

Figure 6.1. Mass spectra of nascent ions from 10 sccm, 50 W (a) C_3F_8 and (b) C_4F_8 plasma molecular beams.

Figure 6.1 indicates that there is no significant signal from ions with m/z > 200. Note that for these spectra, the signal for a specific m/z ratio was collected at the peak of a selected IED (CF^+ for the C_4F_8 and CF_3^+ for the C_3F_8 data). The ion intensities discussed below were calculated by integrating the areas under the peaks of the IEDs for each individual ion; as each ion has a wide energy distribution (FWHM>5 eV), this is a more accurate representation of the contribution of each ion to the total ion intensity. Multiple consecutive scans of a single ion result in up to 40% variance in the measured intensity, so only changes greater than this can be reasonably considered as significant. Typically, when discussing ion fluxes in the literature, the detected signal is corrected for ion mass dependent transmission and the detection efficiency of the MS, then divided by the area of the sampling aperture of the MS to yield a flux.[12] Assuming the ion detection is not greatly dependent on mass, and the aperture size is constant for all these measurements, the intensities present are reasonable representations of the flux.

Figures 6.2 and 6.3 show the intensities of the six major ions present in C_3F_8 and C_4F_8 plasma molecular beams as a function of *P*, with the source flow set at 10 sccm (gas pressure ~ 45 mTorr). A sharp increase in overall ion intensity occurs at $P > 125$ W in the C_3F_8 system, Figure 6.2. The C_4F_8 total ion intensity increases with *P*, with a slight drop at $P = 150$ W, Figure 6.3. Figure 6.4 shows the ion intensity data collected for 50 W C_4F_8 plasmas as a function of gas pressure. There is an increase in total ion flux as the pressure increases from 15 to 25 mTorr, and then a decrease at higher pressures.

Ion energy distributions have been studied in various FC plasma systems.[8,9,13] There are two primary ways of analyzing these data: examining the shapes and widths of the

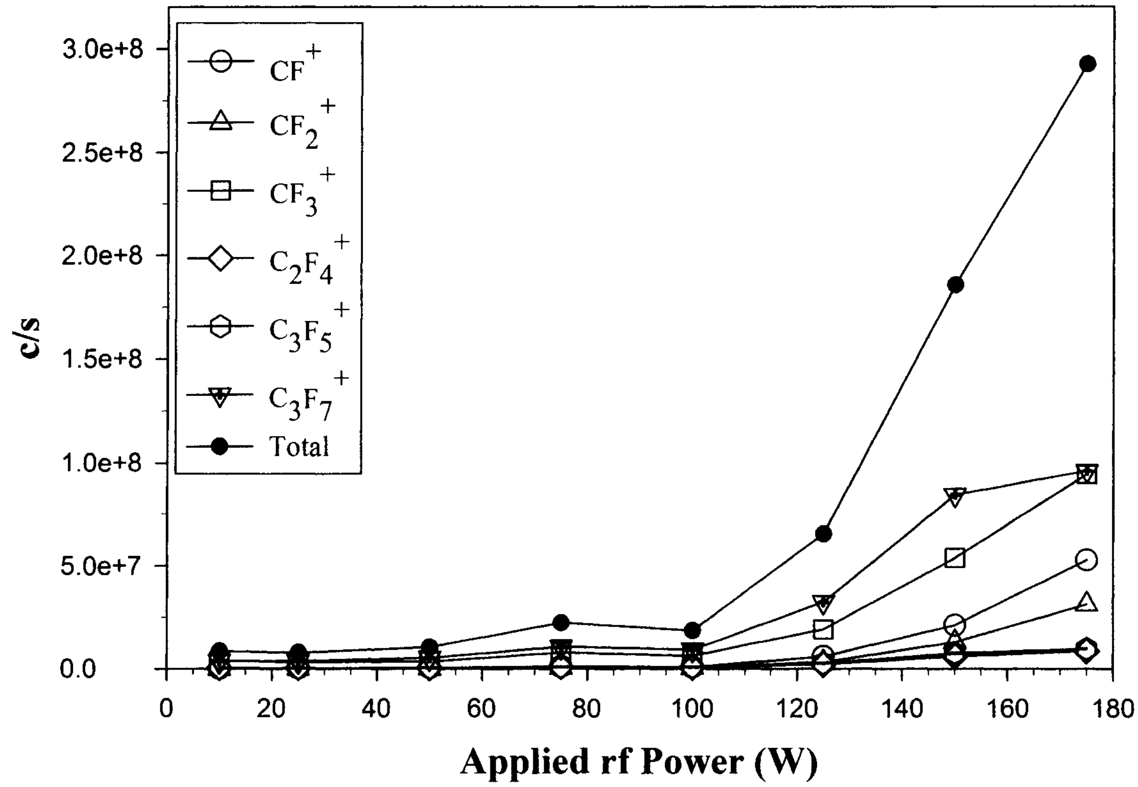

Figure 6.2. Ion intensity as a function of applied rf power for 10 sccm C_3F_8 plasma molecular beams.

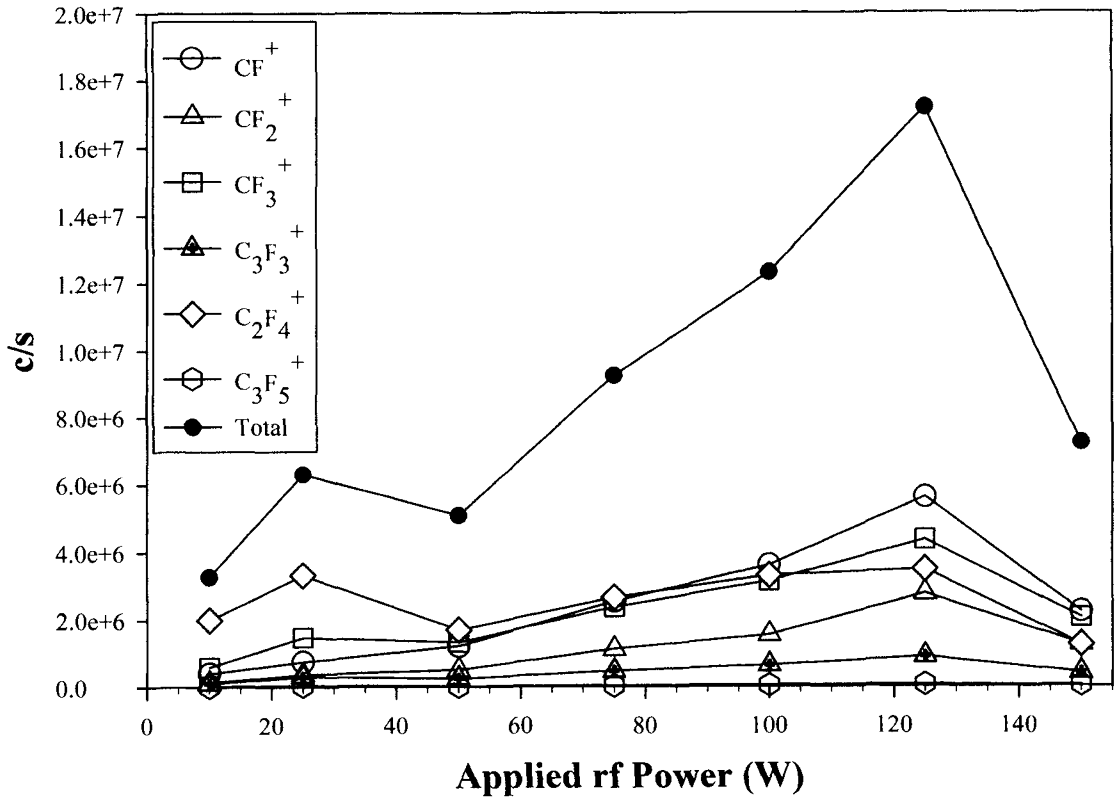

Figure 6.3. Ion intensity as a function of applied rf power for 10 sccm C_4F_8 plasma molecular beams.

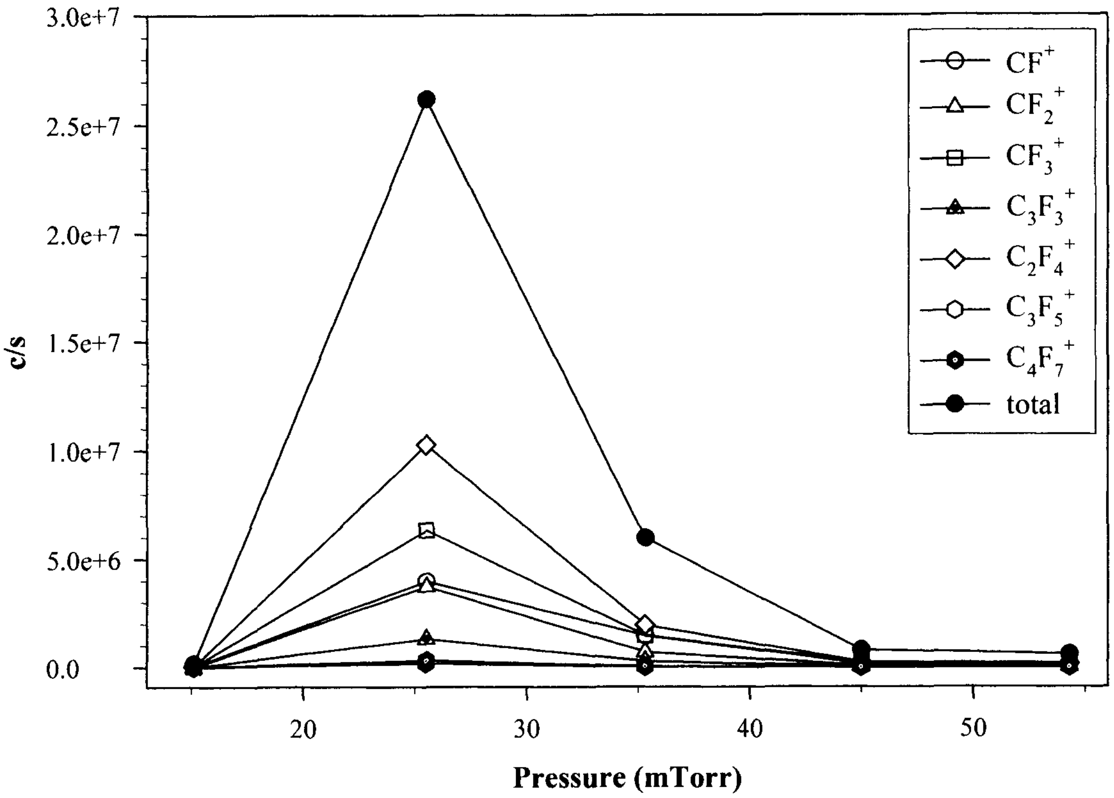

Figure 6.4. Ion intensity as a function of plasma source pressure for 50 W C_4F_8 plasma molecular beams.

distributions, and calculating the mean energy for the individual IEDs. The shape of the ion energy distribution can yield information on how ions gain their energy in the plasma, whereas mean energies provide a simple way to quantify and compare ion energies.

When examining the shapes of IEDs for plasma ions, it is instructive to consider ion formation mechanisms. Plasmas are capable of generating ions with a variety of distributions that range from single, narrow, monoenergetic peaks to broad, complex, multimodal structures. Ions gain their energy via acceleration through the sheath; their resulting energy distributions depend on collisions with neutrals within the sheath and their transit time through the sheath (τ_{ion}) relative to the rf period (τ_{rf}). Ion-neutral collisions within the sheath typically result in broad energy distributions that contain multiple peaks.[4,5] Bimodal energy distributions are also present when the rf field modulates the ion energy.[5,14] Specifically, when $\tau_{ion}/\tau_{rf} << 1$, ions respond to the instantaneous sheath voltage. As a result, the phase of the rf cycle in which they entered the sheath affects their final energies, resulting in broad, bimodal IEDs. In contrast, when $\tau_{ion}/\tau_{rf} >> 1$, the ions need numerous rf cycles to cross the sheath, and therefore respond to the average sheath potential, which results in a narrow, monoenergetic IED (FWHM~ 5eV).[6,14]

Figure 6.5 shows the IEDs of CF^+ in 25 W, 10 sccm C_3F_8 and C_4F_8 plasma molecular beams. Note that the detection range for our MS is 100 eV. If ions exist with energies > 100 eV in our systems, they are not detected. The shapes of our IEDs do, however, resemble IEDs measured in other rf plasmas, including FC systems, and are consistent with $<E_i>$ values used in Graves' work.[4-6,8,13] Figures 6.6 and 6.7 show the CF^+ IEDs from C_4F_8 and C_3F_8 plasma molecular beams as a function of *P*. For the C_4F_8

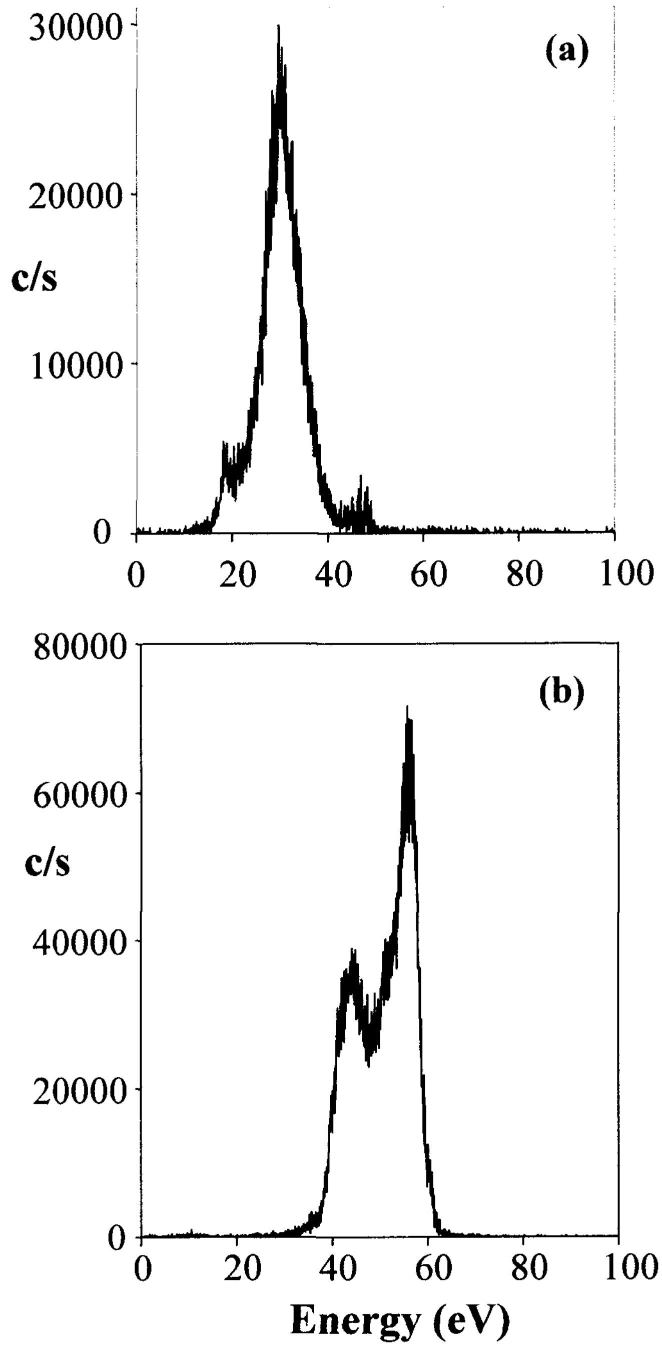

Figure 6.5. Ion energy distributions of CF^+ in 10 sccm, 25 W (a) C_3F_8 and (b) C_4F_8 plasma molecular beams.

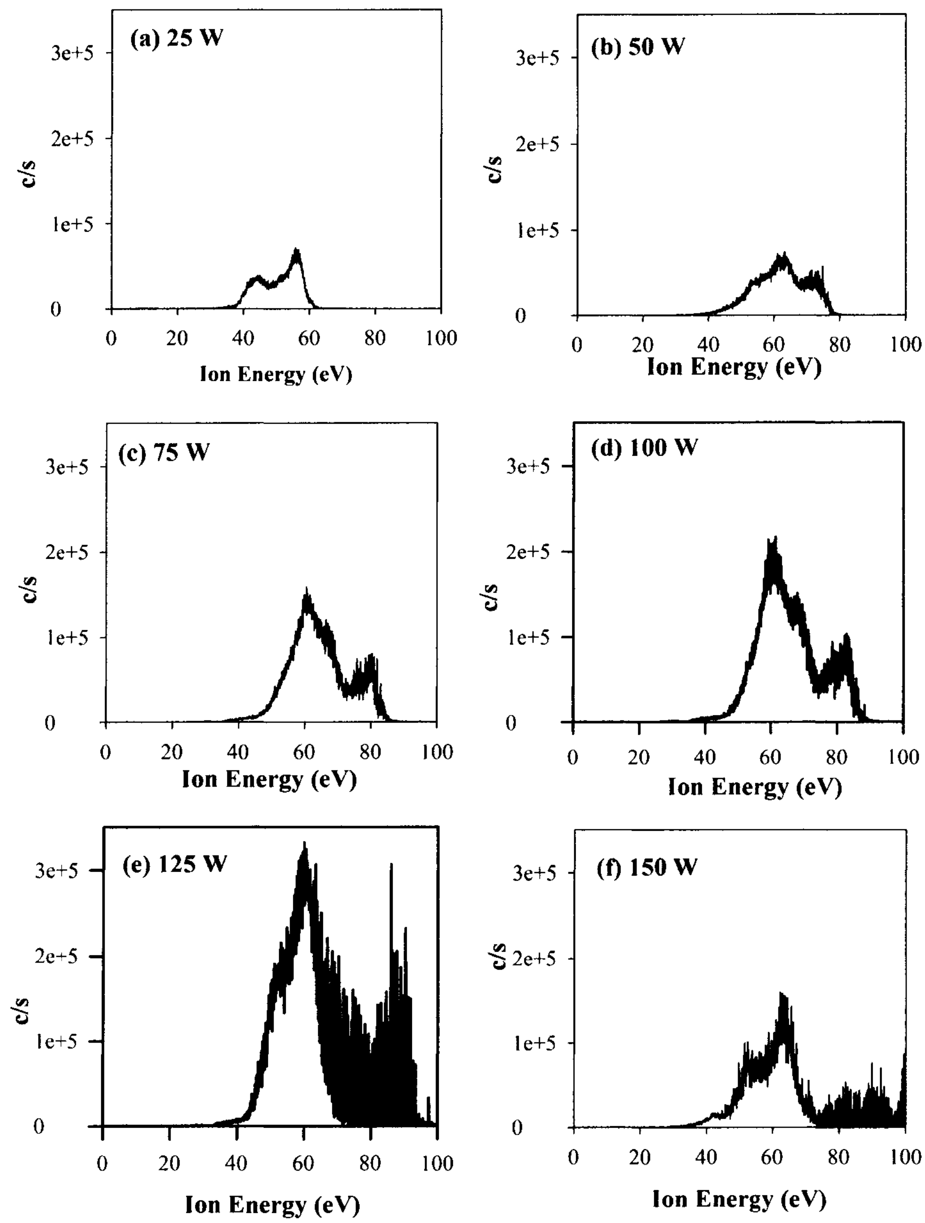

Figure 6.6. Ion energy distributions of CF^+ in 10 sccm (a) 25 W, (b) 50 W, (c) 75 W, (d) 100 W, (e) 125 W, and (f) 150 W C_4F_8 plasma molecular beams. All plots are on the same scale.

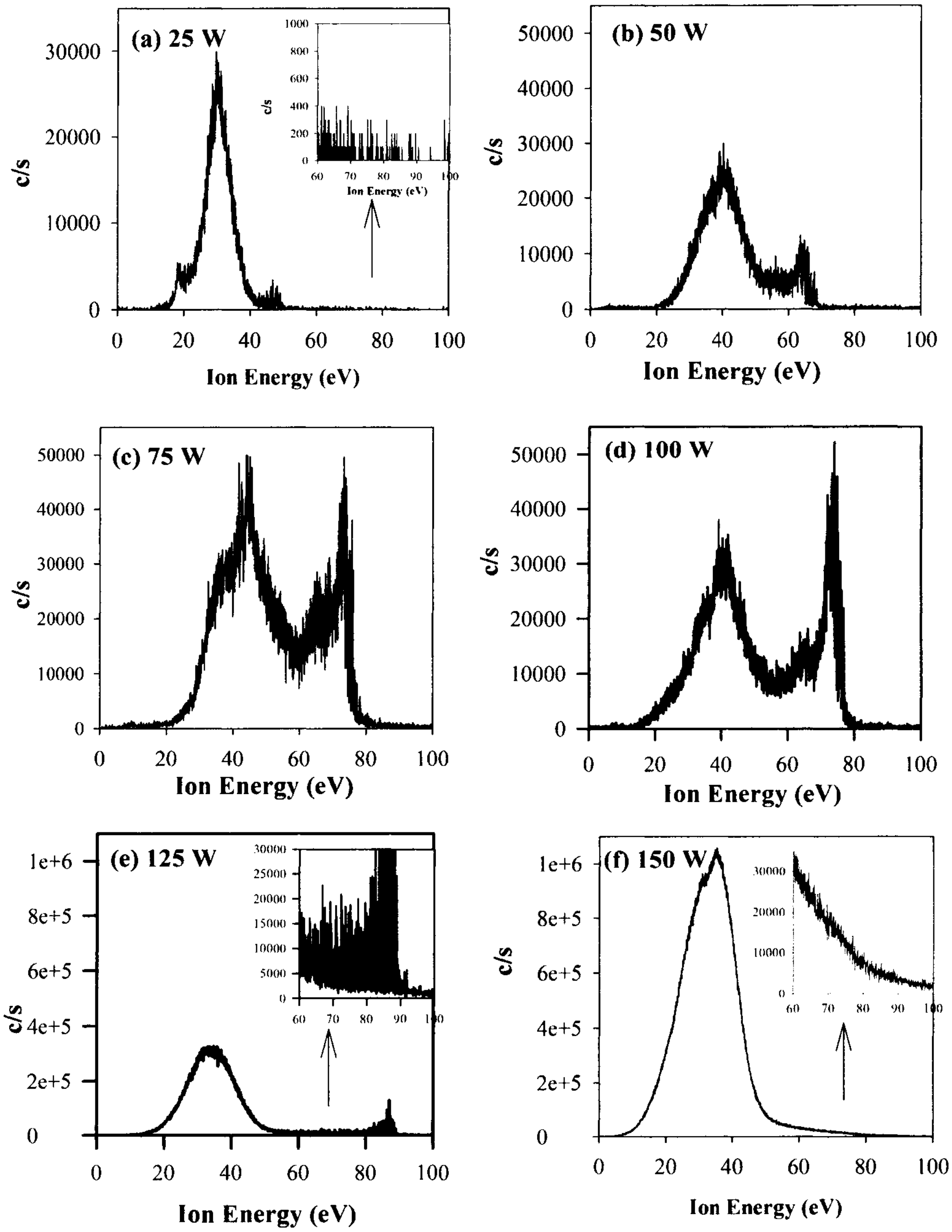

Figure 6.7. Ion energy distributions of CF^+ in 10 sccm (a) 25 W, (b) 50 W, (c) 75 W, (d) 100 W, (e) 125 W, and (f) 150 W C_3F_8 plasma molecular beams. The insets in (a), (e), and (f) are magnifications of the 60-100 eV region for the 25 W, 125 W, and 150 W data respectively. (a) – (d) and the insets of (e) and (f) are on the same scale.

system, Figure 6.6, the IEDs shift to a higher energy with increasing *P*, and the structure becomes broader and more complex. The same trend is exhibited in the C_3F_8 system, Figure 6.7, except at $P \geq 125$ W, where the IEDs shift to a lower energy, with an extremely broad distribution. Figure 6.8 shows the IEDs of CF^+ and $C_2F_4^+$ from 50 W C_4F_8 plasma molecular beams as a function of pressure. At increased pressure, the IEDs are broader, more complex, and shifted to a lower energy. Similar results for CF^+ IEDS were measured by Goyette et al. in C_4F_8 plasmas in a GEC rf reference cell reactor (pressure 5-20 mTorr).[15] The CF^+ and $C_2F_4^+$ distributions in our plasmas are very similar. Overall, the IEDs do not appear to be mass dependent: for a given set of plasma parameters, the IEDs are similar, independent of mass.

Recall that the IEDs in our systems are measured from plasma molecular beams. The high energies measured for these ions indicate that they experience sheath effects as they leave the bulk plasma and enter the main chamber. The broadness and complexity of the structures suggest contributions from a collisional sheath and/or some rf modulation of the ion energies. These data are evidence that the plasma molecular beams are representative of plasma compositions.

Mean ion energies, $\langle E_i \rangle$, were calculated using the following equation:[16]

$$\langle E_i \rangle = \int_0^\infty \frac{f(E)EdE}{f(E)dE} \qquad (6.1)$$

$\langle E_i \rangle$ values for the major ions in 10 sccm C_3F_8 (triangles) and 10 sccm C_4F_8 plasmas (circles) are shown in Figure 6.9 as a function of *P*. The mean ion energies of the different ions formed within the same plasma do not vary significantly. Multiple consecutive scans of a single ion result in <1% variance in mean ion energy. Overall, C_4F_8 plasma ions have higher $\langle E_i \rangle$ than C_3F_8 plasma ions at all *P*, and the two plasma

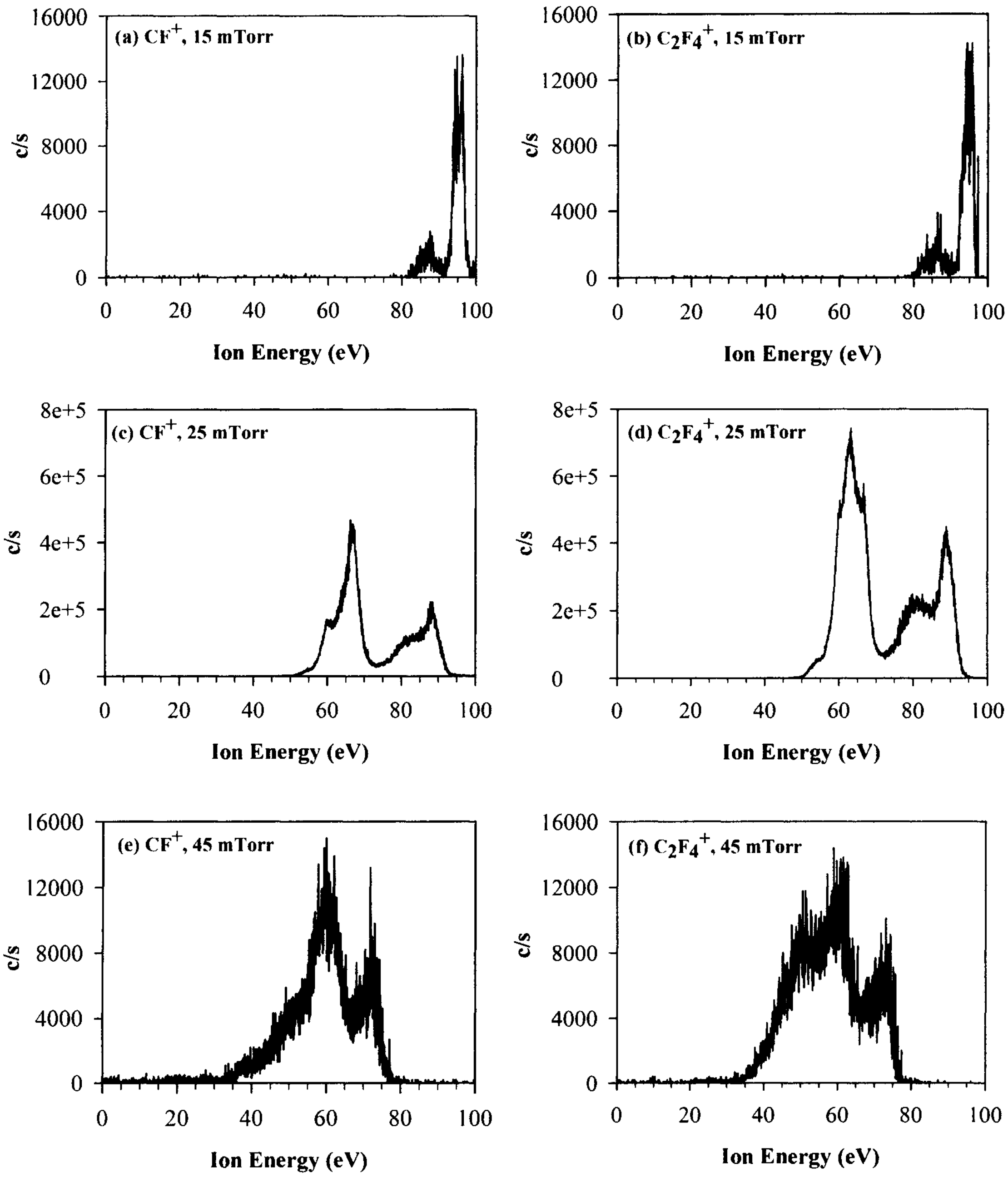

Figure 6.8. Ion energy distributions of CF^+ and $C_2F_4^+$ in (a), (b) 2.5 sccm, (c), (d) 5 sccm, and (e), (f) 10 sccm 50 W C_4F_8 plasma molecular beams. Graphs in the same row are on the same scale.

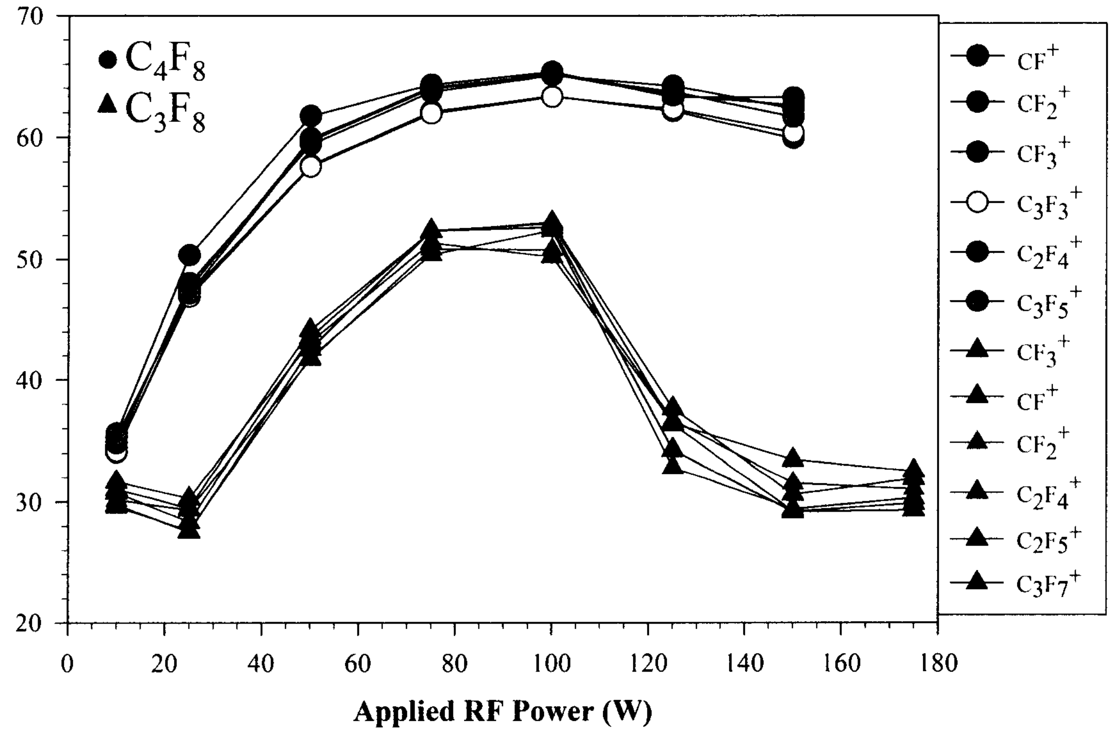

Figure 6.9. Mean ion energies of the major ions present in 10 sccm C_3F_8 (triangles) and C_4F_8 (circles) plasma molecular beams as a function of applied rf power.

systems exhibit different trends with increasing *P*. The mean energy of ions created in C_4F_8 plasmas increases with *P* initially, and then levels off at $P \geq 75$ W. In contrast, the mean energies of ions in C_3F_8 plasmas decrease at $P \geq 125$ W. Note this is the same *P* threshold that results in significantly greater ion intensities in the C_3F_8 system; this is further discussed below.

Figure 6.10 shows mean ion energies as a function of gas pressure for 50 W C_4F_8 plasma molecular beams. As with the C_3F_8 data, ions within a plasma have similar $\langle E_i \rangle$ values. As the source pressure increases in these systems, the mean ion energies decrease. This is consistent with basic plasma theory: increased pressure results in decreased electron energy and shorter particle mean free paths, leading to lower ion energies.[17]

Chapter 5 demonstrates that ions contribute to CF_2 surface production during FC plasma molecular beam processing of thin FC films on Si substrates. IRIS was used to measure the fraction of CF_2 molecules scattering off of the surface relative to those impacting the surface. This ratio, the scattering coefficient, *S*, is greater than unity when there is net surface production of a molecule, as is the case with CF_2. Table 6.1 shows $S(CF_2)$ values from Chapter 5 and $\langle E_i \rangle$ measured on the IRIS for the same systems. Figure 6.11 is a graph of $S(CF_2)$ as a function of $\langle E_i \rangle$. There is a clear correlation between mean ion energy and CF_2 surface production: higher ion energies result in greater surface production of CF_2. The outlier to this trend is for the 45 mTorr, 150 W C_3F_8 system (circled in the figure). Possible explanations for this are discussed below.

Table 6.1. $S(CF_2)$ measured during FC plasma molecular beam processing of Si and mean ion energies measured in the same beams.[a,b]

Plasma	*P* (W)	Pressure (mTorr)	$S(CF_2)$	Mean ion energy (eV)
C_3F_8	25	45	1.12 (0.04)	28.8 (1.1)
C_3F_8	50	45	1.13 (0.10)	42.8 (1.0)
C_3F_8	75	45	1.34 (0.11)	51.6 (0.9)
C_3F_8	100	45	1.56 (0.25)	52.0 (1.2)
C_3F_8	150	45	1.70 (0.14)	30.6 (1.7)
C_4F_8	25	45	1.27 (0.12)	47.9 (1.3)
C_4F_8	50	45	1.42 (0.08)	59.4 (1.5)
C_4F_8	75	45	1.65 (0.26)	63.4 (1.0)
C_4F_8	100	45	1.61 (0.34)	64.6 (1.0)
C_4F_8	150	45	1.65 (0.15)	61.7 (1.3)
C_4F_8	50	15	1.90 (0.14)	91.6 (2.2)

[a] $S(CF_2)$ values are from Table 5.1.

[b] Mean ion energies were calculated using Equation 6.1. The values presented are the average of the mean ion energies of the major ions in the system. One standard deviation from the mean is shown in parentheses.

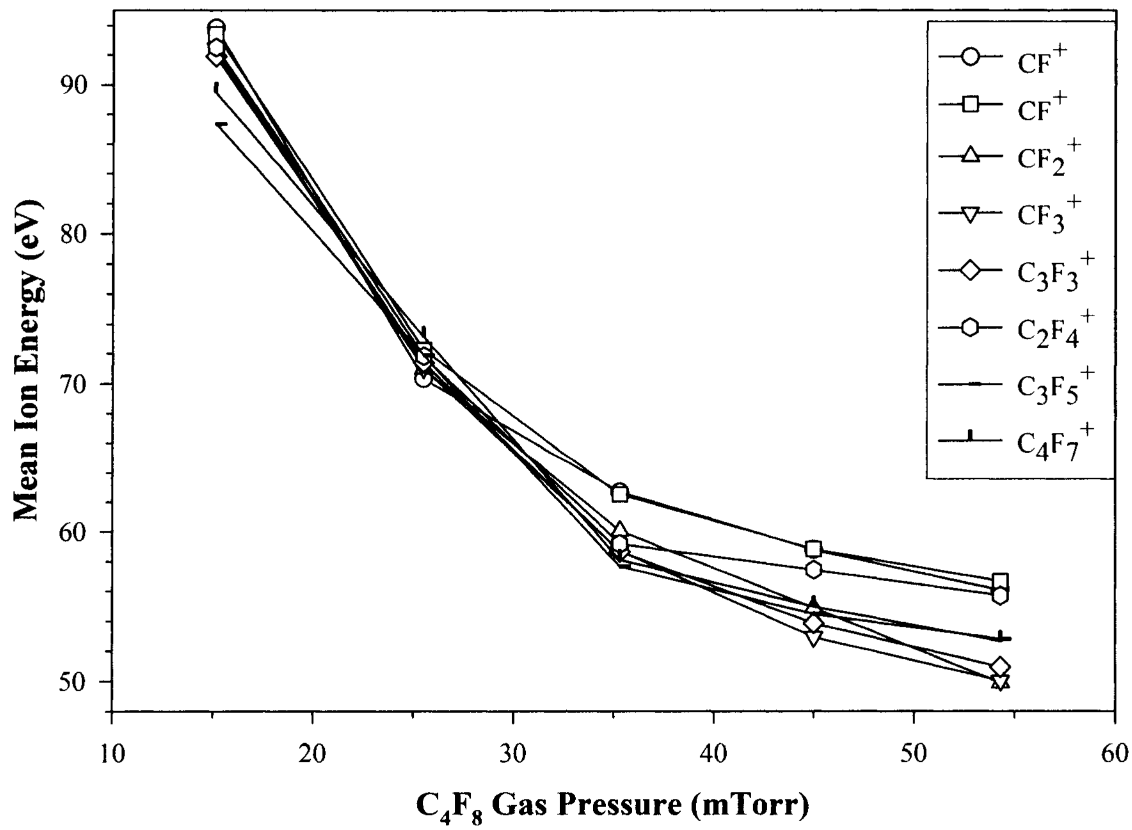

Figure 6.10. Mean ion energies of the major ions present in 50 W C_4F_8 plasma molecular beams as a function of plasma source pressure.

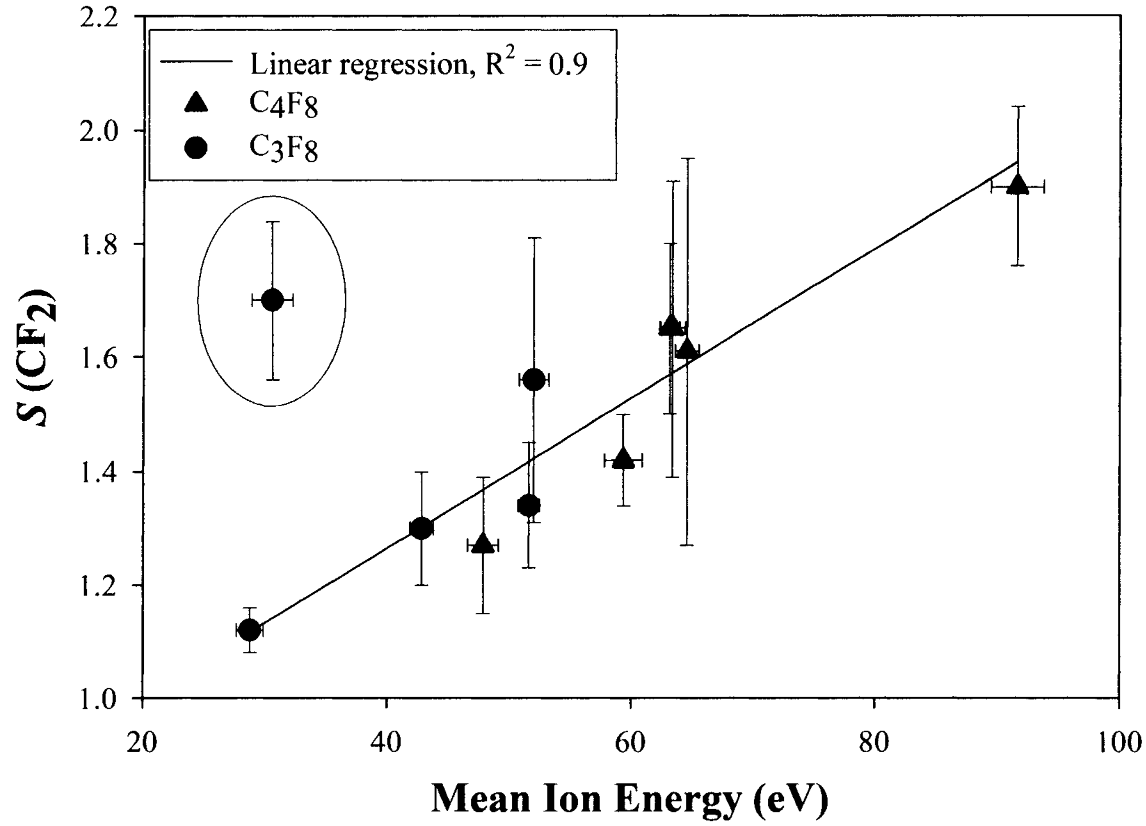

Figure 6.11. CF_2 scatter coefficients (*S*) measured during C_3F_8 (circles) and C_4F_8 (triangles) plasma processing of Si as function of average ion energy. All of the data except the circled outlier, are fit with a least squares linear regression analysis with R^2 = 0.9.

6.4. Discussion

6.4.A. IEDs and ion intensities. IEDs presented in this chapter are the first data of this type collected for plasma molecular beams on the IRIS. Notably, the IED shapes of the major ions present in C_4F_8 plasma molecular beams, Figure 6.6, resemble those of ions measured in low pressure C_4F_8 rf plasmas by Goyette et al. and others.[8,9,13] A primary principle governing our IRIS work is that the apparatus is designed to form molecular beams that contain virtually all of the species present in the plasma.[18] Because of this, our beam studies provide fundamental molecular level information for plasma systems. The IED results show that the ions in the beams are representative of plasmas, providing further evidence that supports the relevancy of our technique.

The IEDs measured in this system corroborate several assumptions made in Chapter 5. As discussed in Section 5.3, increasing applied rf power in a plasma typically leads to an increase in ion energy.[19] Figure 6.9 validates this for our systems at $P \leq 100$ W. Although ions with higher energies are produced at $P > 100$ W in the C_3F_8 system, $\langle E_i \rangle$ decreases significantly. This is attributed to a change in the plasma mode at these powers. In inductively coupled plasmas it is well known that two modes exist: a dim E mode, and a bright H mode. The former is a weak capacitive discharge, whereas the latter is the true inductive discharge, which is characterized by an increase in optical emission and plasma density.[20] Recent work in the Fisher group characterized this transition in DLC deposition systems with similar operating pressures; the transition to the H mode occurred at ~ 90 W.[3] This is consistent with results for the C_3F_8 system, with the transition occurring at ~ 100 W.

6.4.B. Ion energies and CF_2 surface production. Chapter 5 discussed a model of CF_4 discharges by Zhang and Kushner. Interestingly, their results demonstrated that increasing ion energies result in increasing CF_2 surface production. CF_3^+ and larger FC ions contribute to CF_2 formation by dissociation on the surface (reaction 6.1) or through ion sputtering of the deposited FC film (reaction 6.2),[7] where P_s and W_s represent polymer passivated surface sites and bare surface sites respectively.

$$C_xF_y^+ + P_s \rightarrow CF_2(g) + C_{x-1}F_{y-2}(g) + P_s \qquad (6.1)$$

$$C_xF_y^+ + P_s \rightarrow C_xF_y(g) + CF_2(g) + W_s \qquad (6.2)$$

Zhang and Kushner's calculations also show that dissociation and sputtering reaction probabilities are nearly the same, with that for process (6.1) being slightly higher depending on process conditions.[7]

The clear correlation between $S(CF_2)$ and $\langle E_i \rangle$ shown in Figure 11 is experimental evidence that CF_2 surface production increases with ion energy. This is consistent with both modeling results discussed above, and experimental work by Booth and coworkers. As discussed in Chapter 5, they investigated CF_x radical production and loss in CF_4 plasmas under both fluorine rich and fluorine poor conditions, and found that ions contribute to CF_2 surface production in both cases.[21-24] Specifically, the powered electrode in their configuration acted as a net source of both CF and CF_2, whereas the grounded electrode acted as a net sink. The production mechanism for the former was directly linked to energetic ion bombardment, with higher ion fluxes and energies associated with the net CF_x source. The data presented in this chapter are consistent with these results; additionally, we show a linear correlation between $\langle E_i \rangle$ and CF_2 surface production measured in the same system.

As a final note, there is an obvious outlier in Figure 6.11, where the CF_2 surface production does not follow the trend visible in the other data points. This can be explained by comparing two data points: the 25 W and the 150 W C_3F_8 systems. The measured mean ion energies are similar (28.8 and 30.6 eV, respectively), whereas the $S(CF_2)$ values are quite different: 1.12 and 1.70. If we look beyond the $\langle E_i \rangle$ values to the actual distributions we see that the IED of CF^+ in the 25 W system contains detected energies that range from 15-50 eV, whereas that for the 150 W system has detected energies ranging from 0 to 100 eV. Thus, the mean energy in the latter case is not a reasonable representation of energy of the ions impacting the surface. The inset in the CF^+ IED for the 150 W C_3F_8 system in Figure 6.6 shows the ion intensity between 60-100 eV on the same scale as the 25-100 W data. Although $\langle E_i \rangle \sim 31$ eV, there are clearly high energy ions in the tail of the distribution that could contribute to CF_2 surface production.

6.5. Summary

This chapter further characterizes ions present in C_3F_8 and C_4F_8 plasma molecular beams introduced in Chapter 5. The IEDs of the ions in these systems are broad, with complex structures resembling literature IEDs in other FC plasma systems. Mean ion energies in our systems range from 28 to 92 eV, and the IEDs are affected by source gas, pressure and applied rf power. The mean ion energy is correlated with CF_2 surface production measurements discussed in Chapter 5.

References

1. Smirnov, V. V.; Stengach, A. V.; Gaynullin, K. G.; Pavlovsky, V. A. *J. Appl. Phys.* **2005**, *97*, 093303.
2. Fuoco, E. R.; Hanley, L. *J. Appl. Phys.* **2002**, *92*, 37.
3. Zhou, J.; Martin, I. T.; Ayers, R.; Adams, E.; Liu, D.; Fisher, E. R. *Plasma Sources Sci. Technol.* **2005**, *to be submitted.*
4. Ishikawa, I.; Sasaki, S.; Nagaseki, K.; Saito, Y.; Suganomata, S. *Jpn. J. Appl. Phys.* **1997**, *36*, 4648.
5. Hirose, Y.; Ishikawa, I.; Sasaki, S.; Nagaseki, K.; Saito, Y.; Suganomata, S. *Jpn. J. Appl. Phys.* **1998**, *37*, 5730.
6. Sobolewski, M. A.; Wang, Y.; Goyette, A. *J. Appl. Phys.* **2002**, *91*, 6303.
7. Zhang, D.; Kushner, M. J. *J. Vac. Sci. Technol. A* **2000**, *18*, 2661.
8. Li, X.; Ling, L.; Hua, X.; Oehrlein, G. S.; Wang, Y.; Anderson, H. M. *J. Vac. Sci. Technol. A* **2003**, *21*, 1955.
9. Li, X.; Ling, L.; Hua, X.; Oehrlein, G. S.; Wang, Y.; Vasenkov, A.; Kushner, M. J. *J. Vac. Sci. Technol. A* **2004**, *22*, 500.
10. Williams, K. L.; Martin, I. T.; Fisher, E. R. *J. Am. Soc. Mass Spectrom.* **2002**, *13*, 518.
11. Martin, I. T.; Fisher, E. R. *J. Vac. Sci. Technol. A* **2004**, *22*, 2168.
12. Singh, H.; Coburn, J. W.; Graves, D. B. *J. Vac. Sci. Technol. A* **2001**, *19*, 718.
13. Goyette, A. N.; Wang, Y.; Misakian, M.; Olthoff, J. K. *J. Vac. Sci. Technol. A* **2000**, *18*, 2785.

14. Kawamura, E.; Vahedi, V.; Lieberman, M. A.; Birdsall, C. K. *Plasma Sources Sci. Technol.* **1999**, *8*, R45.

15. Goyette, A. N.; Wang, Y.; Olthoff, J. K. "Comparison of the identities, fluxes, and energies of ions formed in high density fluorocarbon discharges"; *Characterization and Metrology for ULSI Technology: 2000 International Conference*, 2001.

16. Edelberg, E. A.; Perry, A.; Benjamin, N.; Aydil, E. S. *J. Vac. Sci. Technol. A* **1999**, *17*, 506.

17. d'Agostino, R.; Cramarossa, F.; Fracassi, F. Plasma Polymerization of Fluorocarbons. In *Plasma Deposition, Treatment, and Etching of Fluorocarbons*; d'Agostino, R., Ed.; Academic Press, Inc.: San Diego, 1990; pp 95.

18. McCurdy, P. R.; Bogart, K. H. A.; Dalleska, N. F.; Fisher, E. R. *Rev. Sci. Instrum.* **1997**, *68*, 1684.

19. Lieberman, M. A.; Lichtenberg, A. J. *Principles of Plasma Discharges and Material Processing*; Wiley and Sons: New York, 1994.

20. Turner, M. M.; Lieberman, M. A. *Plasma Sources Sci. Technol.* **1999**, *8*, 313.

21. Cunge, G.; Booth, J. P. *J. Appl. Phys.* **1999**, *85*, 3952.

22. Booth, J. P.; Cunge, G.; Chabert, P.; Sadeghi, N. *J. Appl. Phys.* **1998**, *85*, 3097.

23. Booth, J. P. *Plasma Sources Sci. Technol.* **1999**, *8*, 249.

24. Booth, J. P.; Hancock, G.; Perry, N. D.; Toogood, M. J. *J. Appl. Phys.* **1989**, *66*, 5251.

CHAPTER 7

PRELIMINARY IRIS RESULTS FOR CF IN FLUOROCARBON PLASMAS

This dissertation chapter contains preliminary work involving IRIS investigations of CF in C_3F_8 and C_4F_8 plasmas. Relative density measurements and rotational temperature measurements as a function of different plasma parameters are discussed.

7.1. Introduction

The importance of fluorocarbon (FC) plasmas to both etch and deposition processes is discussed earlier in this dissertation. The overall effect of the plasma on the substrate depends on the concentration and energies of different plasma species. Chapters 5 and 6 discuss the interactions of CF_2 with the surface during the deposition of a thin FC film on Si. Additionally, these works reveal that ions and ion energies strongly affect both film composition and CF_2 surface production. Previous work in the Fisher group has demonstrated that studying multiple molecules in the same plasma system aids in the explanation of the chemistry of the plasma-surface interface.[1-3]

This chapter discusses expanding our IRIS studies of FC plasmas to include CF and C_2. CF in particular has been cited as a potential film deposition precursor in FC plasmas.[4] In contrast, experimental results by Kadota and coworkers suggest that C_2 is not a deposition precursor in C_4F_8 plasmas. Specifically, Kadota and coworkers used LIF measurements to examine the spatial variations of C_2 in high density CF_4/H_2 and C_4F_8 plasmas generated by helicon wave discharges.[5,6] C_2 surface production was insignificant in pure CF_4 systems but was enhanced with H_2 addition. In this case, hollow-shaped spatial distributions of C_2 were observed, with increased C_2 density near the chamber walls. This distribution supports C_2 surface production from the deposited FC film, which makes it an unlikely deposition precursor in these systems. Similar distributions were observed in C_4F_8 plasmas. Additionally, in C_4F_8 systems, positive ion bombardment of the FC film was necessary for C_2 surface production, and the presence of CF_x ions and radicals in the gas phase was deemed critical to the surface production mechanism. Based on the above information, CF and C_2 are interesting molecules to study using IRIS, with an emphasis on how ions affect their surface interactions.

In addition to relative density measurements, this chapter discusses rotational temperature measurements (Θ_R) of CF in C_3F_8 and C_4F_8 plasmas. One of the advantages of using low pressure plasmas to make and modify materials is that the low bulk temperatures of these systems can prevent or minimize thermal damage to the substrate.[7] When discussing the temperature of a plasma system, it is important to realize that plasma energetics are quite complex, and energy can partition differently into the various degrees of freedom of a molecule. This may result in non-thermalized systems where the rotational, vibrational, and translational temperatures are different for a particular molecule, or between different molecules. Studying the energetics of molecules is important for the elucidation of mechanistic details of both formation mechanisms and plasma surface interactions.[8]

7.2. Results and Discussion

7.2.A. CF and C_2 LIF measurements. Figures 7.1 shows the LIF excitation spectrum collected from 223.500 – 224.200 nm in 0.001 nm increments. Comparison to the literature confirms the presence of CF with no interference from other species.[9,10] The most prominent feature in the spectrum is the P_{11} bandhead of the $A^2\Sigma^+$ - $X^2\Pi$ (1,0) vibronic system at 223.837 nm. This transition was used for the density and attempted reactivity measurements discussed below. Figure 7.2 shows the relative density of CF in C_3F_8 and C_4F_8 plasma molecular beams as a function of *P*. Similar to CF intensity data collected for CF_4, C_2F_6 and CHF_3 plasmas,[11] increasing *P* generally leads to increased CF

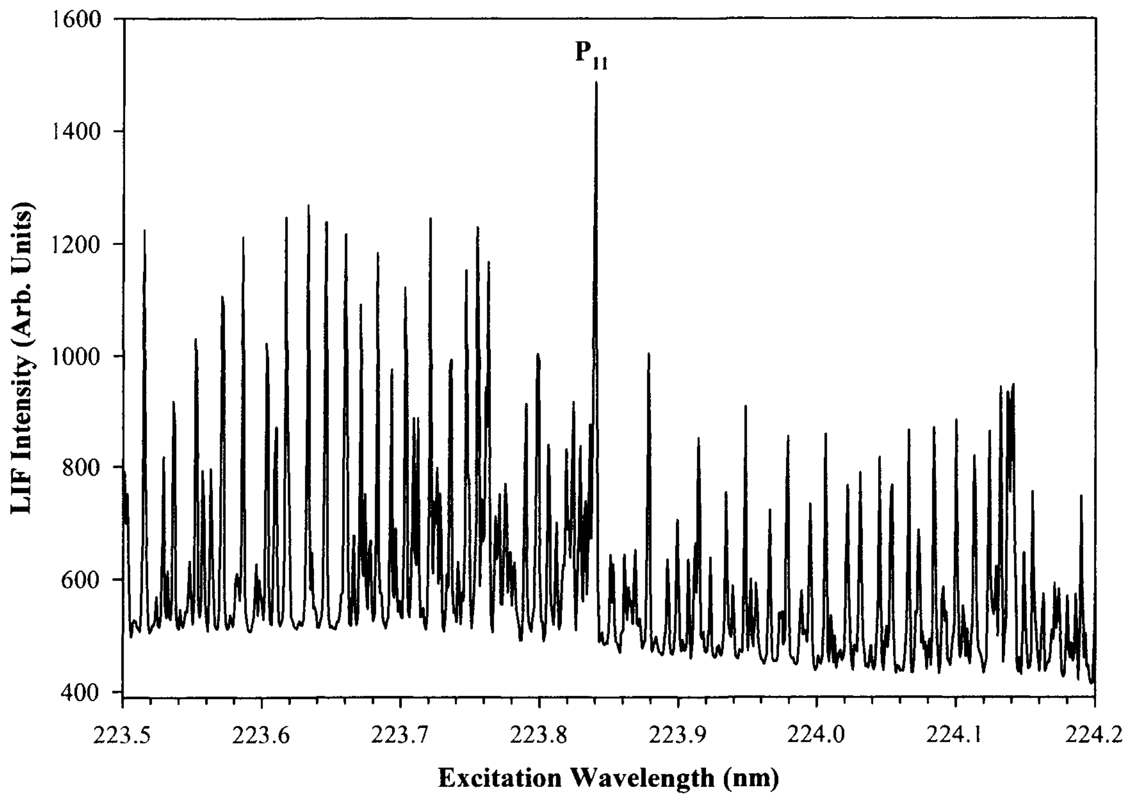

Figure 7.1 Experimental LIF excitation spectrum of CF in the molecular beam formed from a 200 W C_4F_8 plasma.

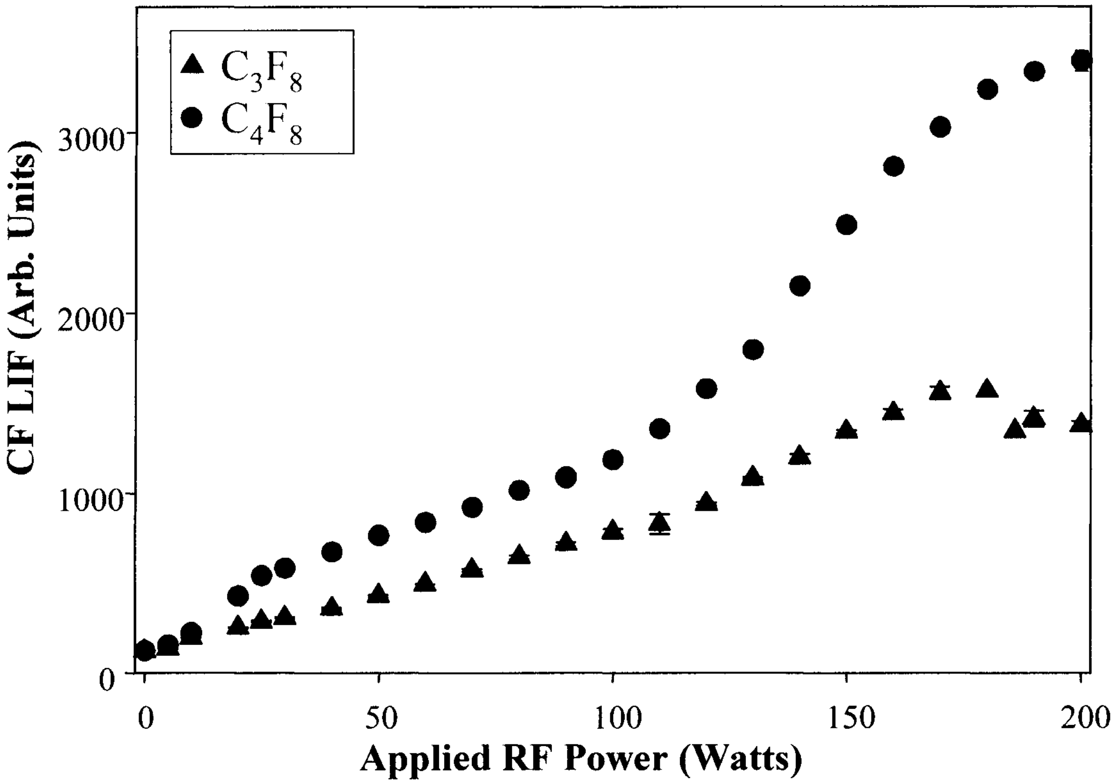

Figure 7.2 Relative LIF intensities of CF radicals in C_4F_8 (circles) and C_3F_8 (triangles) plasma molecular beams as a function of *P*.

production in both plasma systems, although in the C_3F_8 system, CF production reaches a maximum at $P = 180$ W. The increased CF production with P is a trend seen in other systems discussed in this dissertation (CF_2, $SiCl_2$) and is attributed to increased fragmentation of the monomer gas. Additionally, similar to CF_2 in these plasmas, C_4F_8 produces more CF than C_3F_8 does under the same conditions.

LIF detection of C_2 in C_4F_8 plasmas was attempted using the Swan system ($d^3\Pi_g$-$a^3\Pi_u$). The lower state of the Swan system is a metastable, and this LIF scheme was successfully used by Kadota and coworkers to detect C_2 in high density (2-20 mTorr, 100 – 1500 W) C_4F_8 plasmas generated by helicon wave discharges.[6] For our experiments, the dye laser was tuned to 516.550 nm, the C_4F_8 flow was set at either 5 sccm (22.6 mTorr), 10 sccm (41 mTorr) or 17 sccm (59 mTorr), and P was set to 100 W. Various excitation spectra were also collected from 516.495-516.550 nm or 516.440 – 516.540 nm in 0.001 nm increments for the 10 sccm and 17 sccm systems. Images were collected with up to 10000 laser shots. In all cases, there was no LIF signal present that was distinguishable from the background noise in the images.

7.2.B. Surface interactions of CF. Abundant LIF signal was available for CF density and rotational temperature measurements. Therefore, S(CF) measurements were attempted on numerous occasions. Ultimately, the cross-sections of the beam and scatter of the CF data were not suitable for the model used to quantify S. When the slits were not cooled with N_2 (l), the cross-sections were too broad due to spurious scattering off the slits. Cooling the slits to minimize the scattering resulted in greatly decreased LIF signals, effectively making the measurements impossible. Additionally, the fluorescence lifetime of CF (~26 ns) makes measurements of this molecule challenging because there is a very short window available to collect the fluorescence.[10] In a typical IRIS measurement, the gate delay is set so that the camera starts to collect signal at ~ 40 ns after t_0, where t_0 the time required for the laser to reach the chamber to excite the LIF. Since the lifetime of CF is 26 ns, the gate delay for this system is set to t_0 + 5 ns. As a result, any reflections from the laser in the chamber become significant because a longer gate delay cannot be used to avoid them.

7.2.C. CF rotational temperature measurements. Θ_R of a molecule is based on the population of different rotational states; these can be measured by collecting experimental excitation spectra.[8] For CF, Θ_R is deduced from the relative heights of the neighboring P_{12}, J = 17.5 (224.149 nm) and J = 1.5 (224.155 nm) lines. This relationship is sensitive to Θ_R because of the large difference in rotational quantum numbers. Both lines are scanned in an excitation LIF spectrum with a step size of 0.001 nm, and compared to data simulated using the program LIFBase.[12] Figure 7.3 shows an example of CF Θ_R collected for a 50 W C_4F_8 plasma molecular beam. The simulated Θ_R = 378 K is clearly a reasonable fit for the experimental data. The average of multiple data sets yields a value of $\Theta_R = 349 \pm 25$ K for these plasma conditions. These data were collected for numerous powers in both C_3F_8 and C_4F_8 plasma molecular beams, and the results are shown in Figure 7.4. Interestingly, Θ_R (CF) increases with *P* in C_3F_8 plasma molecular beams, whereas it is independent of *P* in the C_4F_8 plasma molecular beams. Previous work in our group has demonstrated that Θ_R of a molecule is related to its formation pathway.[8] The different trends Θ_R exhibits with increasing *P* may be related to different CF formation mechanisms in the 2 plasma systems. One obvious difference between the monomer gases is that one is linear (C_3F_8) and the other is cyclic (C_4F_8). Measuring Θ_R

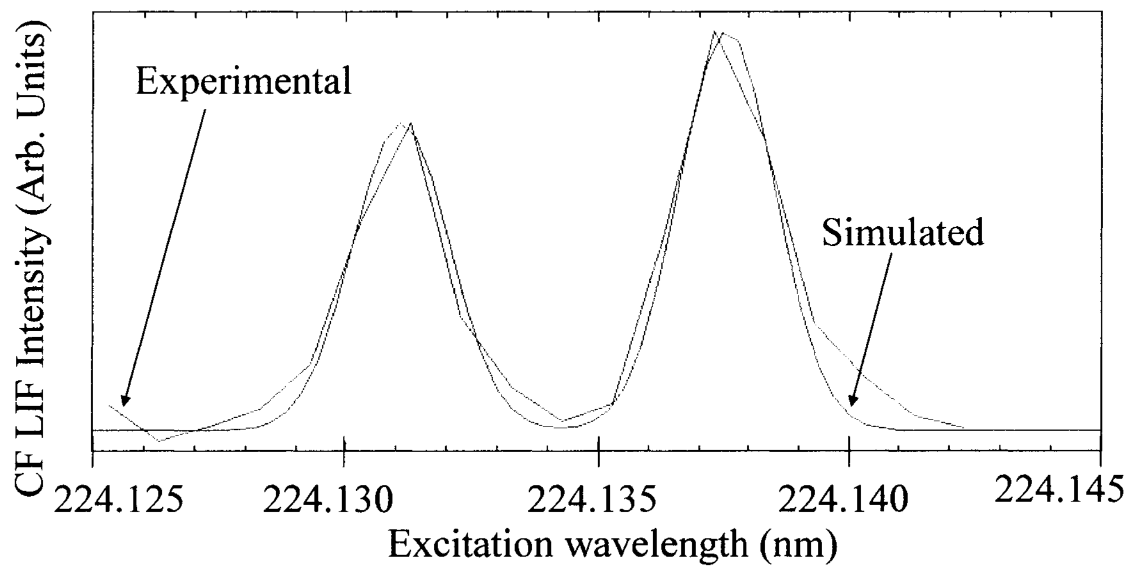

Figure 7.3 Experimental LIF excitation spectrum of CF in a 100% C_4F_8 plasma molecular beam (P = 50 W) from 224.125 to 224.145 nm (0.001 nm resolution). The simulated line intensities for a 378 K CF molecule are also shown.

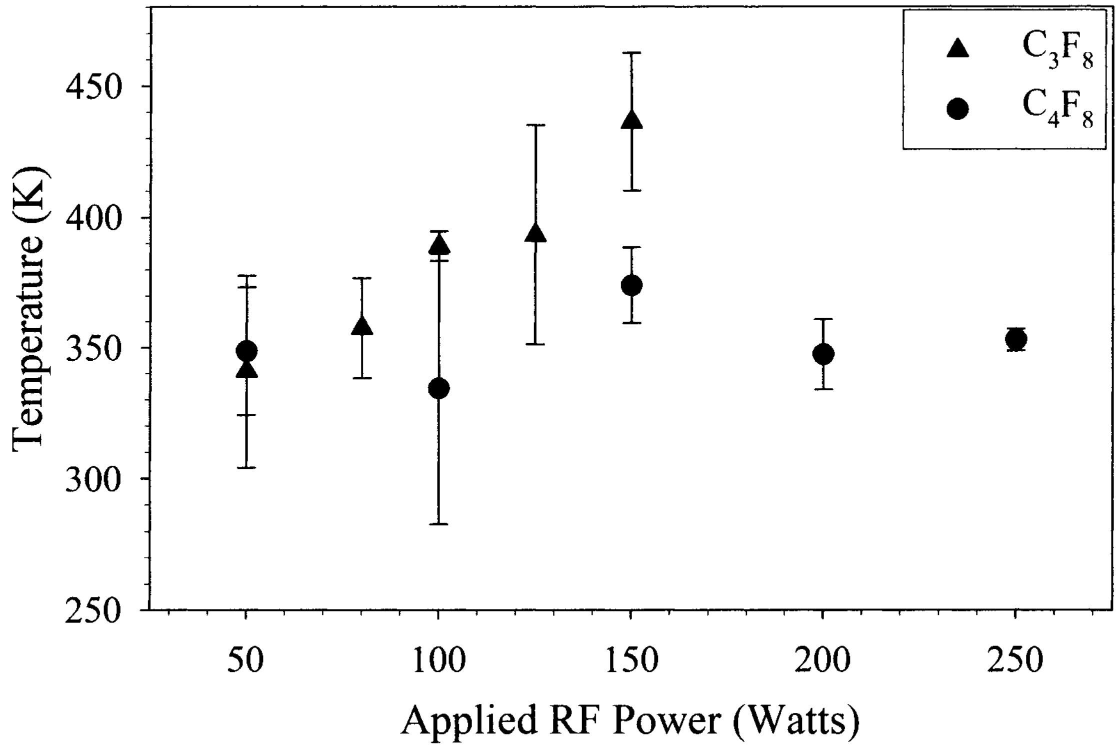

Figure 7.4 Average rotational temperatures (Θ_R) of CF in C_3F_8 (triangles) and C_4F_8 (circles) plasma molecular beams as a function of P.

in other FC plasmas with linear monomers (C_2F_6, C_4F_{10}) would help to explain these measurements.

7.3. Summary

CF has been detected in both C_3F_8 and C_4F_8 plasma molecular beams with the same parameter space used for CF_2 studies discussed in Chapters 5 and 6 of this dissertation. Initial relative density measurements and characterization of Θ_R have been performed. Initial attempts at C_2 detection have been unsuccessful, however additional attempts using different pressures and powers, and with the C_3F_8 monomer should be explored.

References

1. Williams, K. L.; Fisher, E. R. *J. Vac. Sci. Technol. A* **2003**, *21*, 1024.

2. Liu, D.; Zhou, J.; Martin, I. T.; Fisher, E. R. *J. Phys. Chem* **2005**, *To be submitted.*

3. Liu, D.; Martin, I. T.; Zhou, J.; Fisher, E. R. *Pure Appl. Chem.* **2005**, *Submitted.*

4. d'Agostino, R.; Cramarossa, F.; Fracassi, F. Plasma Deposition, Treatment, and Etching of Polymers. In *Plasma Deposition, Treatment, and Etching of Polymers*; d'Agostino, R., Ed.; Academic Press, Inc.: San Diego, 1990; pp 95.

5. Sasaki, K.; Furukawa, H.; Kadota, K. *J. Appl. Phys.* **2000**, *88*, 5585.

6. Suzuki, C.; Sasaki, K.; Kadota, K. *Jpn. J. Appl. Phys.* **1999**, *38*, 6896.

7. Grill, A. *Cold Plasma in Materials Fabrication: From Fundamentals to Applications*; IEEE Press: New York, NY, 1994.

8. Kessels, W. M. M.; McCurdy, P. R.; Williams, K. L.; Barker, G. R.; Venturo, V. A.; Fisher, E. R. *J. Phys. Chem. B* **2002**, *106*, 2680.

9. Andrews, E. B.; Barrow, R. F. *Proc. Phys. Soc.* **1950**, *165*, 890.

10. Booth, J.-P.; Hancock, G.; Toogood, M. J.; McKendrick, K. G. *J. Phys. Chem* **1996**, *100*, 47.

11. Mackie, N. M. Investigation of Mechanisms for Plasma Polymerization of Organic Thin Films. Dissertation, Colorado State University, 1998.

12. Luque, J.; Crosley, D. R. **1999**, *SRI International Report MP 99-009.*

CHAPTER 8

INVESTIGATIONS OF $SiCl_2$ SURFACE INTERACTIONS DURING CHLOROSILANE PLASMA PROCESSING OF SILICON

This dissertation chapter contains preliminary work involving tetrachlorosilane ($SiCl_4$) plasmas, including gas-phase and $SiCl_2$ gas-surface interaction data collected for $SiCl_4$ and $SiCl_4/H_2$ plasma systems. Results are discussed and compared with previous IRIS results from the Fisher group for SiF_4 and SiF_4/H_2 plasma systems.

8.1. Introduction

In semiconductor device manufacturing, halogen-containing plasmas have been traditionally used for etching Si-based materials. Specifically, the fluorine and chlorine etch products of Si, SiF_2 and SiF_4, and $SiCl_2$ and $SiCl_4$, are sufficiently volatile to allow efficient material removal.[1,2] Fluorocarbon and fluorosilane plasmas have been studied extensively in the Fisher group in both deposition and etch systems.[3-12] The next step in our research is towards Cl-based plasmas used primarily in etching systems. The general mechanism for Cl_2 plasma etching of Si has been studied extensively, and is further discussed below. Chlorine-based plasmas are also used to etch III-V semiconductor materials and metals such as GaAs, GaN and Al.[2,13-17] Chlorine is actually preferable to fluorine in these systems because metal chloride etch products have a higher volatility. This is also true for the etching of a number of new materials being explored for replacement gate oxides such as HfO_2 and ZrO_2.[18]

Cl_2 plasma etching of Si has been thoroughly investigated in the literature. In these systems, Cl and Cl_2 react with the Si surface to form a chlorinated adlayer, and the $SiCl_x$ layer is subsequently removed by ion bombardment.[14,19] Ion energy (E_i) and substrate temperature (T_S) are both cited as significantly affecting the process efficiency, and resulting etch products. For example, molecular dynamics simulations by Graves and coworkers suggest the Si etch yield is dependent on E_i.[20,21] Furthermore, Karahashi et al. have examined the temperature dependence of desorption products and find that above 600 °C, mostly dichloride species are desorbed.[22] Above 800 °C, desorption of monochloride species also occurs.

$SiCl_2$ in $SiCl_4$ plasmas has been chosen as the test system to initiate mechanistic IRIS studies of Cl-based plasmas. This system was chosen for several reasons. First, in addition to being a Cl-source for etch studies, $SiCl_4$ has been used in the deposition of various Si-based materials such as amorphous Si and silicon nitride.[23-25] Previous work in the Fisher group has demonstrated that studying the same molecule in plasmas with different overall regimes (etching vs. deposition) helps clarify the role of that molecule in the overall process.[7,10,12] Second, SiF_4 and SiF_4/H_2 plasmas have been extensively studied using IRIS, and interesting comparisons are possible between the fluorosilane systems and their chlorine analogues. Comparison can also be made between $SiCl_2$ measurements and studies of isoelectronic CF_2 in the FC plasma systems discussed in this dissertation.

IRIS studies of $SiCl_4$ and $SiCl_4/H_2$ plasmas have been initiated to obtain mechanistic information pertinent to both etch and deposition processes. Basic gas-phase composition and relative $SiCl_2$ density data are presented as a function of *P*, pressure and gas-composition for these systems. $SiCl_2$ reactivity measurements show that $SiCl_2$ is produced during $SiCl_4$ and $SiCl_4/H_2$ plasma processing of Si, although the addition of H_2 decreases the surface production of $SiCl_2$. These results are compared to previous IRIS studies in the Fisher group involving SiF_4 and SiF_4/H_2 plasma processing of Si.[10] These data show the feasibility of studying chlorine-based systems on the IRIS, and provide the basis for a rich new experimental system in our laboratories.

8.2. Results and Discussion

8.2.A. Gas phase analyses. Optical emission spectroscopy (OES) and LIF measurements were used to examine the gas phase composition of 100% $SiCl_4$ and $SiCl_4/H_2$ plasmas. These techniques provide complementary information, identifying excited state species and ground state species respectively. Figure 8.1a shows the OES data for a 100 W $SiCl_4$ plasma. Emission from Cl, SiCl and $SiCl_2$ dominate the spectrum, which also has contributions from H atoms. The same reactor was used for both $SiCl_4$ and $SiCl_4/H_2$ treatments; the H content is most likely a result of residual contamination from the latter film deposition systems. Figure 8.1b is the spectrum of emission from a 100 W, 50:50 $SiCl_4/H_2$ plasma. H_2 addition results in the same emitting species, although the H_α line is the prevailing feature. The inset shows a magnification of the region from 250-400 nm, clearly indicating that excited state $SiCl_x$ species are present in the $SiCl_4/H_2$ system.

The OES data confirmed the presence of excited state $SiCl_2$ in $SiCl_4$ and $SiCl_4/H_2$ plasmas. Ground state $SiCl_2$ was identified in $SiCl_4$ plasma molecular beams on the IRIS using laser-induced fluorescence (LIF) measurements. LIF is a nonintrusive and highly selective analytical technique which allows the study of a single plasma species in a molecular beam populated by a variety of different ions and molecules and atoms. Figure 8.2 shows the LIF excitation spectrum collected from 315.000 – 323.000 nm in 0.010 nm increments from a 100 mTorr, 100 W $SiCl_4$ plasma. Comparison to the literature verifies that the fluorescing species is indeed $SiCl_2$.[26] The predominant feature in this spectrum is the 2^8_0 band of the $\tilde{A}\,^1B_1 - \tilde{X}\,^1A_1$ transition, which was used to acquire the $SiCl_2$ density and reactivity data for this chapter.

Figure 8.3a shows the relative density of $SiCl_2$ in 100% $SiCl_4$ and 50:50 $SiCl_4$:H_2 plasmas as a function of *P*. In the pure $SiCl_4$ system, the vapor pressure was 100 mTorr

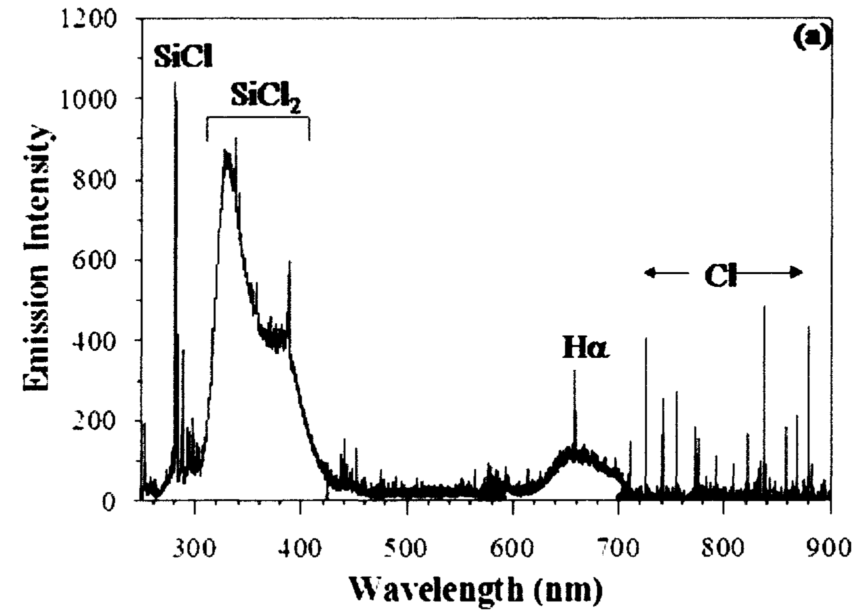

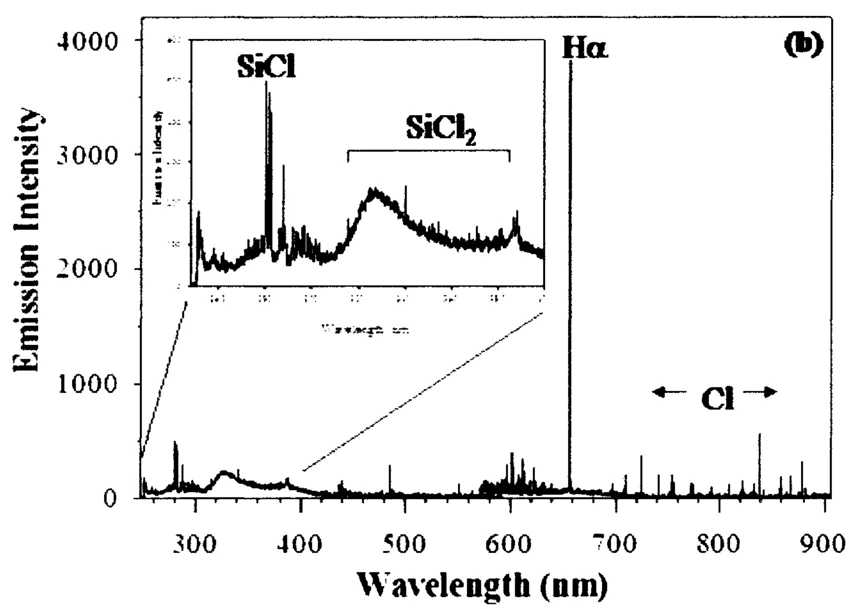

Figure 8.1. Optical emission spectra of 100 W (a) $SiCl_4$ and (b) 50:50 $SiCl_4/H_2$ plasmas. Total gas pressure for both systems was 100 mTorr.

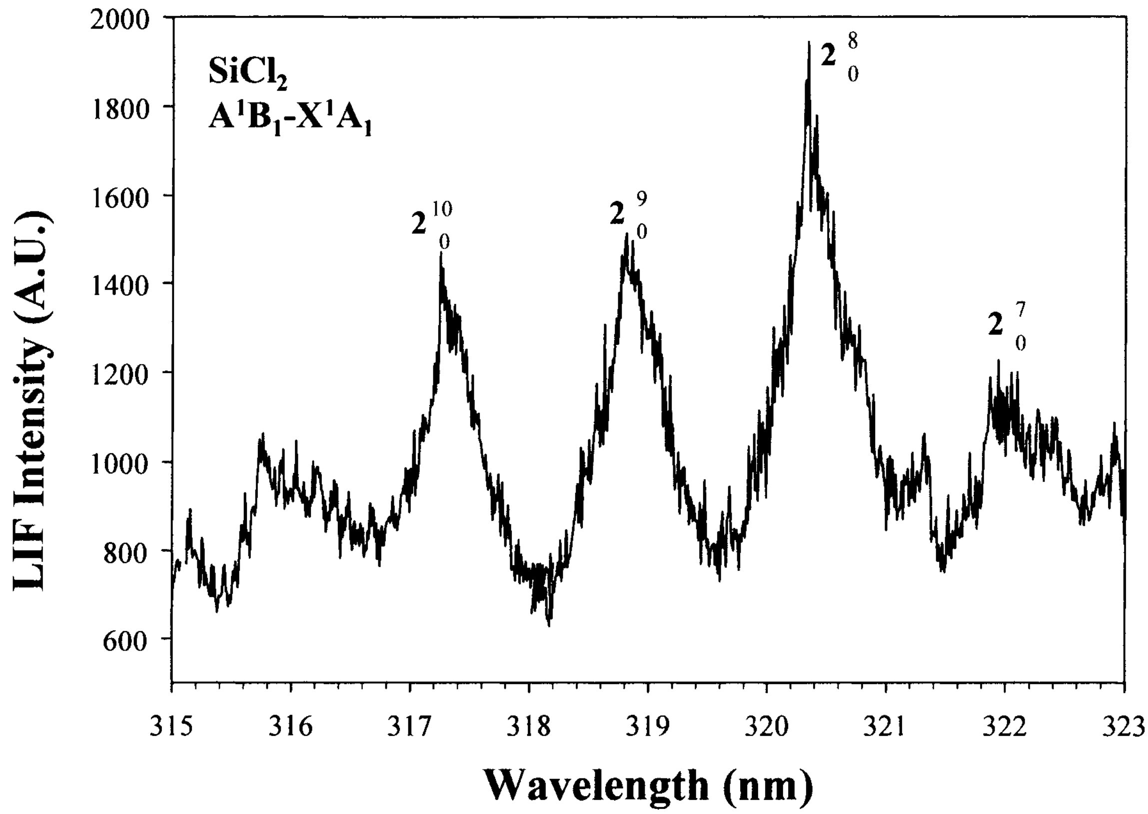

Figure 8.2. Experimental fluorescence excitation spectrum of $SiCl_2$ in the molecular beam formed from a 50 mTorr, 100 W $SiCl_4$ plasma. The transition used for all density and reactivity measurements was the 2^8_0 vibronic band of the $\tilde{A}^1B_1$- $\tilde{X}\,^1A_1$ transition.

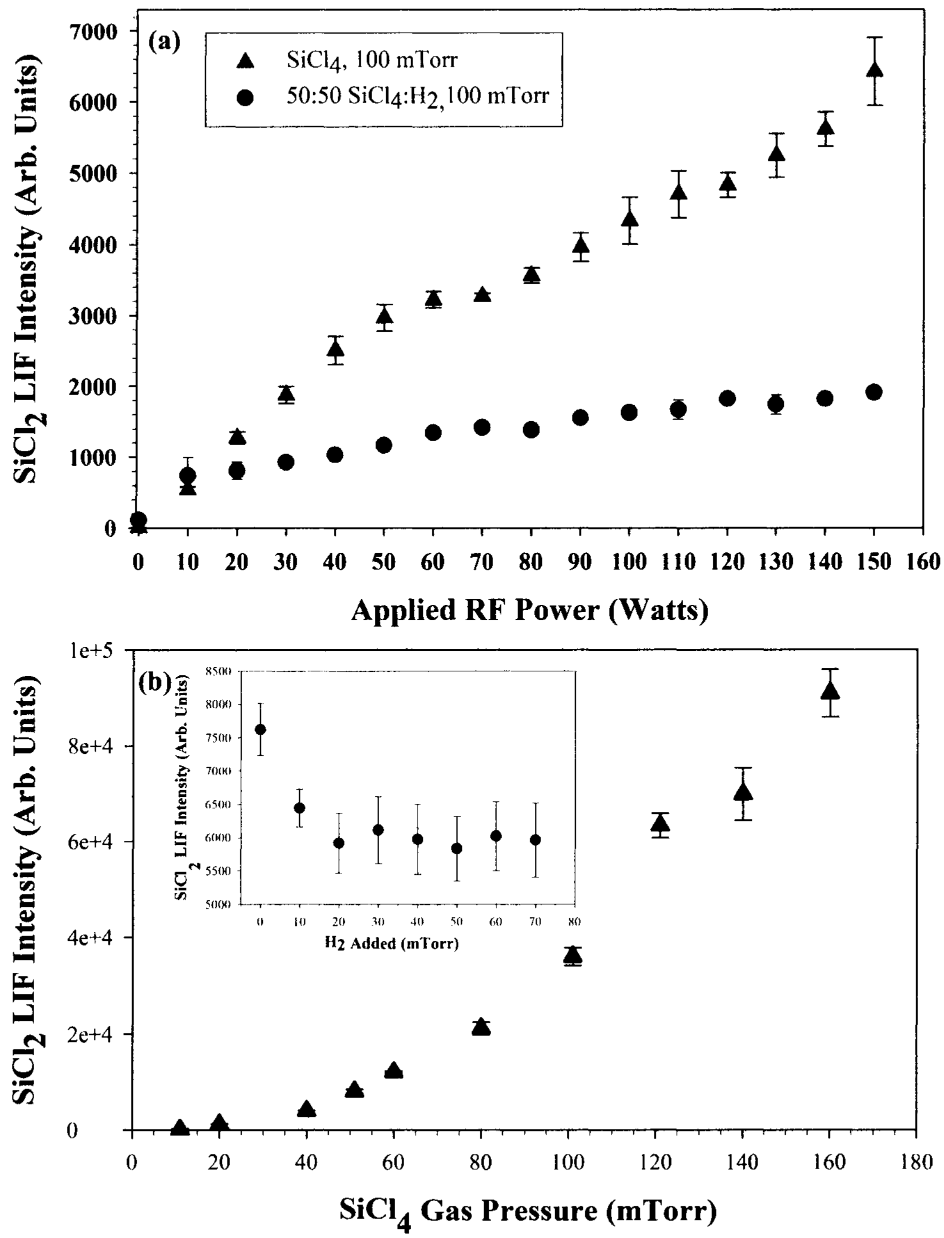

Figure 8.3. Relative LIF intensities of $SiCl_2$ radicals in $SiCl_4$ (triangles) and 50:50 $SiCl_4$:H_2 (circles) plasmas as a function of (a) applied rf power (total pressure = 100 mTorr), and (b) pressure (*P*=50 W). The inset in Figure 8.3b shows the relative LIF intensities of $SiCl_2$ radicals in 50 mTorr $SiCl_4$ plasmas as a function of H_2 addition (*P*=50 W).

before the plasma was lit, and the pressures recorded after lighting the plasma were 117 mTorr and 220 mTorr at 10 W and 150 W respectively. The observed pressure increase supports greater monomer dissociation at higher *P*, which leads to increased $SiCl_2$ production.[27] Clearly, the 50:50 $SiCl_4$:H_2 plasmas have lower relative $SiCl_2$ densities than the pure $SiCl_4$ systems. This is due to the lower $SiCl_4$ monomer vapor pressure used for these experiments (50 mTorr). There is a slight increase in relative $SiCl_2$ density with increasing *P* in the 50:50 $SiCl_4$:H_2 plasmas. The gas-phase species densities are the net result of complex gas-phase reactions. The addition of H_2 to the system increases the types of reactions possible. Mass spectrometry measurements will allow us to identify molecules such as $SiCl_xH_y$ to better characterize the gas-phase molecules present.

Figure 8.3b shows the relative density of $SiCl_2$ in $SiCl_4$ plasmas as a function of $SiCl_4$ vapor pressure in 50 W $SiCl_4$ plasma molecular beams. The vapor pressure was increased by increasing the flow of the $SiCl_4$ vapor into the system; this resulted in increased $SiCl_2$ production. When the initial $SiCl_4$ vapor pressure (no plasma) is 11 mTorr, the pressure when the plasma is ignited increases ~64%. When the initial $SiCl_4$ vapor pressure is 160 mTorr (no plasma), the pressure when the plasma is ignited increases ~44%. Using the pressure increase as a gauge for dissociation efficiency, there is more efficient dissociation of the monomer at lower pressures, although the relative $SiCl_2$ densities are highest at the highest pressures.

The inset in Figure 8.3b shows the $SiCl_2$ density as a function of H_2 addition in a 50 W plasma molecular beam. The $SiCl_4$ pressure was set at 50 mTorr for this experiment, and the H_2 flow was increased to increase the total gas pressure by 10 mTorr increments. The relative $SiCl_2$ density decreases with H_2 addition, and is independent of the amount of H_2 added. This is another area where MS measurements will be useful in explaining changes in gas-phase composition that occur when H_2 is added.

8.2.B. $SiCl_2$ surface interactions. Figure 8.4 shows a series of ICCD images of $SiCl_2$ LIF from a 50 mTorr, 50 W $SiCl_4$ plasma. Figure 8.4a contains the LIF signal from $SiCl_2$ molecules present only in the molecular beam. For Figure 8.4b, a Si substrate was rotated into the path of the molecular beam, so the LIF signal imaged is from $SiCl_2$ molecules present in both the molecular beam and those scattered off the surface. Figure 8.4c is the difference between Figures 8.4b and 8.4a, and shows only the $SiCl_2$ molecules scattered off the substrate surface. Clearly, there is significant $SiCl_2$ surface production. To quantify the $SiCl_2$ scatter, 20 columns of pixels along the laser beam were averaged and this was plotted as a function of distance along the laser axis to yield the cross-sections plotted in Figure 8.5. The signal from the scatter is very intense. The dashed lines in Figure 8.5 are the simulated curves for the incident beam and scattered molecules, assuming an adsorption-desorption mechanism, with $S = 3.60 \pm 0.10$. A weighted average of multiple data sets yields $S = 3.51 \pm 0.08$ for this set of parameters.

Table 8.1 contains the $S(SiCl_2)$ values measured during $SiCl_4$ plasma processing of Si as a function of P, source pressure and gas composition. These data are also depicted graphically in Figure 8.6. $S(SiCl_2) >> 1$ under all conditions studied. Indeed, $S(SiCl_2)$ for the 50 mTorr, 160 W $SiCl_4$ system is 4.94 ± 0.10, the highest scatter coefficient measured to date using IRIS. There are several possible surface reactions that could account for the measured $S > 1$, including

$$Cl\ (g) + Si\ (s) \rightarrow SiCl_2\ (g) \qquad (8.1)$$

$$I^+ + SiCl_2\ (ads) \rightarrow SiCl_2\ (g) \qquad (8.2)$$

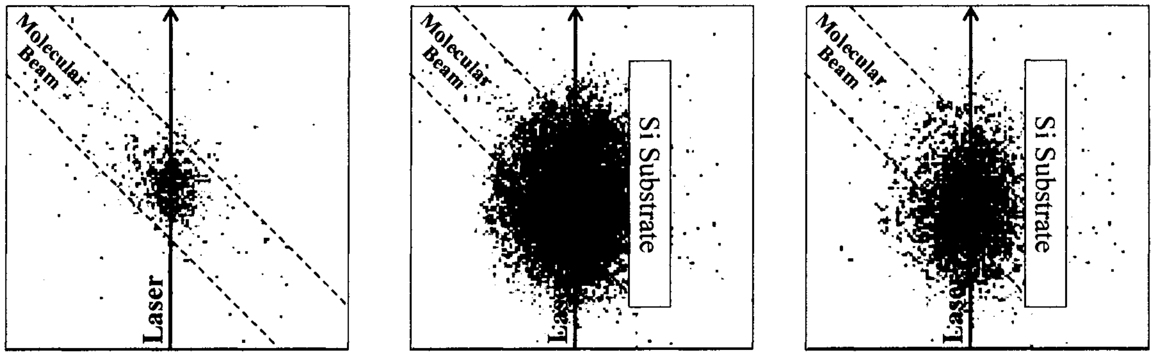

(a) **(b)** **(c)**

Figure 8.4. Spatially resolved 2D ICCD images of the LIF signal for the $SiCl_2$ 2^8_0 vibronic band of the $\tilde{A}^1B_1$ - $\tilde{X}\,^1A_1$ transition from (a) a 50 W $SiCl_4$ plasma molecular beam and (b) with a Si substrate rotated into the path of the molecular beam (laser-surface distance = 3.3 mm). The image in (c) is the difference between (a) and (b) and shows only the $SiCl_2$ molecules scattering from the surface. LIF signals with the highest intensity appear as the darkest regions, and lines indicate the location of the molecular and laser beams. The images have equivalent intensity scales.

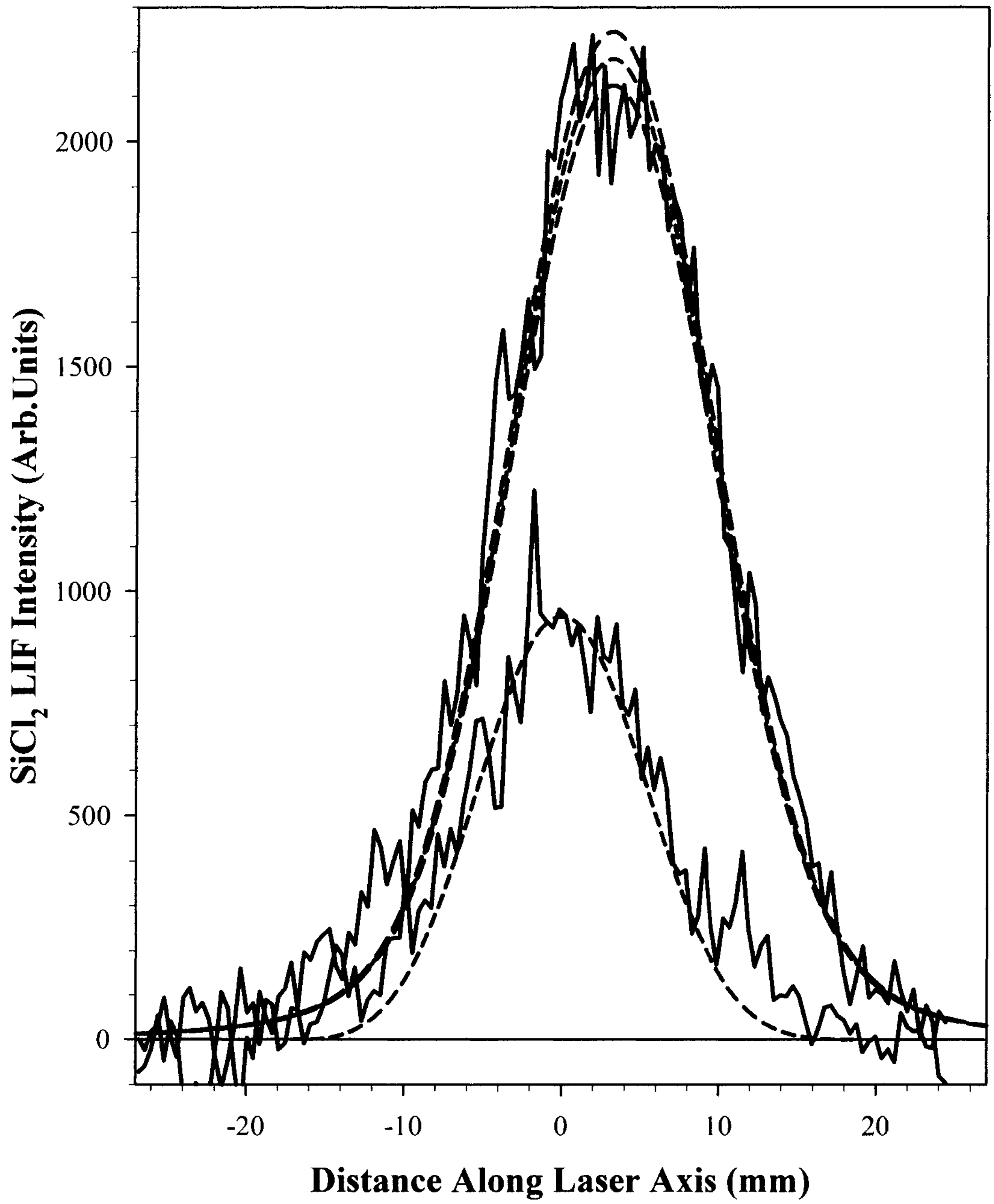

Figure 8.5. Cross-sections of the $SiCl_2$ LIF images shown in Figures 8.4a and 8.4c (solid lines). Dashed lines represent the simulation results for $S = 3.60 \pm 0.10$ with a laser-surface distance of 3.3 mm.

Table 8.1. $SiCl_2$ scatter coefficients for $SiCl_4$ plasma processing of Si.[a]

$SiCl_4$ (mTorr)	H_2 (mTorr)	*P* (W)	*S* ($SiCl_2$)	SiF_4 (mTorr)	H_2 (mTorr)	*P* (W)	Corrected *S* (SiF_2)[b]
50	---	25	2.31 (0.04)	---	---	---	
50	---	50	3.51 (0.08)	50	---	40	0.42 (0.01)
50	---	80	3.90 (0.07)	50	---	80	3.63 (0.17)
50	---	120	4.21 (0.07)	---	---	---	---
50	---	160	4.94 (0.10)	50	---	170	4.00 (0.14)
50	50	50	2.44 (0.11)	50	50	40	0.72 (0.03)
50	50	100	2.43 (0.12)	50	50	80	2.33 (0.05)
100	---	40	3.20 (0.20) *	100	---	40	1.21 (0.01)

[a] *S*($SiCl_2$) values are the weighted averages and errors of 3-7 data sets, except for the system marked with an *. This value is from a single data point; the error is representative of the upper and lower limit of a fit similar to that shown in Figure 8.5.

[b] *S*(SiF_2) values are from reference 10.

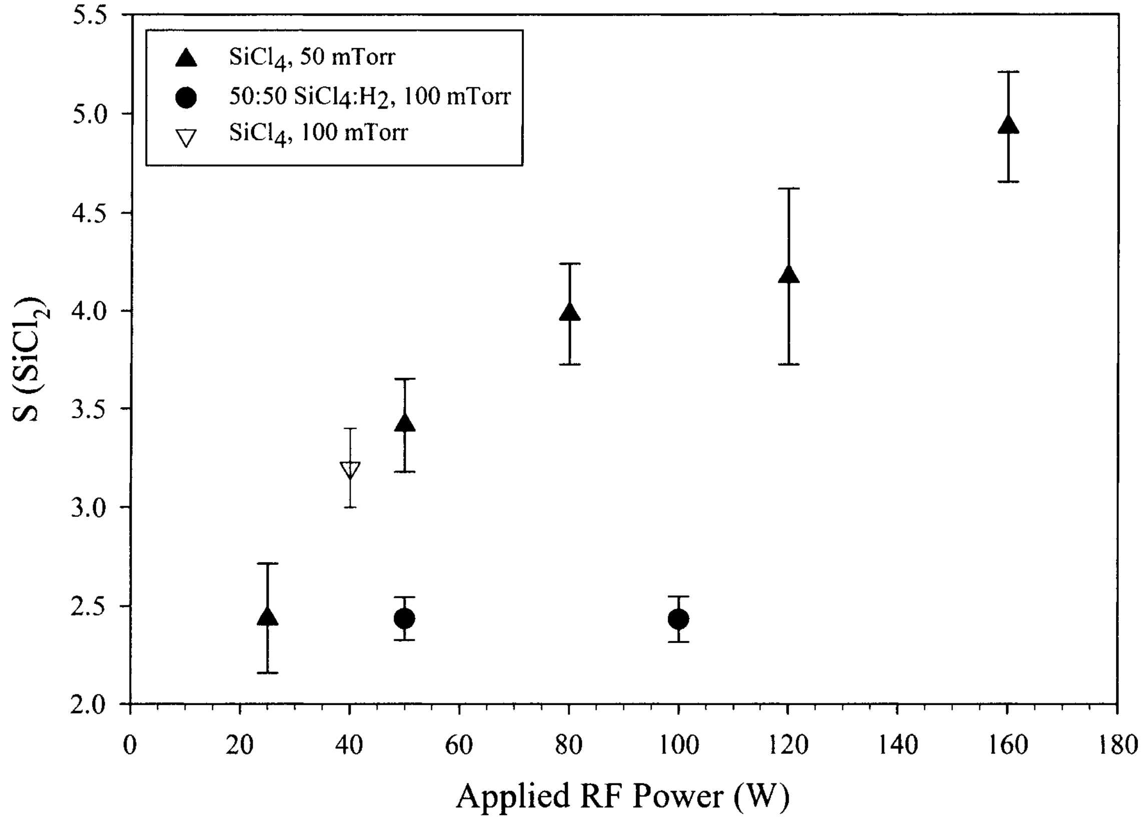

Figure 8.6. $SiCl_2$ scatter coefficients (*S*) measured during $SiCl_4$ (triangles) and $SiCl_4/H_2$ (circles) plasma processing of Si as a function of applied rf power (W). The $SiCl_4$ vapor pressure in the source was either 50 mTorr (filled triangles) or 100 mTorr (open triangle). Circles denote measurements taken in 50:50 $SiCl_4$:H_2 plasmas (total pressure = 100 mTorr). Values are the weighted averages and weighted errors of 3-7 data sets, except the data point for the 100 mTorr system, which is the value obtained for a single data point.

$$SiCl (g) + Cl (ads) \rightarrow SiCl_2 (g) \quad (8.3)$$

Reaction 8.1 represents the surface production of $SiCl_2$ as a Cl atom etch product of Si. Reaction 8.2 represents ion-induced $SiCl_2$ surface production, and reaction 8.3 is one example of a neutral-mediated production mechanism.

The 50 mTorr $SiCl_4$ data have a noticeable dependence on *P*. As discussed earlier, higher *P* leads to greater monomer dissociation. The increase in $S(SiCl_2)$ with *P* may be due to greater Cl atom densities as a result of greater dissociation of the source gas. This would lead to increased $SiCl_2$ production via reaction 8.1. Alternately, increased *P* may lead to higher ion energies, which have been known to enhance the Si etch yield.[20,21] As $SiCl_2$ is an etch product, $S(SiCl_2)$ would increase as well. Ion energy measurements such as those discussed in Chapter 6 could elucidate the contribution of reaction 8.2 to $S(SiCl_2)$.

A comparison between the 100 mTorr, 100% $SiCl_4$ and 100 mTorr, 50:50 $SiCl_4$:H_2 systems suggests that the source gas composition has a greater effect on $SiCl_2$ surface production than the total pressure. The data point for the 100 mTorr $SiCl_4$ plasma is close to that of the 50 mTorr $SiCl_4$ system. The values for the $SiCl_4$:H_2 system, however, are much lower than those measured at either pressure for the 100% $SiCl_4$ systems. Additionally the values measured in the hydrogen containing system are independent of *P*.

Additional measurements made under ion-limited and ion-enhanced conditions will allow us to quantify the effect of ions on $S(SiCl_2)$, and thus determine the effect of reactions such as 8.2 on $SiCl_2$ surface production. Mass spectrometry measurements will allow us to determine the role of ion energies and fluxes in these systems.

8.2.C. Surface analysis. Although a thorough surface analysis study has not been completed, preliminary etch rate data allow some interesting points to be made. Si etch rates measured in an independent reactor for 25 and 100 W $SiCl_4$ plasma treatment of Si are 19 ± 2 and 51 ± 8 Å/min respectively. $S(SiCl_2)$ measured for the former system is 2.31 ± 0.04, and it is anticipated that the 100 W system would yield $S(SiCl_2) \sim 3.9$-4.2 based on results for 80 and 120 W. As $SiCl_2$ is a major etch product of Cl etching of Si, it is reasonable that higher etch rates are measured in systems with greater $SiCl_2$ surface production.

Net deposition was observed in 20:80 and 50:50 $SiCl_4$:H_2 plasmas. XPS analysis of materials deposited on a zirconia substrate in the 20:80 system show 30% Si, 57% O, 11% C, and ~1% Cl. The binding energy of the Si peak is 103 eV, which is consistent with the oxide peaks of Si. These data suggest the net deposition is not of a-Si:H, but of SiO_2, possibly from etching of the glass reactor. XPS analysis of an etched Si substrate shows ~10% Cl incorporation from the 50 W, 80:20 $SiCl_4$:H_2 plasma treatment. Additional surface analysis measurements are clearly needed to achieve a complete picture of the overall effects of the $SiCl_4$ and $SiCl_4/H_2$ plasma treatments on Si.

8.3. Comparison to SiF_4 Systems

Previous work in the Fisher group includes a comprehensive study of the effect of plasma parameters (P, gas composition), Ts and ions on SiF and SiF_2 surface interactions during SiF_4 and SiF_4/H_2 plasma processing of Si.[10,11,28] Three plasma types were defined within these systems, and SiF_2 surface production was sensitive to the overall plasma regime. In net etch systems, SiF_2 was produced at the surface; both surface loss and production of SiF_2 were found in systems resulting in F incorporation with no net etching or deposition; and in a-Si:H,F film deposition systems, SiF_2 was typically lost at the surface.

The $S(SiF_2)$ values presented in Table 8.1 were scaled to take into account different velocity distributions of molecules in the beam (ν_{mb}) vs. those scattering from the surface (ν_{sc}). If the velocity distributions of the two populations are significantly different, this can affect their densities in the laser. This was accounted for by scaling S by the ratio of the velocities: ν_{mb}/ν_{sc}. Because ν_{sc} is based on T_S, when T_S is room temperature the scaling ratio is > 1. Although the $SiCl_2$ data have not been corrected for velocity, these values can be considered as a lower limit because ν_{mb} will not be less than ν_{sc} when $T_S \sim$ room temperature.

$SiCl_2$ surface production greatly exceeds SiF_2 surface production in analogous systems at low P, Table 8.1. For example, $S(SiCl_2)$ for 50 mTorr $SiCl_4$ systems is 2.31 ± 0.04 and 3.51 ± 0.08 at 25 W and 50 W respectively. $S(SiF_2)$ in a 40 W, 50 mTorr SiF_4 system is 0.42 ± 0.01, considerably lower. At $P \geq 80$ W, the S values bear a greater resemblance, but $S(SiCl_2)$ remains greater than $S(SiF_2)$ in analogous systems.

8.4. Suggested Future Studies

Previous studies of SiF_4 plasmas showed that in systems where the surface production of a molecule is enhanced by ion bombardment, S values increase with the application of a negative substrate bias and decrease with the application of a positive substrate bias.[10] This is because the negative bias accelerates positive ions into the substrate, whereas the positive bias repels them, limiting ion bombardment. Similar investigations of the $SiCl_4$-based systems would yield insight into the effects of ion bombardment on $SiCl_2$ surface production. Additionally, the ion composition and ion energies could be measured using the Hiden MS discussed in Chapter 6. If these data show similar trends to the isoelectronic SiF_4 system, i.e. if ions contribute to $SiCl_2$ surface production, the effect of the ion energies of these systems could be clarified.

There are several other molecules accessible via LIF in $SiCl_4$-based plasma systems, including SiCl,[29] SiH (for $SiCl_4/H_2$ plasmas)[30] and SiN ($SiCl_4/N_2$ or $SiCl_4/NH_3$ plasmas).[25] Studying multiple molecules in a single system allows for greater insight into the overall chemical processes that occur. There is a much interesting work that can be done on the chlorosilane systems now that the groundwork has been laid.

8.5. Summary

$SiCl_2$ surface interactions were investigated during $SiCl_4$ plasma processing of Si using our IRIS instrument. $S(SiCl_2)$ values >1 show that there is net production of $SiCl_2$ at the Si surface during $SiCl_4$ plasma processing, with higher values corresponding to systems where etching of the Si substrate is the dominant process.

References

1. Kuo, Y. *J. Electrochem. Soc.* **1995**, *142*, 2486.
2. Rahman, M.; Deng, L. G.; van den Berg, J.; Wilkinson, C. D. W. *J. Phys. Chem. D* **2001**, *34*, 2792.
3. Butoi, C. I.; Mackie, N. M.; Barnd, J. L.; Fisher, E. R.; Gamble, L. J.; Castner, D. G. *Chem. Mater.* **1999**, *11*, 862.
4. Butoi, C. I.; Mackie, N. M.; Gamble, L. J.; Castner, D. G.; Barnd, J.; Miller, A. M.; Fisher, E. R. *Chem. Mater.* **2000**, *12*, 2014.
5. Mackie, N. M.; Dalleska, N. F.; Castner, D. G.; Fisher, E. R. *Chem. Mater.* **1997**, *9*, 349.
6. Mackie, N. M.; Venturo, V. A.; Fisher, E. R. *J. Phys. Chem. B* **1997**, *101*, 9425.
7. Martin, I. T.; Fisher, E. R. *J. Vac. Sci. Technol. A* **2004**, *22*, 2168.
8. Martin, I. T.; Malkov, G. S.; Butoi, C. I.; Fisher, E. R. *J. Vac. Sci. Technol. A* **2004**, *22*, 227.
9. Williams, K. L.; Martin, I. T.; Fisher, E. R. *J. Am. Soc. Mass Spectrom.* **2002**, *13*, 518.
10. Williams, K. L.; Butoi, C. I.; Fisher, E. R. *J. Vac. Sci. Technol. A* **2003**, *21*, 1688.
11. Williams, K. L.; Fisher, E. R. *J. Vac. Sci. Technol. A* **2003**, *21*, 1024.
12. Butoi, C. I.; Mackie, N. M.; Williams, K. L.; Capps, N. E.; Fisher, E. R. *J. Vac. Sci. Technol. A* **2000**, *18*, 2685.
13. Hope, D. A. O.; Monnington, G. J.; Gill, S. S.; Borsing, N.; Smith, J. A.; Rees, J. A. *Vacuum* **1993**, *44*, 245.
14. Sung, K. T.; Pang, S. W. *Jpn. J. Appl. Phys.* **1994**, *33*, 7112.

15. Giehl, A. R.; Gumbel, M.; Kessler, M.; Herhammer, N.; Hoffmann, G.; Fouckhardt, H. *J. Vac. Sci. Technol. B* **2003**, *21*, 2393.

16. Baek, K. H.; Kim, K. H.; Hwang, C. H.; Lee, D. H. *J. Vac. Sci. Technol. B* **2001**, *19*, 2104.

17. Dienelt, J.; von Sonntag, J.; Zimmer, K.; Rauschenbach, B. *J. Vac. Sci. Technol. B* **2004**, *22*.

18. Sha, L.; Cho, B. O.; Chang, J. P. *J. Vac. Sci. Technol. A* **20**, *20*, 1525.

19. Mendicino, M. A.; Seebauer, E. G. *Appl. Surf. Sci.* **1993**, *68*, 285.

20. Barone, M. E.; Graves, D. B. *J. Appl. Phys.* **1995**, *78*, 6604.

21. Graves, D. B.; Wu, H.; Porteous, R. K. *Jpn. J. Appl. Phys.* **1993**, *32*.

22. Karahashi, K.; Matsuo, J.; Hijya, S. *J. Vac. Sci. Technol. B* **1992**, *60/61*, 126.

23. Lejuene, M.; Beyer, W.; Carius, R.; Muller, J.; Rech, B. *Thin Solid Films* **2004**, *450-451*, 280.

24. Bruno, G.; Capezzuto, P.; Cicala, G.; Cramarossa, F. *J. Appl. Phys.* **1987**, *62*, 2050.

25. Peng, L.; Fan, W. Y. *Chem. Phys. Lett.* **2002**, *367*, 645.

26. Suzuki, M.; Washida, N.; Inoue, G. *Chem. Phys. Lett.* **1986**, *131*, 24.

27. Li, X.; Ling, L.; Hua, X.; Oehrlein, G. S.; Wang, Y.; Vasenkov, A. V.; Kushner, M. J. *J. Vac. Sci. Technol. A* **2004**, *22*, 500.

28. Williams, K. L.; Martin, I. T.; Fisher, E. R. *J. Am. Soc. for Mass Spectrom.* **2002**, *13*, 518.

29. Jeffries, J. B. *Mater. Res. Soc. Symp. Proc.* **1988,** *117*, 41.

30. Kessels, W. M. M.; McCurdy, P. R.; Williams, K. L.; Barker, G. R.; Venturo, V. A.; Fisher, E. R. *J. Phys. Chem. B* **2002**, *106*, 2680.

CHAPTER 9

RESEARCH SUMMARY AND FUTURE DIRECTIONS

This dissertation chapter addresses general considerations for the utility of plasma processes. Additionally, suggested future directions based on this research are discussed.

Low temperature plasmas are essential to numerous manufacturing fields including semiconductor, aerospace, biomedical and automotive development.[1-4] As discussed in this dissertation, halogen-containing plasmas are especially important for microelectronic device fabrication, particularly the etching of Si-based materials with small device sizes.[4-8] As feature sizes in integrated circuits decrease, control of etch processes and development of new dielectric materials becomes more important.[9] The continuous refinement of known protocols and the development of new processes are necessary to accommodate shrinking device sizes, and the use of new materials with their accompanying manufacturing challenges. Understanding the fundamental chemistry that occurs in plasma processes is critical for continued success in this field.

This dissertation discusses uses of plasmas in both etch and deposition systems. One of the overarching goals of this work is to combine gas-phase and surface analyses data with the chemistry that occurs at the plasma-surface interface. This was achieved by the correlations presented in Chapters 5 and 6 between CF_2 surface production, the resulting film properties, and the mean ion energies measured in the plasmas.

This work has discussed the utility of plasmas for the deposition of thin films such as FC materials. Chapter 4 pertains to the first use of plasmas in our laboratories to modify microfluidic devices with PECVD. The use of plasmas to treat microfluidic devices is gaining popularity in the literature.[10,11] This is an area that could be easily expanded upon in the Fisher laboratories. Different plasma treatments to investigate include non-depositing plasma treatments such as H_2O and CO_2 plasmas to modify the hydrophobicity of the PDMS surface. Additionally, there are numerous thin-film systems to explore, such as plasma deposited polyethylene glycol. Lastly, it would be interesting to apply the treatments we have developed to microfluidic devices constructed out of polymers other than PDMS, such as PMMA to determine if the same plasma treatments lead to similar EOF modification in different base devices.

Chapter 6 discusses ion energy distributions in FC plasmas and their relationship to CF_2 surface production during C_3F_8 and C_4F_8 plasma processing of Si. The Fisher group has published $S(CF_2)$ data for a multitude of FC systems, including CF_4, C_2F_6 and HFPO. It would be interesting to measure the IEDs in these systems to further investigate the correlation between ion energy and $S(CF_2)$ discussed in Chapter 6. The CF rotational temperature studies presented in Chapter 7 could also be expanded to include other FC monomers.

Lastly, the initial $SiCl_4$ studies presented in Chapter 8 are ready for expansion. Conducting a study similar to the fluorosilane system discussed in that chapter would yield insight into the roles of $SiCl_x$ molecules in both etch and deposition systems. NH_3 could be added to $SiCl_4$ plasmas to explore silicon nitride systems, which are of particular interest as anti-reflection coatings and diffusion barriers in microelectronic devices.[12,13] It would be possible to study up to six molecules using IRIS in this system: SiCl, $SiCl_2$, SiN, SiH, NH and NH_2. Additionally, ion energy analysis in these systems would contribute to explaining the role of ion energy in the etching or deposition process.

References

1. Grill, A. *Cold Plasma in Materials Fabrication: From Fundamentals to Applications*; IEEE Press: New York, NY, 1994.

2. Li, X.; Ling, L.; Hua, X.; Oehrlein, G. S.; Wang, Y.; Anderson, H. M. *J. Vac. Sci. Technol. A* **2003**, *21*, 1955.

3. Li, X.; Ling, L.; Hua, X.; Oehrlein, G. S.; Wang, Y.; Vasenkov, A.; Kushner, M. J. *J. Vac. Sci. Technol. A* **2004**, *22*, 500.

4. Hope, D. A. O.; Monnington, G. J.; Gill, S. S.; Borsing, N.; Smith, J. A.; Rees, J. A. *Vacuum* **1993**, *44*, 245.

5. Li, X.; Ling, L.; Hua, X.; Oehrlein, G. S.; Wang, Y.; Vasenkov, A. V.; Kushner, M. J. *J. Vac. Sci. Technol. A* **2004**, *22*, 500.

6. Barone, M. E.; Graves, D. B. *J. Appl. Phys.* **1995**, *78*, 6604.

7. Fuller, N. C. M.; Telasca Jr., D. A.; Donnelly, V. M.; Herman, I. P. *Appl. Phys. Lett* **2003**, *82*, 4663.

8. Graves, D. B.; Wu, H.; Porteous, R. K. *Jpn. J. Appl. Phys.* **1993**, *32*.

9. McCurdy, P. R.; Sturgess, L. J.; Kohli, S.; Fisher, E. R. *Appl. Surf. Sci.* **2004**, *233*, 69.

10. Bouaidat, S.; Winther-Jensenb, B.; Flygenring Christensena, S.; Jonsmanna, J. *Sens. Actuators, A* **2004**, *110*, 390

11. Tsai, S. W.; Loughran, M.; Hiratsuka, A.; Yano, K.; Karube, I. *Analyst* **2003**, *128*, 237.

12. Asinovsky, L.; Shen, F.; Yamaguchi, T. *Thin Solid Films* **1998**, *313*, 198.

13. Klaus, J. W.; Ott, A. W.; Dillon, A. C.; George, S. M. *Surf. Sci.* **1998**, *418*, L14.